EXPLORATION OF CAT STRIATE CORTEX DURING NATURAL SCENE STIMULATION

by

Jonathan Lee Baker

A dissertation submitted in partial fulfillment
of the requirements for the degree

of

Doctor of Philosophy

in

Neuroscience

MONTANA STATE UNIVERSITY
Bozeman, Montana

November 2013

©COPYRIGHT

by

Jonathan Lee Baker

2013

All Rights Reserved

APPROVAL

of a dissertation submitted by

Jonathan Lee Baker

This dissertation has been read by each member of the dissertation committee and has been found to be satisfactory regarding content, English usage, format, citation, bibliographic style, and consistency and is ready for submission to The Graduate School.

Dr. Charles M. Gray

Approved for the Department of Cell Biology and Neuroscience

Dr. Frances Lefcort

Approved for The Graduate School

Dr. Ronald W. Larsen

STATEMENT OF PERMISSION TO USE

In presenting this dissertation in partial fulfillment of the requirements for a doctoral degree at Montana State University, I agree that the Library shall make it available to borrowers under rules of the Library. I further agree that copying of this dissertation is allowable only for scholarly purposes, consistent with "fair use" as prescribed in the U.S. Copyright Law. Requests for extensive copying or reproduction of this dissertation should be referred to ProQuest Information and Learning, 300 North Zeeb Road, Ann Arbor, Michigan 48106, to whom I have granted "the right to reproduce and distribute my dissertation in and from microform along with the non-exclusive right to reproduce and distribute my abstract in any format in whole or in part."

Jonathan Lee Baker

November 2013

DEDICATION

This thesis is dedicated to my late grandfather, Charles Livingston, an illiterate farmer and laborer, WWII veteran and hero who truly understood the value of education and was the lone private supporter of my undergraduate studies. I would also like to acknowledge my late friend and consummate source of optimism and support, Donald Stitt. He will be missed considerably while I pursue a career in academia and business. His spirit and enthusiasm will live on.

TABLE OF CONTENTS

1. BACKGROUND, SIGNIFICANCE AND SUMMARY OF THESIS CONTENTS ….1

1.1 Introduction 1
1.2 Background and Significance 2
1.3 Visual Cortical Responses to Natural Scene Stimulation 4
1.4 Oscillatory Activity within Visual Cortex 9
1.5 Outline of Thesis 13

2. RESPONSE HETEROGENEITY AMONG ADJACENT CAT STRIATE CORTICAL NEURONS TO NATURAL SCENE STIMULATION.....…….15

2.1 Background and Introduction 15
2.2 Materials and Methods 17
2.2.1 Surgery 17
2.2.2 Electrophysiology 19
2.2.3 Spike Sorting 19
2.2.4 Visual Stimulation 22
2.2.5 Data Analysis 24
2.2.6 Compensation for Extra Syncs 25
2.2.7 Response Reliability 26
2.2.8 Sparsity 26
2.2.9 Firing Rate Calculations 28
2.2.10 Comparison of the Time Course of Neuronal Responses 28
2.2.11 Detection of Response Events 29
2.3 Results 30
2.3.1 Summary of Data Collected 30
2.3.2 Response Reliability 32
2.3.3 Response Sparsity 37
2.3.4 Response Heterogeneity 42
2.3.5 Response Events 50
2.4 Discussion 54
2.4.1 Summary of Main Results 54
2.4.2 Methodological Issues 55
2.4.3 Response Heterogeneity with Cortical Columns 57
2.4.4 Implications for Pooling Models of Visual Cortex 63
2.4.5 Sparse Coding 65
2.4.6 Outstanding Issues 65
2.4.7 Natural Scenes 66

TABLE OF CONTENTS – CONTINUED

3. DYNAMICS OF SPIKING AND LOCAL FIELD POTENTIAL ACTIVITY IN CAT STRIATE CORTEX DURING NATURAL SCENE STIMULATION....68

3.1 Background and Introduction 68
3.2 Materials and Methods 74
3.2.1 Surgery 74
3.2.2 Electrophysiology 74
3.2.3 Silicon Polytrodes 75
3.2.4 Histology 76
3.2.5 Silicon Tetrode Probe Spike Sorting 78
3.2.6 Silicon Polytrode Spike Sorting 79
3.2.7 Visual Stimulation using Natural Scenes 80
3.2.8 Visual Stimulation with Sinewave Gratings 81
3.2.9 Visual Stimulation with Black and White Spots and Bars 81
3.2.10 Local Field Potentials 82
3.2.11 Multitaper Spectral Analysis 84
3.2.12 Z-transformed Multitaper Spectral Analysis 86
3.2.13 Z-Spectra Events 88
3.2.14 Correlation between Z-Spectra and Spiking Activity 91
3.2.15 Spike-LFP Coherence 92
3.2.16 Additional Spiking and LFP Analysis 95
3.2.17 Global Scene Transitions 97
3.3 Results 97
3.3.1 Summary of Data Collected 97
3.3.2 Spiking Activity during Natural Scene Stimulation 102
3.3.3 Local Field Potential Activity during Natural Scene Stimulation 112
3.3.4 Dynamics of Spiking and Local Field Potential Activity 118
3.3.5 Evoked Responses during Scene Transitions within the Movies 130
3.3.6 Summary of Results and Main Findings 132
3.4 Discussion 134
3.4.1 Summary of Main Results 134
3.4.2 Natural Scenes in the Study of Striate Cortex 135
3.4.3 The Origin and Spatial Scale of Local Field Potentials 138
3.4.4 Gamma Frequency Band Activity within the Striate Cortex 138
3.4.5 Dynamics of Spiking and Gamma Band Activity during Natural Scene Stimulation 145

TABLE OF CONTENTS – CONTINUED

4. MAIN FINDINGS, CONTRIBUTIONS AND CONCLUSIONS …….151

4.1 Summary of Main Findings and Primary Contributions..... 151
4.2 Contributions in the Context of Cortical Microcircuits 152
4.3 Future Experimentation and Analysis..... 157

REFERENCES CITED..... 161

LIST OF TABLES

Table Page

2.3.1 Number of cells isolated at each recording site 31

LIST OF FIGURES

Figure Page

1.3.1 Heterogeneous responses between neighboring cells 8

1.4.1 Laminar profile of spiking and LFP activity 13

2.2.1 Tetrode recoding of neuronal activity in cat striate cortex 20

2.3.1 Response heterogeneity during natural scene stimulation 34

2.3.2 Response reliability during natural scene stimulation 35

2.3.3 Diversity of response reliability among recording sites 37

2.3.4 Lifetime and population sparseness 38

2.3.5 Population sparseness 42

2.3.6 Signal correlations among pairs of cells 44

2.3.7 Diversity of signal correlations among recording sites 45

2.3.8 Firing rate differences among a neighboring cell pair 48

2.3.9 Distribution of peak firing rates during natural scenes 49

2.3.10 Differences in peak firing rates among pairs of cells 50

2.3.11 Detection of individual and joint firing events 52

2.3.12 Similarity index for cell pairs 54

2.4.1 Natural scene responses and spatiotemporal receptive fields 59

2.4.2 Heterogeneous responses to a jittering grating stimulus 61

2.4.3 Heterogeneous responses to natural and classical stimuli 63

3.2.1 Laminar profile of spiking and LFP activity to a movie 83

3.3.1 Schematic of multicontact silicon recording probes 101

LIST OF FIGURES – CONTINUED

Figure Page

3.3.2 Select laminar profiles of spiking and LFP activity to movies 103

3.3.3 Distribution of response reliability to short and long movies 106

3.3.4 Distribution of sparsity to short and long movies 107

3.3.5 Distribution of signal correlations to short and long movies 109

3.3.6 Laminar profiles of signal correlations to short movies 110

3.3.7 Laminar profiles of signal correlations to long movies 111

3.3.8 Average power spectra in recording sites during short movies 113

3.3.9 Average power spectra in recording sites during long movies 114

3.3.10 Spectrogram of LFP power during a short movie 115

3.3.11 Laminar profile of Z-spectrogram during a short movie 117

3.3.12 Distribution of PSTH-LFP correlations during short movies 120

3.3.13 Distribution of PSTH-LFP correlations during long movies 121

3.3.14 Laminar profile of PSTH-LFP correlations for short movies 122

3.3.15 Laminar profile of PSTH-LFP correlations for long movies 123

3.3.16 Spatial and temporal dynamics of spike-LFP coherence 125

3.3.17 Peak spike-LFP coherence difference profiles 126

3.3.18 Scatterplot of peak spike-LFP coherence differences 128

3.3.19 Average spiking and LFP profiles during scene changes 131

3.4.1 Average spike-LFP coherence profiles during short movies 143

ABSTRACT

The mammalian visual system evolved to process and represent objects within the complexities of the natural world to appropriately guide behavior in order to ensure survival and reproduction. Visual neuroscience has long sought to understand the neural basis of these processes, but the complexity of both the visual world and the brain has traditionally required a highly reductionist approach. The classical approach has led to the development of models of visual perception that are largely based on the analysis of how single cells within the visual system respond to simple and parametrically defined visual stimuli. However our ultimate goal is to understand how the visual system operates in the natural world. The experiments and results contained in this thesis were conducted, in part, to explore the cat's visual system during the presentation of time varying natural scenes, i.e. movies, and to attempt to validate our current working models of the visual system. Novel large-scale recording methods were employed to record from and characterize responses of large populations of cat primary visual cortex neurons during classical as well as movie stimulation. Contrary to the current models and our general understanding of how visual cortex represents information, groups of adjacent neurons responded heterogeneously to the movies presented and individual responses were very brief and highly sparse in time. The diversity and dynamics of the spiking activity was also significantly correlated with fluctuations of the ongoing local field potentials, specifically within the gamma frequency band, ranging from 25 to 90Hz. These gamma band oscillations also exhibited rich spatiotemporal dynamics throughout the movie presentations. In conclusion, time-varying natural scenes evoke response dynamics within the cat primary visual cortex not typically observed under more classical stimulus regimes. Future experimentation and the construction of biologically feasible models of visual cortex should take into account the diversity of responses observed under more natural stimulus conditions.

CHAPTER ONE

BACKGROUND, SIGNIFICANCE AND SUMMARY OF THESIS CONTENTS

1.1 Introduction

The broad objective of this research was to advance our understanding concerning the dynamics of neuronal activity within large populations of striate cortical neurons during the presentation of time varying natural scenes, i.e. movies. To accomplish this, I used novel silicon based electrophysiology probes to record large-scale population activity within the anesthetized cat striate cortex while presenting a series of 'classical' visual stimuli, that included black and white light bars, binary white noise, drifting sinusoidal gratings and the novel addition of repeated presentations of both short (30-40 second) and long (5 minute) movies. In the chapters that follow, I have focused on the main results related to population activity, in terms of single unit activity (SUA), multiple unit activity (MUA) and local field potential (LFP) activity recorded during the presentation of the short and long movies, and when appropriate, I present results obtained from the set of the classical stimuli listed above, primarily in order to make historical comparisons or to point out novel observations and key findings. Overall, this work was to some extent exploratory in nature, through the use of both novel recording technology and time varying natural scene stimulation. However the experiments were guided by well-founded hypotheses concerning how striate cortex is known to respond to visual stimuli, and in the process, I was able to make several key advances toward our collective pursuit of understanding visual perception in the mammalian brain. In chapter

two, I tested the hypothesis that individual striate neurons would respond rarely and briefly to time varying natural scenes and that concurrently recorded groups of closely spaced striate neurons would respond at relatively different rates and times throughout the movie presentations. In chapter three, I tested the hypothesis that robust and reproducible gamma frequency band (25-90Hz) activity, recorded in the local field potentials, would be present throughout the movie presentations and periods of significantly enhanced gamma frequency band activity would be correlated, in both space and time, with concurrently recorded spiking activity. Evidence was obtained to strongly support both of these hypotheses and the key findings and novel contributions are summarized briefly in this chapter and described in more detail in chapters two and three.

1.2 Background and Significance

The mammalian visual system evolved under the constraints of the natural world, thereby enabling and guiding appropriate behavior within the environment. The inherent complexities of the visual world and the incomprehensible number of neurons and density of synaptic connections within mammalian visual cortex necessitated an initial reductionist approach to studying the relationship between the visual stimuli presented to the system under study and the corresponding cortical responses. However, in spite of such complexity, in the pioneering experiments conducted by David Hubel (Hubel, 1959) he approached this stimulus-response problem by conducting a set of technical tour-de force experiments, by chronically implanted microelectrodes in awake and unrestrained cats in order "to make observations in natural sleep and waking states" and "to find the

best types of natural stimuli for activating cortical units". The exploratory nature of this approach was inspired by work conducted in the cat retina by Stephen Kuffler (Kuffler, 1953), who had identified and characterized center-surround organization within retinal ganglion cells of the cat. Although successful in characterizing cortical unit activity in the awake cat, David Hubel and Torstein Wiesel soon transitioned to an acute anesthetized preparation in order to more qualitatively characterize the "spurs and pauses in firing" observed while waving a hand within the 'receptive field' of the cells encountered and while the cat "looked about the room"; where he observed responses that accompanied most eye movements (Hubel, 1959). These experiments (Hubel and Wiesel, 1959; 1962) were conducted within anesthetized cats, allowing them to systematically characterize the response properties of individual striate neurons by using spots and bars of light for stimuli. This approach enabling them to successfully distinguish between several cellular response types, which they termed 'simple', 'complex' and 'hypercomplex' (Hubel and Wiesel, 1959; 1962). These somewhat arbitrary descriptions or classes of striate neuron types were soon confirmed in anesthetized (Hubel and Wiesel, 1968) and awake monkeys (Wurtz, 1969), and the general procedure of describing 'receptive field' properties through the use of parametrically controlled stimuli under anesthetized conditions rapidly expanded, spawning countless explorations within striate and extrastriate regions of the visual system of several mammalian species. The adoption of this 'classical' experimental paradigm by the visual neurophysiology community has generated a considerable wealth of knowledge regarding neuronal response properties in the mammalian visual system and much of our current understanding of the function of the

visual system is derived from the mass use of reduced and parametrically controlled stimuli.

Drawing from this pool of visual response properties and cell types, numerous heuristic models of visual cortex (Hubel and Wiesel, 1977; Adelson and Bergen 1985), all developed in order to better understand visual perception, are more or less based on the implicit assumption that key observations made under the 'classical' paradigm would readily translate under more naturalistic stimulus conditions, like those encountered by the animals being studied. Yet, our knowledge concerning the visual systems response to more 'naturalistic' stimuli is quite minimal and several aspects of the functional organization of striate cortex and the basic underlying mechanisms of visual perception remain poorly understood (Olshausen and Field 2005; Carandini et al., 2005). This dearth of knowledge necessitated this line of exploration. And as stated above, the goal of this research was to provide answers to a specific set of questions regarding the response properties of striate cortical neurons under natural scene stimulation. Therefore I have approached the issues briefly discussed above, while employing modern recording and stimulus presentation techniques.

1.3 Visual Cortical Responses to Natural Scene Stimulation

The natural visual world is endowed with unique properties, containing rich statistical regularities that can be readily characterized and modeled (Field 1987; Simoncelli & Olshausen, 2001). For instance natural visual stimuli contain extensive correlations in both space and time, and as a result, natural scenes contain a high degree

of redundancy (Dong and Attick, 1995). In addition, the visual system is normally confronted with a dynamically moving scene and whether those dynamics are due to internally generated movements, i.e. eye movements, or from objects moving within the visual scene, presents a further challenge to its study under normal operational conditions. Since the presumed function of any visual system is to reliably capture and transmit the visual information relevant to survival, it is a pertinent scientific question to ask how the system normally operates, i.e. processes information under natural conditions. The mechanisms of this process have been extensively explored over the last 60 years, however our current working framework is based on results obtained through the reduced experimental paradigm described above, and the visual systems' of the organisms under study rarely, if ever, encounter the 'classical' set of stimuli presented in the laboratory setting. Therefore, the primary goal in chapter two was to characterize striate neurons under more 'naturalistic' conditions in order to gain an understanding of how the system responds to natural scenes.

Natural scenes contain a high degree of redundancy and early investigators (Attneave 1954; Barlow 1961) hypothesized that sensory systems may efficiently represent information about the environment by reducing this redundancy. A more recent formulation of the 'efficient coding' hypothesis, known as 'sparse coding' (Field 1987; Olshausen and Field, 1996), made the explicit prediction that information about the visual world is represented by a relatively few number of neurons within a given population at any given time, and that those representative neurons responded robustly, yet rarely, during any arbitrary period of time. Indeed 'sparse' models of striate neurons, when

constrained to efficiently represent the information contained in natural scenes, resembled the spatiotemporal profiles of striate neurons derived from the 'classical' approach (Olshausen & Field, 1996; Bell & Sejnowski, 1997; van Hateren JH, Ruderman, 1998). The results described in chapter two lend direct support to the 'sparse coding' hypothesis and provide new insights into how small populations of striate cat striate cortical neurons respond to and process natural scenes.

Recent studies conducted within various mammalian species (rat, cat, ferret and monkey) have shown that spiking activity of primary visual cortex neurons elicited by naturalistic stimuli are both qualitatively and quantitatively different than those elicited by more classical stimuli (Baddeley et al., 1997; Vinje & Gallant 2000, 2002; Smyth et al., 2003; Kayser et al., 2003, 2004; David et al., 2004; Guo et al. 2005; Touryan et al. 2005; Felson et al., 2005; Yen et al., 2007; Yao et al., 2007; Goard & Dan, 2009; Tolhurst et al., 2009; Haider, et al., 2010). In accordance with the sparse coding hypothesis, striate neurons do in fact exhibit sparse and transient responses under natural scene stimulation and the temporal precision of those responses is quite reliable when multiple repetitions of the identical large field stimulus are presented (Vinje & Gallant, 2000; Yen, et al., 2007, Tolhurst et al., 2009; Haider, et al., 2010, Herikstad, et al., 2011). More specifically, results presented in chapter two revealed a high degree of sparse and heterogeneous responses to natural scenes, consistent with the sparse coding hypothesis. As a primer, Figure 1.3.1 illustrates the main results of chapter two and for historical reference the bottom trace includes the spike record of two simultaneously recorded striate neurons under naturalistic stimulus conditions in the awake cat (Hubel, 1959).

These neighboring neurons exhibit similar spatiotemporal response properties, in the classical terms of orientation, direction and spatial frequency, yet their responses under natural scene stimulation are markedly heterogeneous in terms of response amplitude and relative timing, i.e. their responses are decorrelated. The observed level of response diversity is unexpected in the context of the current working framework of striate cortical function where individual response properties have the tendency to be clustered. The columnar organization of receptive field properties among neighboring neurons has been described as a fundamental property of striate and in general sensory cortices (Hubel and Wiesel 1962, 1977; Mountcastle, 1997, 2003; Ohki et al., 2005), yet the utility of this functional model of sensory cortex is still debated (Horton and Adams, 2005). In fact past studies, using 'classical' visual stimuli, have revealed substantial variations of receptive field properties among adjacent striate neurons (DeAngelis et al., 1999; Gray et al., 1995; Maldonado and Gray 1996; Maldonado et al. 1997; Reich et al. 2001) and the results described in chapter two extend these findings using larger sets of simultaneously recorded units under natural scene stimulation. The observed degree of heterogeneity, or degree of response correlation, among these adjacent units is striking and several recent reports have shown that striate neurons within input layer 4 exhibit very low correlations compared to superficial and deep layers (Smith and Kohn, 2008; Smith et al., 2013) and even more striking that striate neurons recorded in awake and behaving monkeys exhibit near zero response correlation, significantly below all other studies sighted (Ecker et al., 2010), however certain methodological issues may have contributed to the low correlations reported in this study. Most importantly, the original findings reported in

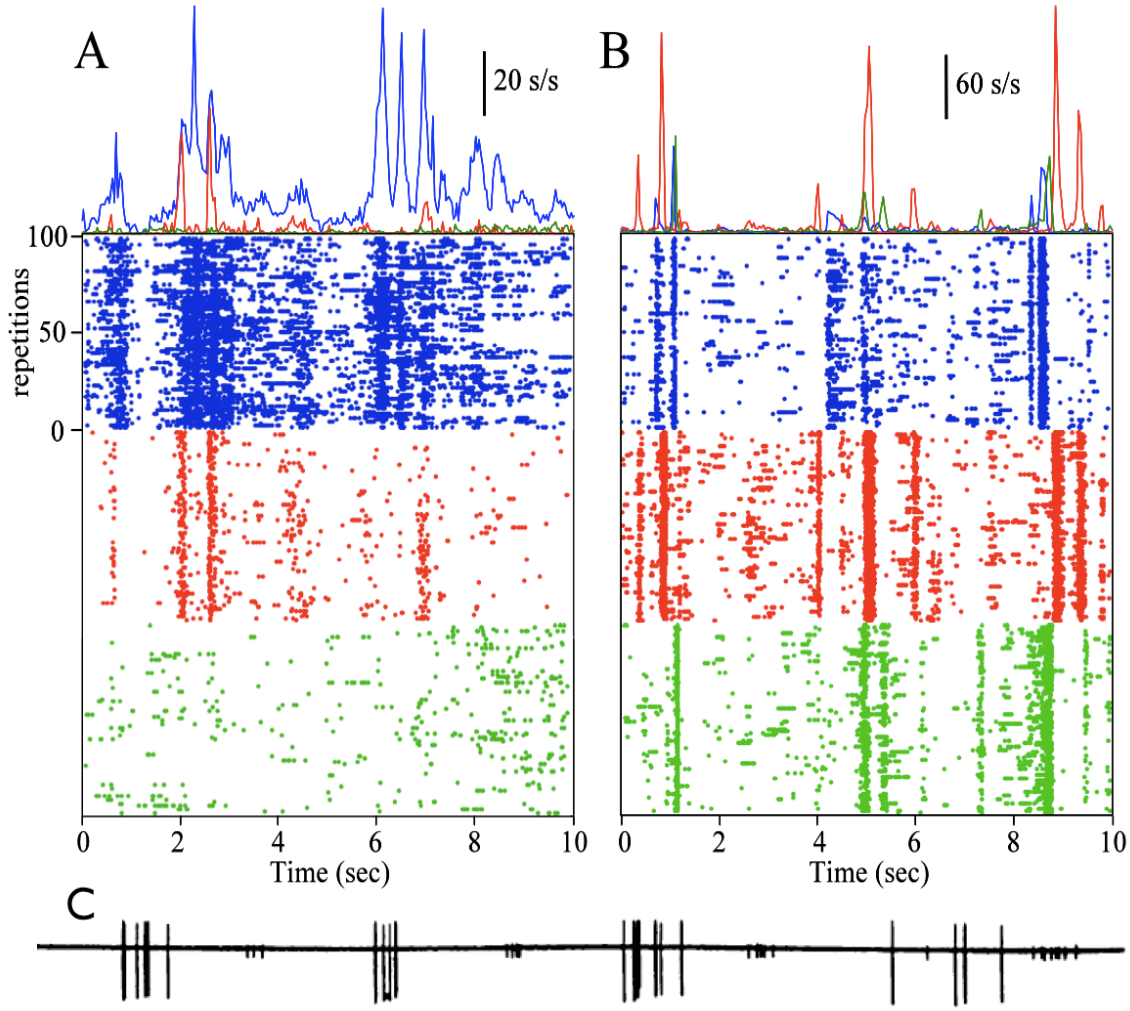

Figure 1.3.1 (A, B) Two example recordings conducted in two separate animals while being stimulated with a 30 second movie, repeated 100 times; only 10 seconds of data are shown. The upper plots display the average spike density functions for three single units recorded from a silicon tetrode probe. The lower color-coded plots display the corresponding spiking responses during each repetition of the movie. Note the brief, yet robust responses exhibited by a majority of the neurons and the degree of heterogeneity, in terms of their relative response amplitudes and timing. (C) For an historical comparison, I've included the spike record (Hubel, 1959, figure 6-C) observed for two simultaneously recorded cat striate units as they respond to "to-and-from hand movements" made by the experimenter's hand. Note the heterogeneity in the response timing of the two units. As noted in the original text, these cells responded to "opposing directions of movement" and several pairs of units, displaying similar response heterogeneity were encountered and noted (Hubel, 1959).

Yen et al., 2007 and those in Chapter Two were recently replicated under nearly identical experimental conditions in cat striate cortex (Martin and Schroder, 2013). Therefore, based on our expanding knowledge about population responses of striate neurons under more naturalistic stimulus conditions and the results described in chapter two and three, a careful reexamination of the current models used to explain receptive field properties of striate cortex is needed, primarily since those models, based on 'classical' experimental data, still inform our understanding of visual perception.

The reexamination of the original classification of 'receptive field' types, those mapped with simple stimuli and using spike triggered techniques (Ringach, 2004), have been validated in the recent years under natural scene stimulation (Smyth et al., 2003; Touryan et al., 2005; Carandini et al., 2005), yet prediction models derived under classical stimulus conditions consistently underperform compared to those derived from natural scene stimulation (David et al., 2004; David and Gallant, 2005; Haslinger et al., 2012). Although highly relevant to the current work and necessary to expanding our understanding of the processing of natural scenes, I did not focus on receptive field characterization under natural scene stimulation, yet future analysis, which takes into account large scale multiple unit and local field potential activity could address these issues. These and other related topics are discussed in more detail in chapter four.

1.4 Oscillatory Activity within Visual Cortex

Oscillatory activity recorded within neurophysiological potentials is a hallmark of nervous systems and has been observed in all examined species, ranging from insects to

humans. Extracellular potentials recorded from within brain tissue results from ionic currents flowing across cellular membranes and the local field potential (LFP) recorded from microelectrodes is thought to result from the integration of this electrical activity, from a large number of surrounding neurons, predominantly reflecting temporally synchronous synaptic currents (Buzsáki et al., 2012). The LFP is most often hypothesized to represent activity related to the inputs of the circuit, explicitly the thalamocortical and cortico-cortical input connections, whereas spiking activity is hypothesized to represent the output of the circuit, explicitly corticothalamic and cortico-cortical output connections. Regardless of its debated origin, the spectral power density of the LFP has been shown to scale, on average, as a $1/f^N$, where f is the frequency and N ranges from 1-3 (Buzsáki and Draguhn 2004; Buzsáki 2007). This scaling property within the LFP has been observed in numerous mammalian species (Leopold et al. 2003; Bedard and Destexhe, 2009) and its origin may result from the filtering properties of brain tissue (Bedard and Destexhe, 2009), or from the resistive properties (Logothetis et al. 2007), which could theoretically modified through firing rate modulations (Milstein et al. 2009). Although the precise origin of the LFP is somewhat irrelevant to these experiments, it can and has been used as a general index of local network activity. The LFP is typically broken up into semi-consistent frequency bands: delta (0.5-3.5Hz), theta (4-8Hz), alpha (8-14Hz), beta (15-30Hz), and gamma (>30Hz). Why the brain generates a range of frequencies and amplitudes and what functions they subserve is generally unknown, however power with the LFP and more broadly, the EEG, lies within a continuum of power across frequencies which change dynamically across time (Buzsáki, 2007).

Gamma band oscillatory activity within striate cortex has been well documented over the past 20 years and the phenomenon has been widely observed throughout the mammalian brain, in both awake and anesthetized preparations, and under a variety of experimental conditions. Chapter three focuses on the characterization of gamma (25-90Hz) and sub-gamma (1-15Hz) band oscillatory activity within the anesthetized cat striate cortex during the presentation of time varying natural scenes in order to quantify the relationship between fluctuations within the two LFP bands and the spiking responses, within and across multiple layers of striate cortex. Novel silicon recording technology, capable of recording simultaneously from up to one hundred single neurons (Blanche et al., 2005), was used to collect broadband neuronal activity across the layers of striate cortex. This approach allowed for the large spatial sampling of LFP and enabled the quantification of the extent of gamma oscillatory activity, in terms of amplitude, frequency and durations, during visual stimulation. Epochs of significantly enhanced gamma and sub-gamma activity were correlated to the concurrently record spiking activity. As discussed in detail in chapter three, I found that significant gamma band activity fluctuated dynamically in both power and frequency throughout natural scene stimulation and these fluctuations were both sparse and brief. These epochs enhanced gamma activity were also highly correlated with the sparse and brief periods of enhanced spiking activity, and in addition, they were more prominently observed in the upper layers of cortex, consistent with known response properties of upper layer 'chattering cells' (Gray and McCormick, 1996; Nowak et. al. 2003) and consistent with the laminar profile of gamma activity recorded in awake monkey visual cortex (Maier et al., 2010).

The results presented in chapter three further illustrate the dynamic relationship between spiking and gamma oscillatory activity under natural scene stimulation and are consistent with various proposals that the primary visual system is constructed to effectively process statistics inherent within natural scenes. A small selection of recent publications (Belitski et al., 2008; Montemurro et al., 2008; Berens et al., 2010) have reported on the dynamic nature of the LFP and spiking activity under natural scene stimulation in anesthetized preparations. Collectively, they have shown that the combined spiking and LFP activity does encode information related to the complex spatiotemporal properties within the natural stimuli, and that the encoding of this information was greatest within the gamma frequency band compared to lower frequency bands in the LFP. In awake and behaving macaque monkeys, the attentional state of the animals has also been shown to influence coupling between spiking and gamma band power (Fries et al., 2001; Womelsdorf et al., 2006) in the visual system, although that relationship is not always clear (Chalk et al. 2010) and some of the variability may be explained by the laminar profile of the coupling due to sub circuit mechanisms (Buffalo et al., 2012) and the intensity of the stimulus (Henry and Shapley, 2005; Roberts et al., 2013). Results presented in chapter three were collected in anesthetized cats and are not directly comparable to the awake and behaving condition, however the laminar profile of gamma frequency band activity and spiking activity under passively viewed movies may provide insights into the circuit mechanisms utilized by the primary visual cortex during awake periods, when the animal freely views and engages the natural world.

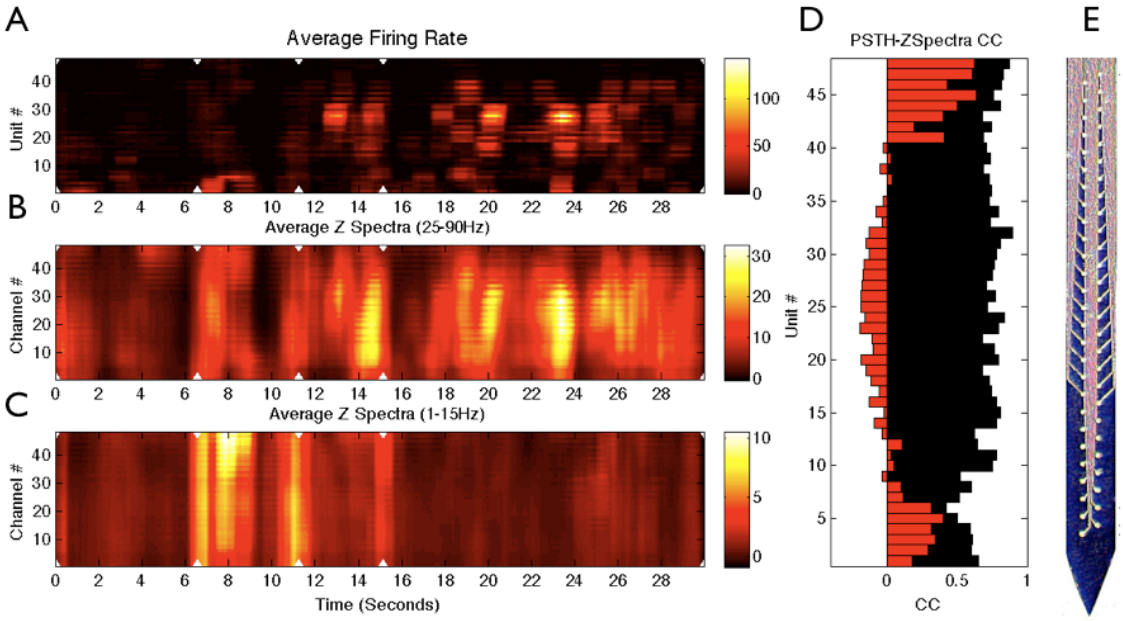

Figure 1.4.1 Example of multiunit and local field potential activity recorded across layers of striate cortex during the presentation of a 30 second movie. (A) The average firing rates of single and multiunit activity recorded from the 54-contact silicon polytrode shown in E, note the heterogeneity in absolute firing rates and the relative timing of activity during the movie. (B) The average Z transformed spectral power within the gamma band (25-90Hz) recorded from 48 polytrode contacts, note the broad spatial and temporal extent of significant gamma activity observed during the movie. (C) The average Z transformed spectral power below the gamma band (1-15Hz) recorded from the same 48 polytrode contacts, note the broad spatial and temporal extent of significant activity observed during the movie. The white triangles in A, B and C mark scene transitions within the movie, note the co-occurrence of sub-gamma spectral power and these scene transitions. (D) Pearson correlation coefficients between the average single and multiunit activity and the average spectral power in the gamma band, values shown in Black, and the average spectral power in the sub-gamma band, values shown in Red. (E) A microscope photo of the silicon polytrode used to record large-scale broadband activity across multiple layers of striate cortex.

1.5 Outline of Thesis

This thesis is organized into three additional, yet related chapters. Chapter two focuses on the characterization of small groups of striate neurons and their responses to natural scenes. Chapter three explores the dynamic relationship between spiking activity

and two fixed frequency bands, the sub-gamma (1-15Hz) and gamma frequency bands (25-90Hz), extracted from local field potentials concurrently recorded with large spatial samplings of populations of striate neurons during time varying natural scene stimulation. Chapter four summarizes the main findings and contributions of this work toward our understanding of striate cortical processing of natural scenes, makes several suggestions for future experiments and analysis, and discusses the relevance of this work in the context of neocortical microcircuits.

CHAPTER TWO

RESPONSE HETEROGENEITY AMONG ADJACENT CAT STRIATE CORTICAL NEURONS TO NATURAL SCENE STIMULATION

2.1Background and Introduction

In the striate cortex, populations of adjacent neurons exhibit common preferences to local stimulus features such as orientation, spatial frequency and direction of motion (Hubel and Wiesel 1977; Hubener et al. 1997; Ohki et al. 2005). This columnar organization is thought to reduce the effects of neuronal variability by enabling the pooling of activity of many nearby neurons that are sensitive to the same features (Mazurek and Shadlen 2002). Adequate coverage of the stimulus space is thought to be achieved by hypercolumnar organization in which the spectrum of feature attributes are represented by continuous variations in the stimulus selectivity of similarly tuned groups of cells (Hubel and Wiesel 1977; Swindale 1991; Swindale et al. 2000).

This model is largely based on the analysis of neuronal responses to simple stimuli, such as bars and sinewave gratings, where parametric variations of individual stimulus features can be easily performed. The widespread use of such stimuli has also revealed that i) striate neurons are tuned to multiple stimulus dimensions including orientation, direction, speed, spatial frequency, binocular disparity and others, ii) the selectivity to one stimulus parameter often depends on the value of other parameters (De Valois et al. 1979; Skottun et al. 1994; Geisler et al. 2001), and iii) influences from beyond the classical receptive field are both non-uniform and non-linear (e.g. Sillito et

al., 1995; Walker et al., 1999; Vinje and Gallant, 2000). This multi-dimensional and non-separable stimulus selectivity, when combined with non-linear surround influences, suggests that striate neurons should rarely be active during natural vision. Support for this has come from several studies demonstrating that striate neurons in cats, monkeys and ferrets respond with low probabilities when presented with a large sample of natural images (Baddeley et al. 1997; Vinje and Gallant 2000, 2002; Weliky et al. 2003).

The sparsity of neuronal responses to natural scenes also predicts a high degree of response heterogeneity (or population sparseness) among populations of adjacent neurons. Support for this comes from several recent studies where multi-neuron recordings have revealed substantial variations of receptive field properties among adjacent striate neurons (Maldonado and Gray 1996; Maldonado et al. 1997; DeAngelis et al. 1999; Reich et al. 2001). Consistent with this finding, serial recordings of neighboring neurons in striate cortex have revealed that natural images evoke highly decorrelated responses (Vinje and Gallant 2000, 2002). These results suggest that the classical picture of columnar organization, derived from the use of simple stimuli, may be substantially different from the one obtained when using complex, time-varying natural images (Horton and Adams 2005).

These issues were investigated through the simultaneous recording of responses of groups of nearby neurons in cat striate cortex during the presentation of time varying natural scenes (movies). The goal of this chapter was to characterize how local populations of neurons jointly represent time-varying natural scenes, and to compare the heterogeneity of the responses for cells recorded on the same or different tetrodes. In

summary, neighboring neurons with the cat striate cortex display markedly different response properties, in terms of firing rate amplitudes and relative response times, during the presentation of natural scenes. This level of decorrelation is not predicted from current functional models of visual cortex and lends strong support to hypothesis that visual cortex utilizes sparse coding to represent information.

2.2 Materials and Methods

2.2.1 Surgery

All experiments were conducted on anesthetized and paralyzed cats (3-4 kg) of both genders. Prior to surgery, each animal was anesthetized with an initial bolus of Ketamine (20 mg/kg) and Acepromazine (5 mg/kg, i.m.) and administered Atropine (0.05 mg/kg, s.c.) to reduce salivation. The animals were then intubated and surgical anesthesia was maintained with Halothane (0.5-1.0%), in a mixture of nitrous oxide and oxygen (2:1), while the animals were artificially ventilated using a Harvard resporator pump. A continuous infusion of Lactated Ringer's solution with 2.5% dextrose was administered intravenously throughout the experiment (4 ml/kg/h). The ECG, heart rate, rectal body temperature and expiratory CO_2 concentration were continuously monitored throughout the experiment, and the latter three were maintained within monitored ranges of 160-200 bps, 37-39ºC, and 3.5%-4.5%, respectively. Once vitals signs were stable, the animals were placed in a Kopf stereotaxic frame and a central scalp incision was made to expose the occipital bone. A unilateral craniotomy (3-5 mm) was made overlying the representation of the area centralis of area 17 (H-C locations). Following the surgery, the

animals were paralyzed with an initial bolus (0.3 mg/kg i.v.) of Pancuronium Bromide (Pavulon), followed by a continuous infusion of 0.3 mg/kg/hr (i.v.). Ophthalmic Neosynephrine (10%) and Atropine (1%) drops were placed in the eyes to retract the nictitating membranes and dilate the pupils, respectively. The eyes were focused on the screen of a computer monitor at a distance of 57cm using the tapetal reflection technique and an appropriate pair of gas permeable contact lenses. With the aid of surgical microscope, a small portion of the dura was reflected to expose the pia matter. In order to protect the pial surface from drying a mixture of 2.5% agar in artificial-CSF solution was applied to the cortical surface. Prior to recording, the agar was removed and a small cut was made in the pial surface. The tetrode or silicon probe was placed atop the pial surface using a Kopf micromanipulator and then slowly advanced into the surface cortex. A 4% mixture of agar in Ringers solution was then applied to the cortical surface to reduce pulsations and stabilize the electrode tip. The assembly was then covered with molten bone wax and mineral oil to maintain the integrity of the agar and bone wax. Upon cessation of the experiment, a lethal dose of Sodium Pentobarbital (60 mg/kg) was administered (i.v.). The protocol used in the experiments was approved by the Institutional Animal Care and Use Committee at Montana State University and conformed to the guidelines recommended in Preparation and Maintenance of Higher Mammals During Neuroscience Experiments, NIH publication No. 91-3207 (National Institutes of Heath, Bethesda, MD, 1991).

2.2.2 Electrophysiology

Recordings were made using either sharp Tungsten electrodes (4 cells) or 16-contact silicon probes (84 cells) provided by the Center for Neural Communication Technology (CNCT) at the University of Michigan. The CNCT probes contained 4 separate tetrodes and were used in two different configurations: one probe type had 4 shanks with a single tetrode at the end of each shank (4x1), and the second type had two shanks with two tetrodes per shank (2x2). In both configurations the center-to-center separation between adjacent tetrodes was 150 μm (Figure 2.2.1). The impedance of each contact ranged from 0.8-1.5 MΩ at 1 kHz. All signals were amplified (4000X), bandpass filtered (0.5 – 6 kHz), digitized at 30 kHz at a resolution of 12 bits, and stored on a personal computer for off-line analysis. Once stable unit signals were obtained, the borders of the receptive fields, the preferred stimulus orientation, and the dominant eye were determined for each recording site using mouse-controlled light bars and sinewave gratings. Movies were displayed to the eye that dominated cellular responses at the majority of recording sites while the non-dominate eye was covered with gauze.

2.2.3 Spike Sorting

Spike waveforms were extracted from the raw signals on each channel of the electrode or tetrode using a multi-step procedure. First, the background signal (i.e. the signal in the absence of spikes) was estimated by removing all data points from the raw signal that exceeded its mean ± 4 standard deviations. Local minima in the original signal (i.e. negative peaks in the spike waveforms) were identified if they exceeded 4 standard deviations of the background signal.

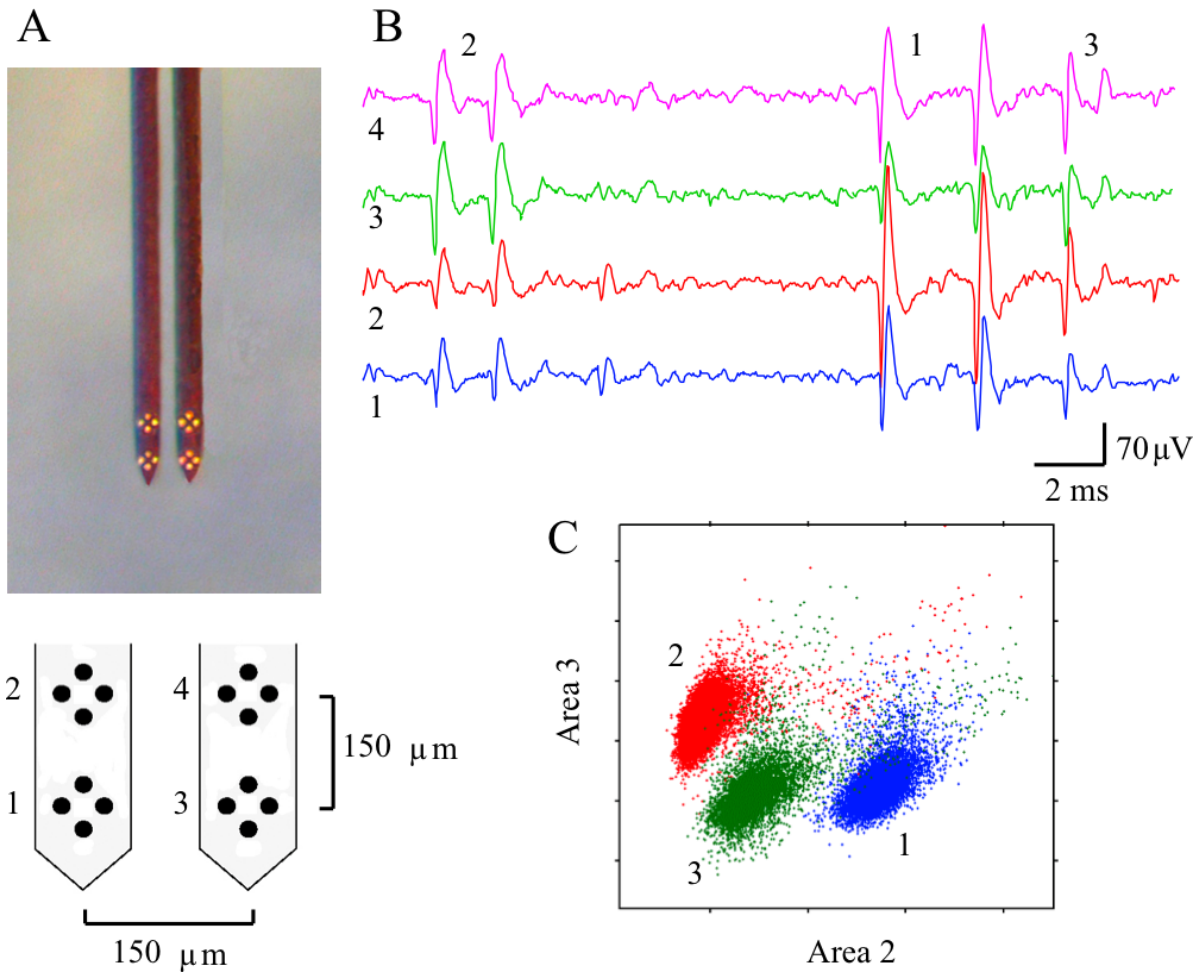

Figure 2.2.1 Tetrode recording of neuronal activity in cat striate cortex. (A) Photograph and schematic of a 4-tetrode silicon probe in the 2x2 configuration. The inter-shank and inter-tetrode separations are both 150 µm. Adjacent contacts within a tetrode are separated by 25 µm. (B) Short segment of raw data showing the spikes of three different neurons (1-3) recorded from the four channels of tetrode #4 of the probe. The signals are plotted in four different colors (blue, red, green, magenta). (C) Scatter plot of waveform area for all spikes of cells 1 (blue), 2 (red) and 3 (green) recorded on channels 2 and 3 of tetrode #4.

Spike waveforms were extracted by storing 32 data points (11 points prior to and including the minimum, and 21 points following the minimum), on each channel. An additional constraint was included to prevent local minima from being within 3 data

points of each other in order to eliminate repeated extractions of the same waveform that might result from the occurrence of high frequency noise. Automated clustering of waveforms was performed using the KlustaKwik software package (Harris et al. 2000) and inspected using the MClust software package (http://www.cbc.umn.edu/~redish/mclust/). Clustering was based on the following parameters extracted from each waveform: area, energy, maximum voltage, minimum voltage, maximum to minimum ratio, waveform width, trigger value, Fast Fourier Transform (FFT) of the waveform, and the 1st and 2nd principal components of the waveform.

Following the initial cluster analysis, several procedures were performed to edit the data and to eliminate artifacts. First, each cluster was carefully inspected and any waveforms clearly deviating from the average pattern were either deleted or moved to another cluster. The latter were treated as unclassified waveforms and subjected to later analysis. Second, artifact clusters were deleted. These typically resulted from double triggering of triphasic waveforms, or were due to waveforms that just exceeded the spike-extraction threshold. Third, clusters having similar waveforms were merged, but only when the inter-spike interval histogram (ISIH) of the resulting cluster had a clear refractory period. Finally, each candidate cluster had to be non-overlapping with all other clusters in at least one classification dimension.

Once these steps were completed, the data from a single tetrode consisted of one or more well-resolved clusters, each corresponding to a distinct single unit, and a non-classified cluster composed of waveforms resulting from superimposed spikes (Goodell

and Gray 2003). In order to identify the single units that contributed to these waveforms, a template-matching algorithm was applied in order to determine which individual or pair of template waveforms obtained from the initial analysis could best account for each unclassified waveform. The mean waveform of each distinct cluster was used as a template. All possible linear superpositions of templates at all possible phase shifts were computed. This yields n(n-1)/2 template pairs, where each pair consists of 125 composite waveforms (±31 phases*2) –1). Each unclassified waveform was then compared to each of the superimposed templates by computing the sum of the squared differences between each pair of waveforms. The template pair that gave the smallest value was chosen as the best match, and the time difference between the two templates used to compute the best match was stored. If this value was less than or equal to the refractory period used for waveform extraction (±3 data points) then a copy of the unclassified waveform was assigned to the clusters for both templates. If the phase difference was greater than the refractory period then the waveform was copied to the cluster whose template had a peak negative value that aligned with that of the triggered waveform. A final editing procedure was performed on each cluster to remove any superimposed waveforms that occurred during the refractory period of the inter-spike interval distribution.

2.2.4 Visual Stimulation

Monochromatic natural movie sequences were presented monocularly, at a distance of 57 cm, using a 20-inch color monitor (Viewsonic P810) at a resolution of 800 x 600 pixels. The luminance distribution of the monitor (0-80 cd/m^2) was gamma-corrected prior to the experiments. During the course of this study, three different

graphics cards were used, with increasing refresh rates of 85.12, 120 and 150 Hz. Movie frames were digitized from a variety of DVD movies covering a wide range of natural and man-made scenes. These included Hollywood movies like “The Big Lebowski”, “The Matrix”, “Everest”, as well as two documentaries called “The Ultimate Guide - Big Cats and House Cats”, and “Animals in the Wild”. The movie files were de-interlaced, and cropped to remove any visible borders. In some movies, the last few frames of one segment were faded into the first few frames of the next segment so the affected frames had to be removed manually. No attempts were made to remove the MPEG2 compression artifacts, as they were fairly minor in the video sequences used. The individual frames were then converted to grayscale and presented at rates of 3, 4 or 6 refreshes per frame (corresponding to the 85, 120 and 150 Hz graphics cards), making the frame rate of the movies 28.3 Hz, 30 Hz and 25 Hz, respectively. No temporal up sampling was attempted, i.e. the identical movie frame was presented for 3, 4, or 6 refreshes. Individual movie frames had dimensions of 640 x 480 pixels and were positioned at the center of the monitor screen, occupying 32º x 24º of visual angle (0.05º/pixel). For each recording site, a short movie sequence was selected, ranging in duration from 15-30 sec, and presented 60-200 times to the dominant eye.

When presenting movie sequences at a resolution of 640x480 pixels, there are occasional times when the computer could not keep pace with the requested frame rate. In these instances, short delays occur in the video presentation that result in particular frames of the movie being displayed for more than the specified number of video refreshes. These “extra syncs” were identified by first converting the vertical sync signal

from the video card into a 1 ms TTL pulse. The pulses were sampled using a counter/timer card (ACCES CTR-05 ISA) and counted the number of vertical syncs occurring between each frame of the movie. The numbers of syncs were checked at the end of each frame, and any additional sync frames were recorded by specifying the frame number in the movie and the number of extra syncs occurring during that frame. The ability of this setup to track extra syncs was verified by matching the records to the signals produced by a photo-diode placed directory on the monitor. Scene changes within the movie were also a concern, because they might cause significant responses due to sudden changes in luminance or contrast in the image. In order to identify scene changes, the difference in gray level of every pixel between consecutive movie frames was computed, and the scene transitions were defined as frames where 60% of the pixels changed by at least 10 gray levels. These were confirmed by visual inspection of the movie frames. It was found that between 2 and 8 scene changes per movie segment were present, with an average of 5.3 scene changes per movie. A simple event-triggered analysis to see how often events (see section 2.2.10) were preceded by a scene change. Only 3.9% (59/1498) of the events occurred within two movie frames of a scene change (a duration of approximately 70 to 80 ms). This led to the conclusion that the effect of scene changes in the dataset was minimal.

2.2.5 Data Analysis

The principal goal of the analysis in this chapter is to characterize the response properties of striate cortical neurons to the presentation of time-varying natural scenes, and to determine how similar or different those properties are among neurons recorded

simultaneously on either the same or different tetrodes. Based on previous studies (Lemon 1984; Gray et al. 1995; Blanche et al. 2005), it can be assumed that cells recorded on the same tetrode primarily lie adjacent to one another, with the probability of their spatial separation falling off exponentially with a space constant of ~30 μm (Gray et al. 1995). Thus, by analyzing the responses of cells recorded simultaneously on the same tetrode, it was possible to obtain a sensitive estimate of the heterogeneity of stimulus selectivity among adjacent groups of cells. Because two types of probe configurations (2x2 and 4x1) were used, it was possible to compare the estimates of heterogeneity among adjacent cells to those obtained from cells lying in vertically, or horizontally non-adjacent positions. However, because the sample size is small, and the number of possible spatial comparisons is large, all inter-group comparisons were grouped together.

2.2.6 Compensation for Extra Syncs

The first step in the analysis was to adjust the spike times for the sessions in which extra syncs were detected on specific frames of the movies. To do this, all spikes that occurred during the extra syncs were removed and subtracted the duration of the extra syncs (i.e. an integer multiple of the vertical refresh) from all subsequent spike times. The resulting inter-spike intervals were checked and removed the first adjusted spike if it occurred within 1 ms of the last unadjusted spike time. Across 20 separate movie presentations the median percentage of extra syncs was 0.007%. Thus, given their rare occurrence, and the analytical compensation for their effects, the influence of extra syncs on the properties of the neuronal responses is likely to be negligible.

2.2.7 Response Reliability

It is well known from physiological experiments in anesthetized animals that there are some neurons in striate cortex that either fail to reliably respond to any stimuli, or that change their responsiveness as a function of the state of the animal, most likely due to the fluctuating levels of anesthesia. Because these effects could have a large impact on the results, a measure of response reliability was developed and evaluated the findings with respect to this measure. Since responses to repeated identical stimulus presentations are likely to be correlated, a simple measure of spike count correlations across trials was devised. On each stimulus repetition, the total number of spikes occurring in each frame of the movie were calculated and the correlation coefficient of those counts, across all frames of the movie and for all possible pair-wise repetitions (n(n-1)/2) was computed. The percentage of correlation values that were statistically significant ($p<0.05$) was then tabulated so that a single value of response reliability could be compared across individual cells and experiments.

2.2.8 Sparsity

To quantify the sparseness of the responses, the non-parametric statistic employed previously by Vinje and Gallant (2000) was used for each cell in the database:

$$S = \{1 - [(\sum_i \frac{r_i}{n})^2 / (\sum_i \frac{r_i^2}{n})]\} / [1 - 1/n]$$

where r_i is the mean number of spikes observed in a neuron during the presentation of frame i of the movie, and n is the number of movie frames. S is 0% if a cell responds with the same number of spikes for every frame, and is 100% if it responds only to one frame.

This measure is often referred to as "lifetime sparseness" to differentiate it from "population sparseness" which is described below (Willmore and Tolhurst 2001). The sparseness was also computed using windows of 10, 50 and 100 ms and although *S* generally decreased with increasing window sizes, the only significant difference in the four distributions was between those computed using 10 and 100 ms ($p=0.04$ using the Kruskal-Wallis non-parametric one-way analysis of variance (ANOVA) for all four distributions, but was $p=0.12$, if the distribution computed using 100 ms was excluded, and $p=0.34$ if the 10 ms distribution was excluded).

The same calculation was used to quantify the population sparseness (PS) for individual frames of the movie. In this case, r_i is the mean number of spikes observed in neuron *i* during the presentation of a movie frame, and *n* is the number of simultaneously recorded neurons. *S* is 0% if all simultaneously recorded cells responded vigorously, and is 100% if only one neuron responded during the presentation of a particular frame. In addition, the concept of dispersal was also investigated (i.e. whether neighboring cells contributed equally to coding a large ensemble of stimuli) for each recording site with more than one cell by creating scree plots (Willmore et al., 2000). This was done by first computing, for each cell, the variance in the mean number of spikes across all movie frames. The variance of all cells at a site were normalized by the highest variance and rank ordered starting with the cell with the highest variance to create the scree plot (see Figure 2.3.5).

2.2.9 Firing Rate Calculations

To assess the distribution of firing rates in response to natural scenes, the peri-stimulus time histogram (PSTH) for each cell was computed using bins equal to the frame duration of the movie, ranging from 33 to 40ms. In one set of measurements, the mean and the peak firing rates were computed for each cell across all bins in the PSTH to inspect the heterogeneity of mean and peak rates for neighboring cells. The instantaneous differences were also compared in firing rates between cell pairs to identify epochs where the cells were responding very differently to the same stimuli (*see Figure 2.3.8 for an example pair*). These differences were compared using the average and the peak values across all bins of the PSTH.

2.2.10 Comparison of the Time-Course of Neuronal Responses

In order to assess variations in the response properties of cells to the movies, the Pearson's correlation coefficient was calculated between the PSTH's of all simultaneously recorded pairs of cells. This measure quantifies the similarity of the time course of the responses (i.e. signal correlation) between each pair of cells, independent of the absolute firing rates (Reich et al. 2001), by normalizing each cell's firing rate. The correlation coefficient was computed using windows of 10, 50 and 100 ms and although the correlation coefficient generally increased with increasing window sizes, the four distributions were not significantly different (Kruskal-Wallis non-parametric one-way ANOVA $p=0.17$ for intra-group pairs and $p=0.09$ for inter-group pairs).

2.2.11 Detection of Response Events

As in previous studies utilizing time-varying stimuli (Bryant and Segundo 1976; Mainen and Sejnowski 1995; Bair and Koch 1996; Berry et al. 1997), individual striate cell responses to time-varying natural scenes were often composed of brief epochs lasting a few 10s to 100s of milliseconds. These epochs of enhances activity were of particular interest, therefore by identifying them at high temporal resolution and characterizing their properties, such as duration, probability and co-occurrence among groups of cells was done by thresholding the PSTH. Significant response events were identified in the PSTH (10 ms bins, shifted in 1 ms steps) by detecting the times when the firing rate exceeded the 75th percentile of the non-zero firing rate distribution. The bins with a zero firing rate were excluded as they constituted a large fraction of the bins (due to the sparseness of the responses) and led to unsuitably low thresholds. An additional criterion was added so that each event was required a minimum of 1 spike on a $1/3^{rd}$ of the stimulus repetitions. This had the effect of eliminating events with highly unreliable responses, while including very brief low firing rate events that were reliable across movie presentations. Once the events had been detected, the durations and probability of occurrence (i.e. sum of all event durations divided by the total stimulus duration) were computed for each cell. For cells recorded at the same time, periods in which events among any pair of cells overlapped in time were determined and these are referred to these as joint-events. The duration and probability of joint events were used the below measure to define a similarity index (SI) for each pair of cells, thereby expressing how often joint events occurred:

$SI_{ij} = [obs_{ij}(p) - exp_{ij}(p)]/[min_{ij}(p) - exp_{ij}(p)]$ if $obs_{ij}(p) - exp_{ij}(p) >= 0$

$SI_{ij} = [obs_{ij}(p) - exp_{ij}(p)]/exp_{ij}(p)$ if $obs_{ij}(p) - exp_{ij}(p) < 0$

where $obs_{ij}(p)$ is the observed joint probability, $exp_{ij}(p)$ is the expected probability (i.e. the product of the two individual event probabilities), and $min_{ij}(p)$ is the minimum of the two individual event probabilities for the i^{th} and j^{th} cells. Positive and negative values of SI indicate joint events that occur more or less often than chance (SI=0), respectively.

2.3 Results

2.3.1 Summary of Data Collected

A total of 88 well-isolated cells were recorded in 8 experiments. Four of the cells were recorded using sharp Tungsten electrodes, while the remaining cells were recorded using silicon multi-tetrode probes provided by the CNCT at the University of Michigan. Once the probes were placed, and a stable recording was obtained, data was acquired during the presentation of time-varying natural scenes (movies) in addition to a battery of simple test stimuli. The natural scene stimulus sets ranged in duration from 10-90 minutes. Data were collected only as long as the unit isolation remained stable and individual cells could be tracked across sessions.

Table 2.3.1 provides a summary of the number of cells recorded at each site. The term “site” refers to recording sessions in which the probe remained at a fixed location in the cortical tissue and stable waveforms could be identified from one or more cells. As shown in Table 2.3.1, it was rare to sample well isolated single units from all four tetrodes of the silicon probe simultaneously. This is primarily due to the rigid

arrangement of tetrodes within a given silicon probe. Across these sites, well-isolated single units were recorded on 2 of the tetrodes and the average number of cells isolated per tetrode was close to 3. This value is somewhat lower than previous studies in which custom made tetrodes were used (Gray et al. 1995; Maldonado and Gray 1996; Maldonado et al. 1997). The difference in yield may be due to the recording properties of the silicon probes. However, in earlier experiments, activity was sampled from only one tetrode at a time, thereby enabled small adjustments in the position of the probe to maximize the recording quality.

Table 2.3.1 Number of cells isolated at each recording site for experiments using either electrodes or tetrodes.

Site	# of Electrodes	# of Cells
1	1	1
2	1	1
3	1	1
4	1	1
Site	# of Tetrodes	# of Cells
1	1	4
2	2	5
3	1	2
4	2	3
5	1	1
6	2	12
7	4	15
8	3	6
9	1	3
10	1	1
11	3	9
12	3	6
13	3	7
14	1	1
15	2	6
16	1	3

Similar adjustments were made with the silicon probes to maximize the yield, but the rigid linkage between the tetrodes meant that attempts to improve the yield on one tetrode often led to decreased yield on one or more of the other tetrodes. A primary goal of this chapter was to assess the differences in response properties among adjacent neurons. It thus became important to evaluate the spatial extent over which the action potentials of individual neurons could be recorded. This was easily accomplished by tracking each instance in which a cell recorded on one tetrode was also recorded by one or more of the other tetrodes surrounding it. (Note that the spike waveforms of a cell recorded on one tetrode usually appear on more than 1 of the 4 channels within the tetrode, almost always on all four contacts, see Figure 2.2.1) Interestingly, only one instance where the same cells were sampled by two separate tetrodes was found. In this case, two cells recorded on one tetrode of a 4x1 probe were also clearly visible in the recording from an adjacent shank of the same probe. Somewhat surprisingly, no instance was found where the same cell was recorded on different tetrodes of the same shank of the probe. It is concluded from this that extracellular spikes recorded from these probes are highly localized, and that activity from different cells on the same tetrode most likely comes from adjacent cells.

2.3.2 Response Reliability

During the course of this study, it became apparent that cells recorded on the same tetrode often responded in markedly different ways to the same movie. Some cells responded vigorously on every stimulus repetition, while others exhibited a much more variable response. Figure 2.3.1 shows two examples of the neuronal activity recorded

from a tetrode in two different experiments in response to 100 repetitions of a 30 sec movie. In each set of plots (A, B), the activities of 3 well-isolated cells are shown. The upper plots show the peri-stimulus-time histogram (PSTH) of each cell, and the lower plots show the corresponding spike rasters for the same 3 cells. In A the overall level of activity, as well as the strength and precision of the responses to specific frames of the movie, varied from cell to cell. Cell 1 fired a total of 26596 spikes during the 50 minutes of recording time, while cells 2 and 3 fired 2059 and 2508 spikes, respectively. A fourth cell (not shown) fired a total of 47 spikes during the same period. The character of the responses to the stimulus was also different. Cell 1 displayed both short and prolonged episodes of evoked activity, while the activity of cell 2 was much more sparse and its responses to the stimulus were very brief. The third cell showed only the slightest hint of responding to the movie, and the fourth cell was essentially inactive. In B the responses to the movie were more uniform. Each cell responded briefly and vigorously to specific frames of the movie, and the responses varied in magnitude and time of occurrence.

As shown in figure 2.3.1, cells that were visually responsive displayed a consistent pattern of discharge across repetitions of the movie. A simple measure was devised to evaluate the similarity of the spike trains across stimulus repetitions. The spike train on each stimulus repetition was converted to a vector of spike counts by calculating the number of spikes in each frame of the movie. Then the correlation coefficient was calculated between all pairs of spike count vectors. This yielded (n(n-1)/2) correlation coefficients, where n is the number of movie repetitions. The percentage of significant

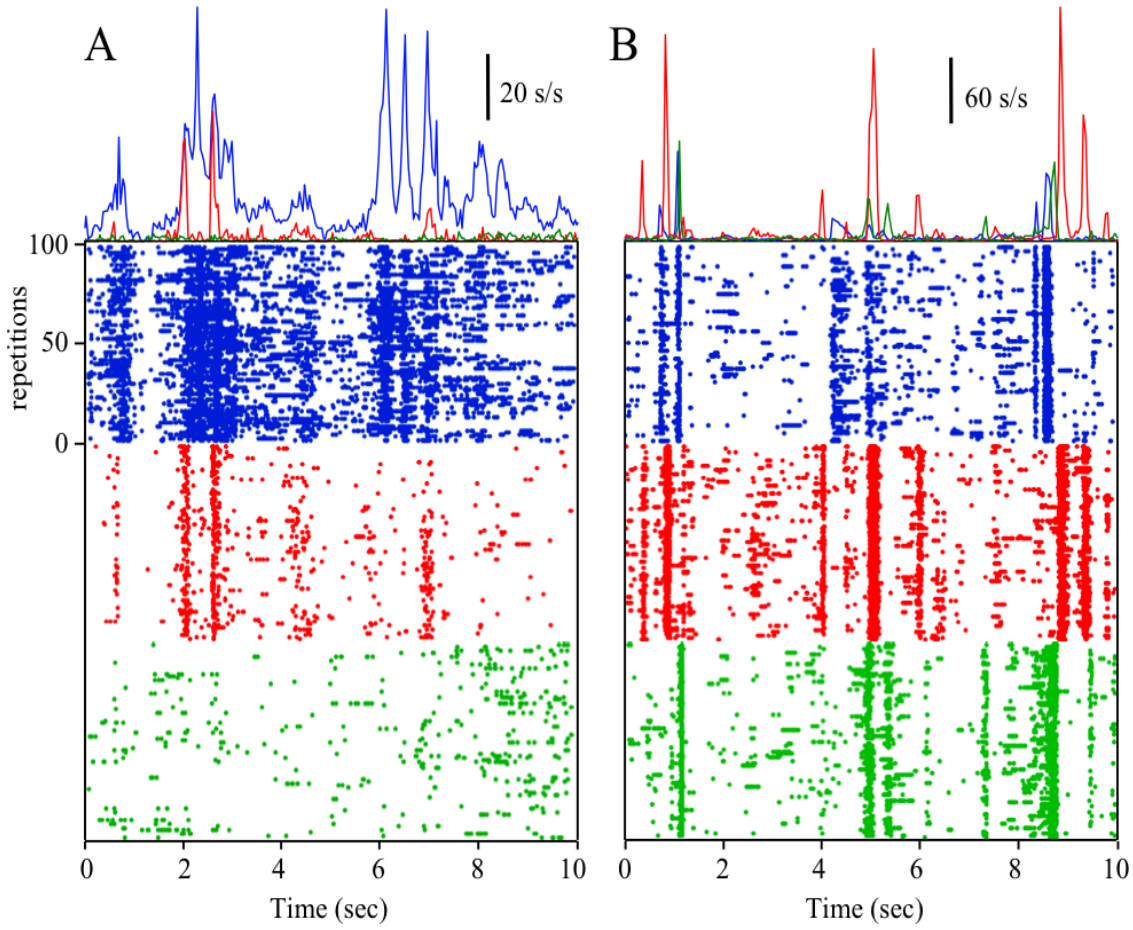

Figure 2.3.1 PSTH and raster plots of the spike times recorded from a single tetrode in two different experiments (A, B) to 100 repetitions of a 30 sec movie (10 sec of data are shown). In both sets of recordings, the activity of three single units is displayed. As in figure 2.2.1, the activities of cells 1, 2 and 3 are shown in blue, red and green, respectively. Responses to specific frames of the movie are apparent from the alignment of spikes across repetitions and the well-defined changes in average firing rate in the PSTHs. These data illustrate that cells recorded on the same tetrode often exhibit clear differences in firing rate, response reliability and time course.

correlation coefficients were used ($p<0.05$) as a measure of response reliability for each cell. The result of this analysis, shown in figure 2.3.2, revealed a broad distribution of values that was skewed to the upper end of the scale. For comparison, the second cell in figure 2.3.1A (red) displayed relatively clear responses in the PSTH, but response variation across trials, evident in the rasters, led to a relatively low peak firing rate (~35

spikes/sec) and a low response reliability value (41.7%). In contrast, the second cell in figure 2.3.1B showed significantly correlated responses on 100% of the comparisons and its peak-firing rate was greater than 300 spikes/sec. The distribution of correlation coefficients obtained for each cell was compared to a distribution of correlation coefficients obtained from 1000 sets of surrogate spike trains in which the spike counts from the data were randomly shuffled between repetitions and frames. The distribution from each of the 88 cells was found to be significantly different from the surrogates (KS-test, $p<0.001$), suggesting that in spite of the wide range of response variability observed, all 88 cells exhibited responses that were significantly different from random spike trains.

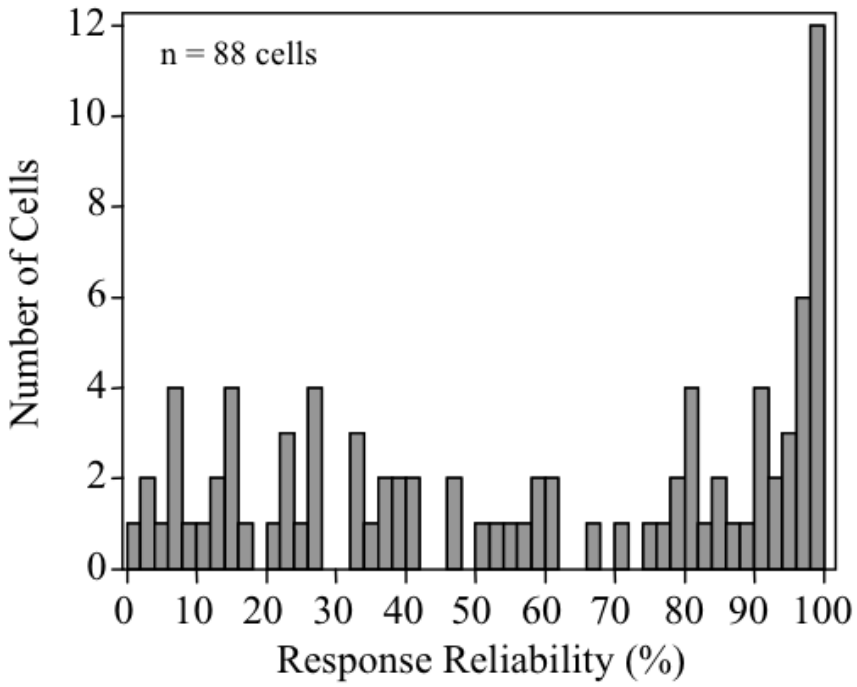

Figure 2.3.2 Histogram of response reliability values calculated for all 88 cells.

There are several possible explanations for the wide variations of response reliability in the sample of cells collected. One possibility is that variations in the level of anesthesia and/or changes in the sleep cycle might have led to a global and thereby local change in excitability of the cells within the larger network (Haider and McCormick, 2009). In this case, it would be expected to find a uniform decrease of response reliability for all the cells at a given recording site. Another possibility is that some cells might have responded unreliably or not at all because the chosen movie clip did not contain features appropriate to the receptive field properties of the cells. In this case, a mixture of reliable and unreliable yet responsive cells would be expected on the same tetrode. A third possibility is that some cells in visual cortex are simply not responsive to visual stimuli. In this case, the background activity of the cell would yield a measure of low response reliability. This alternative is difficult to test, because any chosen stimulus set might not contain the relevant features necessary to activate all the cells. However the current dataset does enabled one to distinguish between the first two possible explanations. Figure 2.3.3 shows a bar chart of cell response reliability for those tetrodes in which more than one neuron was recorded (n=21). On some recordings (e.g. tetrodes 6, 11, 18 and 20) all the cells have low response reliability values, suggestive of a general decrease of excitability. On other recordings (e.g. tetrodes 2-5, 10, 14-16) all of the cells display high levels of response reliability. More interestingly, however, there are a number of recordings (e.g. tetrodes 1, 7-9, 12, 13, 17, 19, 21) in which the response reliability of adjacent cells shows wide variations. These latter findings suggest that at some sites in cortex adjacent cells may have widely differing receptive field properties, or that

regulation of cortical excitability might be cell specific. In either case, it demonstrates that the response reliability of adjacent cortical cells to time-varying natural scenes can be highly heterogeneous.

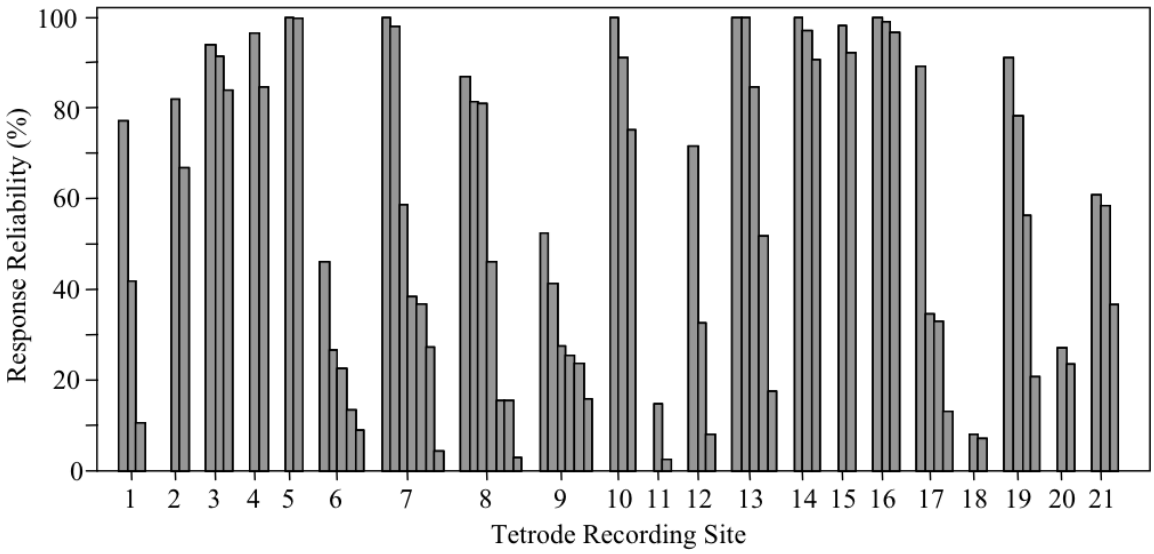

Figure 2.3.3 Bar chart of response reliability values for all tetrode recordings in which more than one cell was recorded on the same tetrode (N=21).

2.3.3 Response Sparsity

A number of theoretical and computational studies have suggested that the efficient coding of natural scenes is best accomplished using a sparse representation (Field 1987; Olshausen and Field 1996b, 2004; Levy and Baxter 1996; Laughlin et al. 1998; Simoncelli 2003). This hypothesis predicts that at any given moment the natural visual environment is represented by only a small fraction of active neurons. In turn, this implies that individual cortical neurons will only rarely be active. This prediction is clearly supported by simple visual inspection of the spike rasters for nearly all responsive cells (see Figure 2.3.1 for multiple examples), making it useful to quantify the magnitude

of the effect across the population. To accomplish this, a measure of response sparsity (*S*) that provides a convenient scale from 0 to 1 measuring how selective the responses of a neuron are to a set of stimuli (Vinje and Gallant 2000) was applied. A value of 0 indicates that a neuron responds to all the frames of the movie with the same number of spikes. A value of 1 indicates that a neuron responds to only one of the frames of the movie. Figure 2.3.4A shows the distribution of *S* for all 88 cells. The mean and median values of this distribution are 71% and 81%, respectively, indicating that cellular responses are indeed sparse.

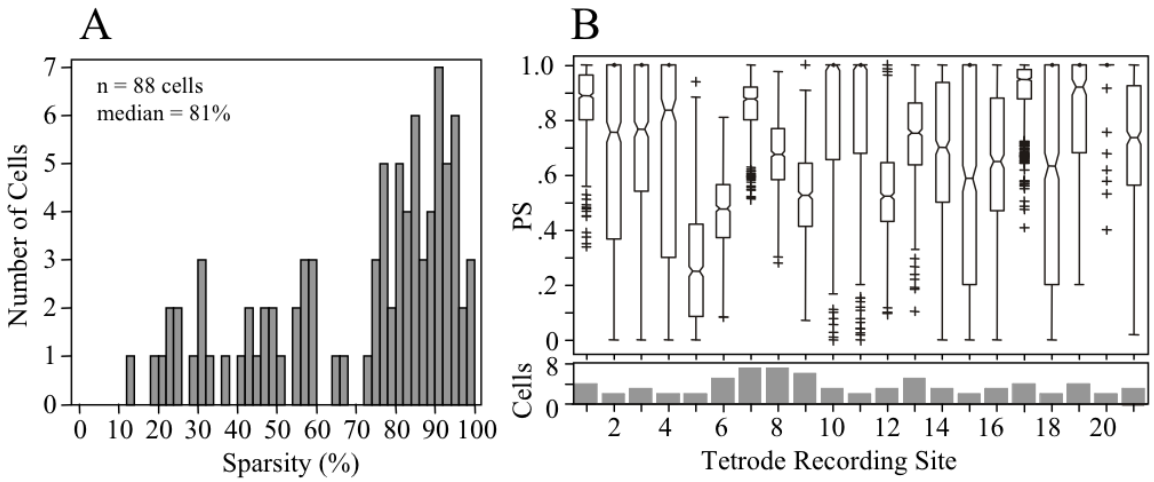

Figure 2.3.4 Lifetime and population sparseness. (A) Histogram of sparsity values for all cells in the database (n=88). The mean and median values of the distribution are 70.7% and 80.5%, respectively. (B) Box plots of population sparseness (PS) values at the 21 recording sites with more than one cell present. The distribution of PS values obtained for each movie frame is described by the medians (horizontal lines) and the quartiles (boxes). The notches denote the uncertainty in the estimation of the medians and the whiskers delineate 1.5 times the inter-quartile range. Individual crosses indicate the outliers. The bar graphs on the bottom indicate the number of cells recorded at each recording site.

The distribution of sparsity values are substantially higher than those reported for cells in the alert monkey (mean = 62%) when stimulated by natural movie sequences having a

diameter 4-fold larger than the classical receptive field (Vinje and Gallant 2000). This difference in sparsity may reflect a species difference, the possible effects of anesthesia, or the fact that the stimuli spanned a larger portion of the visual field (Haider et al., 2010). Bin sizes of 10, 50 and 100 ms were also used to compute *S*, and no significant effect was observed when changing bin size. Unlike with response reliability, there was relatively little heterogeneity in the sparsity measure among adjacent cells recorded at the same site (data not shown). High sparsity appeared to be a general property of the cells in the database. A more direct measure of the sparseness of the neural representation can be obtained using the population sparseness (PS) measure (this is distinct from the sparseness mentioned above, which is usually termed lifetime sparseness). Indeed recent theoretical work has shown that certain codes (e.g. rate codes using cells with Gabor-like receptive fields) may exhibit high lifetime sparseness while simultaneously displaying low population sparseness (Willmore and Tolhurst 2001). In other words, although individual neurons may be rarely active, when they do respond, they respond simultaneously with other neurons. A direct estimate of PS using a metric very similar to the one used to measure lifetime sparseness above was employed (see Methods). The scale also goes from 0 to 1, with a value of 1 indicating that only one neuron responded during the presentation of one movie frame, and a value of 0 indicating that all recorded neurons responded vigorously to the movie frame (frames in which none of the neurons responded were excluded from the analysis). The box plots in figure 2.3.4B show the distribution of PS values for individual movie frames at 21 recording sites with at least two recorded neurons. The PS values covered a wide range, demonstrating that different

movie frames elicited diverse patterns of responses among neighboring neurons. The median PS values at most sites were quite high (except for site 5), with many sites displaying distributions that were highly skewed towards 1 (the extreme being site 20, where the median, upper and lower quartile were all at a PS value of 1). The mean PS value across all 21 sites was 0.67, with a standard deviation of 0.29, which was higher than the values reported in an earlier study of multi-unit activity in ferret visual cortex (Weliky et al. 2003).

In order to look at the relationship between lifetime sparseness and population sparseness the lifetime sparseness values were averaged across all the cells at a site. Since the lifetime sparseness values were fairly uniform at each site, this measure was representative of the lifetime sparseness at each site. Those values are plotted against the median population sparseness in figure 2.3.5A. The data shows a strong correlation between the mean lifetime sparseness and the median population sparseness ($r=0.68$, $p<0.01$). In comparison to an earlier study (Weliky et al. 2003), both the mean lifetime sparseness and median population sparseness values in this dataset were much higher (with the exception of site 5, which had low values for both measures).

It has been suggested that a dispersed code, when evaluated over a large range of stimuli, is one in which all cells contribute equally to coding the stimuli (Willmore et al., 2000). In order to quantify the individual cellular contributions, individual responses were compared to the groups' representation of the visual stimuli. This is usually illustrated in plots called scree plots, in which the variances of all the cells at each site are computed and rank ordered. A flat plot means that the cells contributed equally to coding

the stimulus, while deviations from a flat plot indicate certain cells are more likely to respond than others. In figure 2.3.5B, the variances are normalized by the highest variance at each site, and these are ordered for increasing cell numbers at each site. This allows for the comparison of the values for sites with different numbers of cells. This means for a site with two cells, the data point corresponding to the cell with the higher variance will be plotted at a normalized cell number of 0, while the second cell will be plotted at 1. For a site with four cells, the data points will be at 0, 0.33, 0.66 and 1. The data in figure 2.3.5B has also been grouped according to how many cells were at a site. The six subplots correspond to sites with two (n=7), three (n=6), four (n=3), five (n=2), six (n=1) and seven (n=2) simultaneously recorded neurons. Overall, the plots suggest that the dispersal in the data was fairly low, with one or two cells exhibiting much higher variance than the others.

The area under the scree plot is often used as a measure of dispersal, the mean area and standard deviation was 0.49±0.20. Interestingly, this value is fairly close to the value of 0.56 computed in a theoretical study using sparse coding filters (Willmore et al., 2000). There was an attempt to control for differences in variances due to differences in the firing rate distributions (see Figure 2.3.10) by normalizing each firing rate distribution by its mean before computing its variance. This appeared to increase the dispersal, with the mean area and standard deviation of the scree plots increasing to 0.62±0.23.

These results demonstrate that the neural representation in primary visual cortex exhibits both high lifetime and population sparseness. The contribution of neighboring

cells in coding visual stimuli also appears to be as uniform, if not more so, than predictions from a theoretical model of sparse coding.

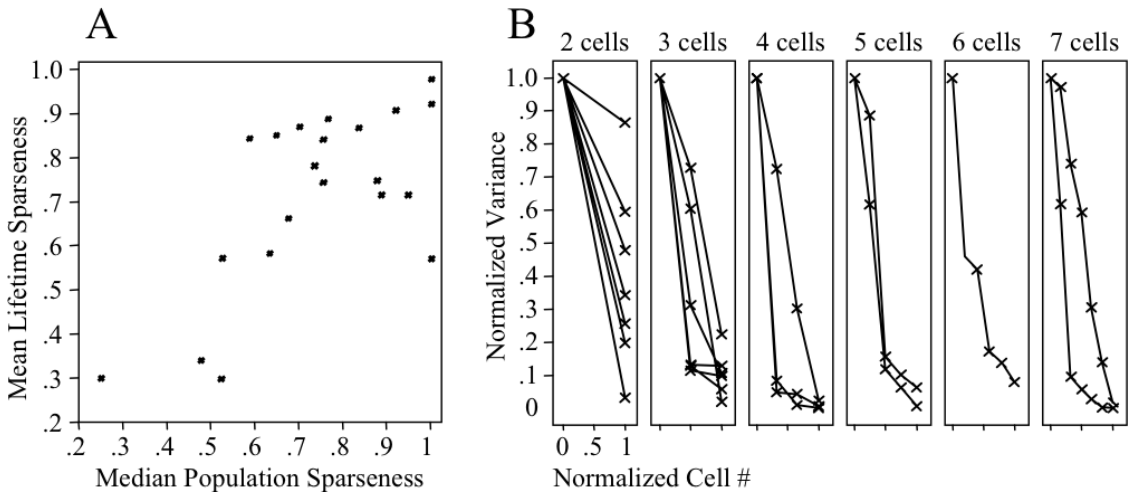

Figure 2.3.5 Population Sparseness. (A) Plot of mean lifetime sparseness versus median population sparseness. (B) Plot of normalized variance versus normalized cell number.

2.3.4 Response Heterogeneity

As is evident from the population sparseness analysis, neurons recorded on the same tetrode often showed striking differences in the time course and magnitude of their responses to the same movie (also reported in Reich et al. 2001 with m-sequence stimuli). An example of these effects is also illustrated in figure 2.3.1B, which reveals three interesting results. First, the responses of each of the cells were vigorous, highly reliable and sparse. The response reliability values were 97%, 100% and 99% for the blue, red and green plots, respectively. The sparsity values for the same 3 cells were 81%, 90% and 85%, respectively. Second, the time course of the responses were very different, even though the cells were presumably adjacent to one another in the cortex. To quantify this

relationship, the signal correlation was computed between the PSTHs (Reich et al. 2001). This measure revealed that the responses of all 3 cells were quite different from one another. The signal correlations between cells 1-2 and 2-3 were zero, indicating that their responses to the movie were independent of one another. Cells 1-3 showed a weak correlation of 0.23 ($p<0.001$). Third, the firing rates of the cells showed marked variations across the movie, and it was rare for any pair of cells to respond at a high rate at the same time. This effect was quantified by calculating the peak difference in the instantaneous firing rates between each pair of cells across all frames of the movie. These numbers (215, 215, and 87 spikes/sec for cell pairs 1-2, 2-3, and 1-3, respectively) revealed that the peak firing rate in all 3 cells occurred when the other cells were firing at near-zero rates.

In order to quantify variations in the time course of responses across the population, the signal correlation was computed for each pair of simultaneously recorded cells. The results were grouped according to whether the cells were recorded on the same tetrode (intra-group) or on different tetrodes (inter-group). This produced 120 intra-group and 170 inter-group pairs of cells recorded from 21 separate tetrode sites.

Figure 2.3.6 shows the results of the signal correlation measure as applied to all pairs of cells recorded on the same (intra-group) (A) and different (inter-group) (B) tetrodes. The distribution of intra-group signal correlation values is plotted in a box plot in A to facilitate comparison with the results from Reich et al. (Reich et al., 2001). In general, the signal correlations spanned a broad range of values in both groups. The mean values were relatively low (intra-group = 0.21 ± 0.23, inter-group = 0.18 ± 0.20 (both

distributions were significantly different from a normal distribution with a mean of 0, t-test $p<0.001$), however, and there was a tendency, as might be expected, for the signal correlations to be stronger among cells recorded on the same tetrode.

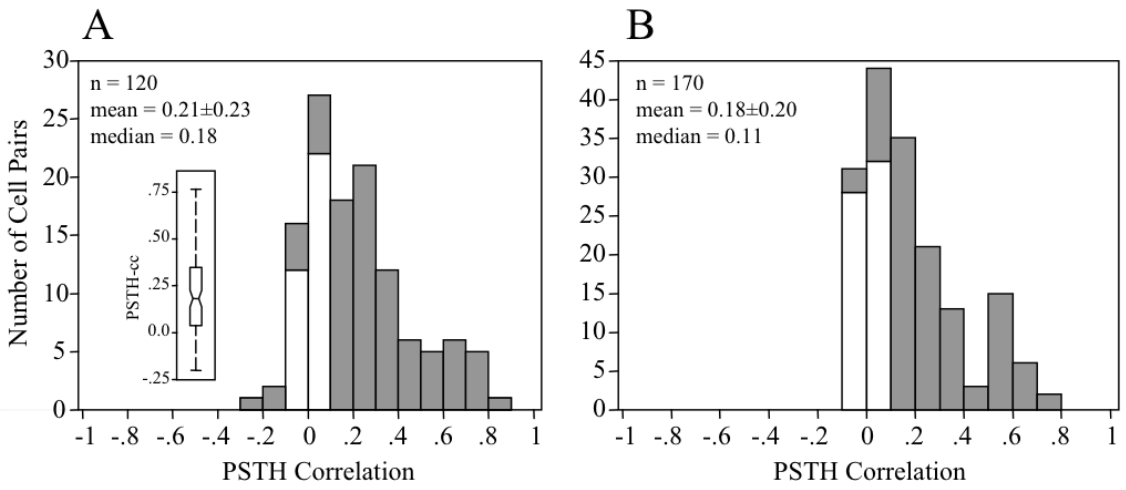

Figure 2.3.6 Histograms of the signal correlations between pairs of cells recorded on the same (A) and different (B) tetrodes. Correlation coefficients that were not significant (i.e. $p>0.05$) are shown in white. The medians and quartiles of the distribution of intra-group signal correlations are shown in a box plot in the inset of A.

However, when the two distributions were compared using a 2-sample KS test, difference was not significant ($p=0.132$). A paired t-test in which the correlation between two neurons recorded on the same tetrode was tested against the correlation between one of the neurons and a third neuron from a different tetrode was also not significant ($p=0.89$, $n=103$ pairs). An similar result was found when using a separation angle measure (Vinje and Gallant, 2000), with mean separation angles of 64±14 for intra-group and 65±13 degrees for inter-group pairs (both distributions were significantly different from a normal distribution with a mean of 0, t-test $p<0.001$, but the distributions were not

significantly different from each other, 2-sample KS test p=0.59). These data indicate, somewhat counter-intuitively, that heterogeneity in the time course of responses is as high among adjacent neurons as it is between those located approximately 150 um apart.

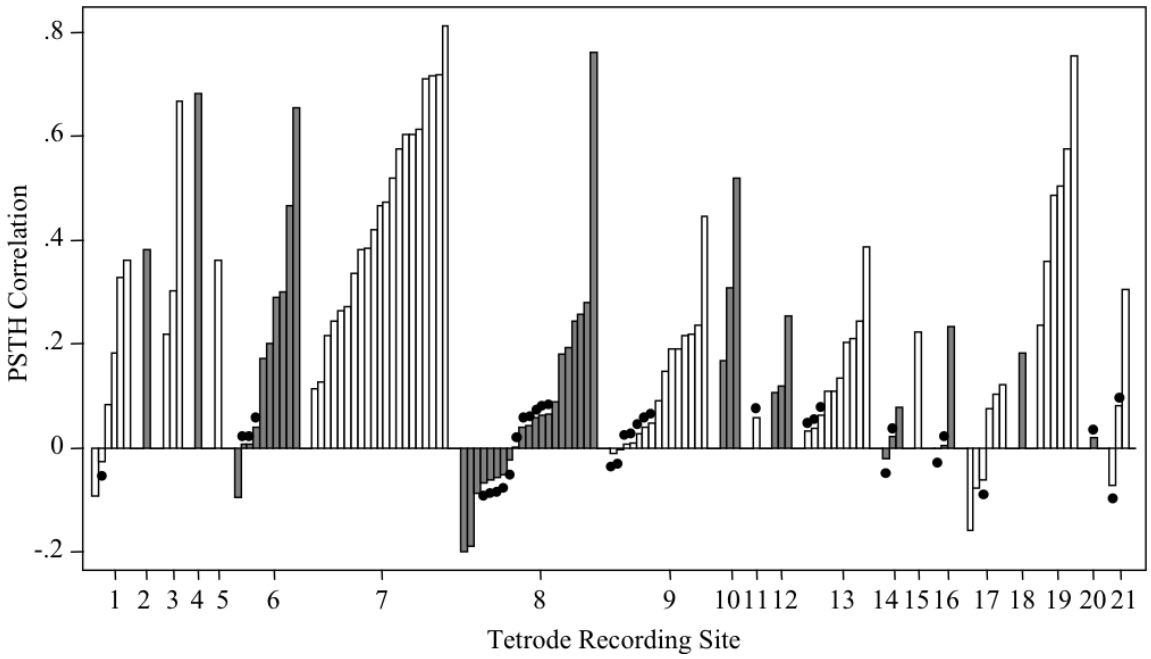

Figure 2.3.7 Bar charts of the signal correlations for all cell pairs recorded at each tetrode site. The cell pairs that exhibited p values greater than 0.05 are marked with filled circles.

To establish a more detailed picture of the response heterogeneity among neighboring neurons, the intra-group PSTH-correlation values are plotted by tetrode recording site (Figure 2.3.7). Pairs that were made up of cells from the same recording site are grouped together (e.g. there were 3 cells at site 3, which yielded 3 pairs of cells). This yielded a total of 21 recording sites where a minimum of 2 cells were recorded at the same time. At some sites, containing only a single pair of cells, the signal correlations were high (e.g. site 4), while at other sites they were low (e.g. site 20). More

interestingly, the sites containing more than 2 cells showed a mixture of signal correlations, often spanning a broad range of values (e.g. sites 6-9). Cell pairs with non-significant correlation coefficients are marked with a filled circle.

It could be postulated that neighboring neurons are conveying the same signal, and that the low response correlations observed were simply due to variability in the neurons' responses. For example, the PSTHs from the two cells at site 4 can be combined to create a putative consensus signal, and then one can generate surrogate PSTHs with some variability added to each bin of the consensus signal. With zero variability, the correlation coefficients between the surrogate PSTHs will always be 1. However, as variability increases, the correlation coefficients start to decrease, until they reach a value that is equal to the experimental data (r=0.68). In the case of the two cells at site 4, this corresponded to variability in which the spike-count variance in each bin was 5 times the mean. Similar variability in spike counts has previously been reported in the cortical neurons of anesthetized animals (Schiller et al., 1976; Tolhurst et al., 1983; Vogels et al., 1989) so it is not entirely implausible that variability could be used to account for the correlation coefficients observed in the data. However there is one crucial prediction from this hypothesis: the correlation between repetitions within the same cell should be equivalent to the correlation between repetitions of different cells. This prediction was tested by computing the correlation coefficients for all unique pair-wise repetitions of the movie (i.e. for 100 repetitions, two sets of 99x100/2=4,950 within-cell correlation coefficients, plus 100x100=10,000 cross-cell correlation coefficients would be calculated). These correlations were computed on the spike counts calculated at the frame

level for each repetition. When the three distributions were compared, the cross-cell distribution was found to be significantly lower than at least one of the within-cell distributions for all 120 intra-group pairs (using the Kruskal-Wallis non-parametric one-way ANOVA, followed by a multiple comparison test of ranks at a significance level of p=0.05). Moreover, in 82% (98/120) of the intra-group pairs, the cross-cell distributions were lower than both within-cell distributions. This shows that the cells individually exhibit significantly higher response correlations between repetitions than when they are grouped together, leading to the conclusion that the response heterogeneity is unlikely to be due to response variability around a common signal. Another striking property of the heterogeneity of responses to natural scenes was apparent in the widespread differences in firing rates among simultaneously recorded cells. An example of this is shown in figure 2.3.8 for a pair of cells recorded on the same tetrode. Part A shows the two PSTHs superimposed for a short segment of the movie, while part B shows the absolute difference in firing rate for each bin of the PSTH. In this example, the cells had a signal correlation of 0.39, but displayed substantially different firing rates during a large number of the movie frames. Even when both cells responded to the same frames of the movie their firing rates tended to be quite different. The mean and the peak firing rate differences were 4.2 spikes/sec and 92.5 spikes/sec, respectively. This demonstrates that even when adjacent cells show high signal correlation in the time course of their responses, there can be marked differences in the magnitude of those responses. To quantify this behavior, the peak firing rate across all bins of the PSTH for each cell (Figure 2.3.9A) was computed. These values showed broad variation, ranging from 0.6 to

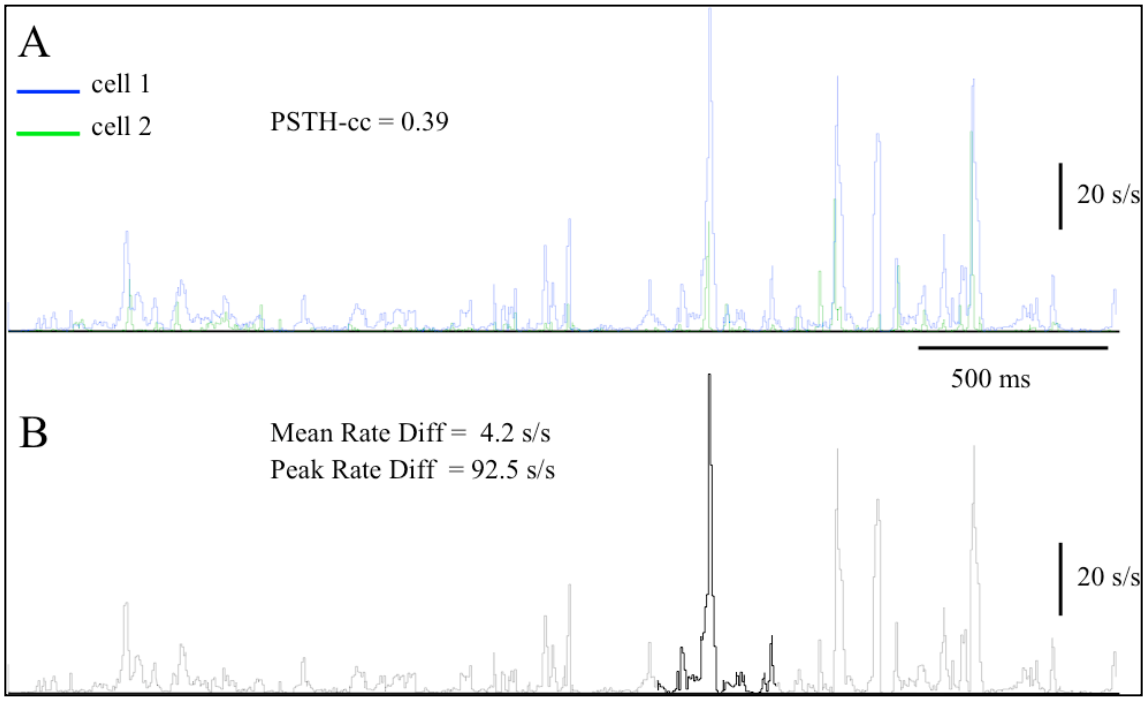

Figure 2.3.8 Neurons recorded on the same tetrode exhibit clear differences in firing rate as a function of time. The plots in panel A show a portion (~3 sec) of the PSTHs, measured in response to a movie, of two neurons (blue, green) recorded on the same tetrode. The signal correlation between the two cells was 0.39. The plot in B shows the bin-by-bin difference in average firing rate between the two cells. The mean difference in rate across the 30-sec movie was 4.2 spikes/sec. The peak difference in rate was 92.5 spikes/sec, indicating that one cell (blue) was firing maximally when the other cell (green) was firing near or below its mean rate.

215 spikes/sec with a median value of 39 spikes/sec. (The mean firing rates were low and tended to show small variations across cells (median=2.1 spikes/sec)). As with the signal correlations, a substantial degree of heterogeneity in peak firing rates was observed among cells recorded on the same tetrode (Figure 2.3.9B). In addition to these differences in peak rate, the relatively low signal correlations indicate that cells tended to respond at different times to the same movie. Moreover, when they did respond to the same frames of a movie, they were likely to fire at substantially different rates. These peak rate differences where calculated using the peak instantaneous difference in firing rate among

all pairs of simultaneously recorded cells. The distributions of rate differences were consistent with the notion that peak firing rates rarely occurred at the same time, or when they did, they often occurred at substantially different rates.

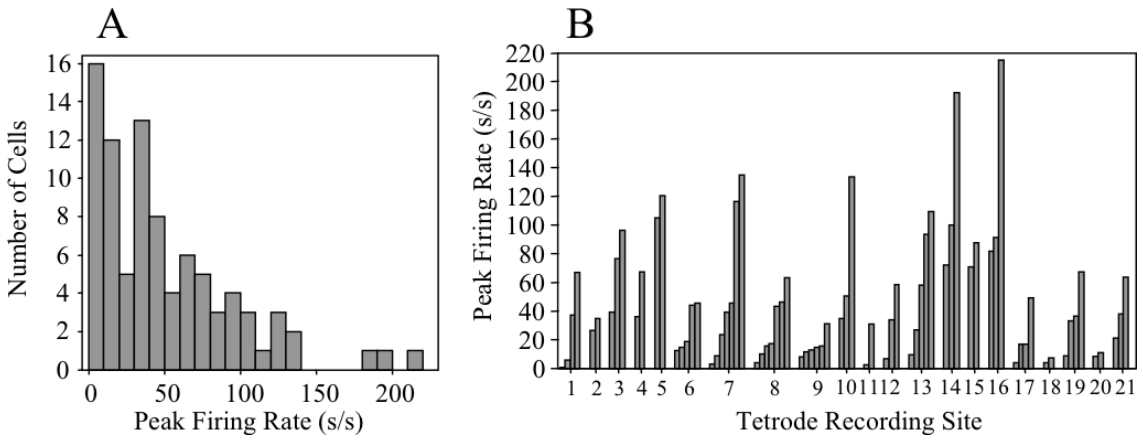

Figure 2.3.9 Distribution of peak firing rates in response to time-varying natural scenes. Panel A shows a histogram of the peak firing rates of all cells (n=88). Panel B shows a bar chart of the peak firing rates for all tetrodes (1-21) in which at least two cells were recorded simultaneously.

No significant difference was observed in the distribution of peak rate differences between intra-group (median difference = 42.7 spikes/sec) and inter-group (median difference = 42.4 spikes/sec) recordings (p=0.49, KS-test), indicating that, similar to the signal correlations, the response heterogeneity among adjacent neurons was equivalent to that between neurons located approximately 150 μm apart. Because the distribution of peak firing rates was broad, it was difficult to compare the rate differences across recordings. To compensate for this effect, each cell's firing rate distribution was normalized to its own peak value (all bins were divided by the maximum) and then the peak rate differences were recalculated. The results shown in figure 2.3.10 reveal that the peak rate differences were shifted towards the upper end of the distribution. The median

values for the intra-group and inter-group recordings were 92% and 91% of the maximum normalized rate, respectively, indicating that the peak rate differences tended to be very close to their maximum possible values. Again, no significant difference between the intra-group and inter-group recordings (p=0.41, KS-test) was found. These data demonstrate that at any point in time, adjacent cells often convey markedly different signals (in the form of different firing rates) in response to the same movie stimulus.

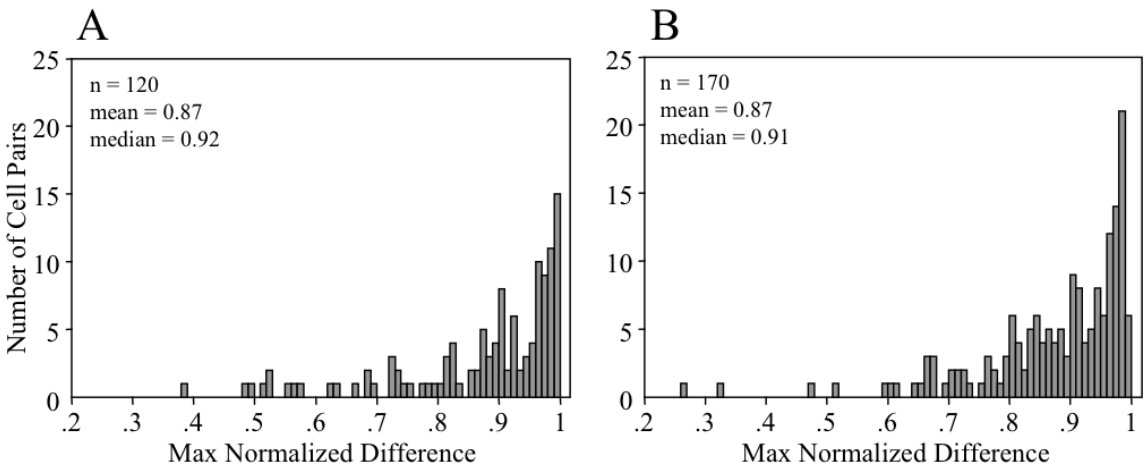

Figure 2.3.10 Histograms of the difference in peak firing rates after each cell was normalized to its respective maximum firing rate. Pairs of cells recorded on the same or different tetrodes are shown in A and B, respectively.

2.3.5 Response Events

As shown in figures 2.3.2 and 2.3.9, the responses of striate neurons to the movies most often consisted of brief periods of elevated activity that varied in duration and firing rate. In order to detect these events and characterize their properties it was necessary to condition the threshold for each cell individually. For this, the PSTH of each cell was computed using a sliding window of 10 ms advanced in 1 ms steps, and then response

events were defined as those periods in the PSTH when the firing rate exceeded the 75th percentile of the cell's non-zero firing rate distribution. An additional arbitrary criterion was included so that each event had to have at least 1 spike on 33% of the trials in the session. This nicely excluded unreliable events from the analysis and reduced the number of cells containing a least a single event to 77 out of 88 cells. Varying the threshold, from 75th, 85th, 95th and mean firing rate did result in a varying number of events, yet the distributions were qualitatively similar to the 75th percentile. Figure 2.3.11 shows examples of the events detected in three cells during a brief segment of the response to 100 repetitions of a movie. Response events are indicated by the colored horizontal bars above the individual PSTHs. For these three cells, the average event durations and probabilities measured for the entire 30 sec movie were 105, 105, 104 ms and 0.07, 0.087, 0.066, respectively, demonstrating that the cells rarely engaged in response events and when they did, those responses were quite brief. Note the lack of an event mark, between the first and third event mark, for the blue cell. This putative event did not reach criterion for response reliability. This analysis was applied to all cells and the median event duration was 53 ms while the median event probability was 0.045 (i.e. the proportion of time a cell was engaged in a response event). Thus, a defining characteristic of striate neuronal responses to the time-varying natural scenes used in the experiments, are brief periods of elevated firing which span a broad range of firing rates and occur with very low probability.

The same analysis was used to identify periods when response events in pairs of cells overlapped in time. To characterize these joint events across the population, the

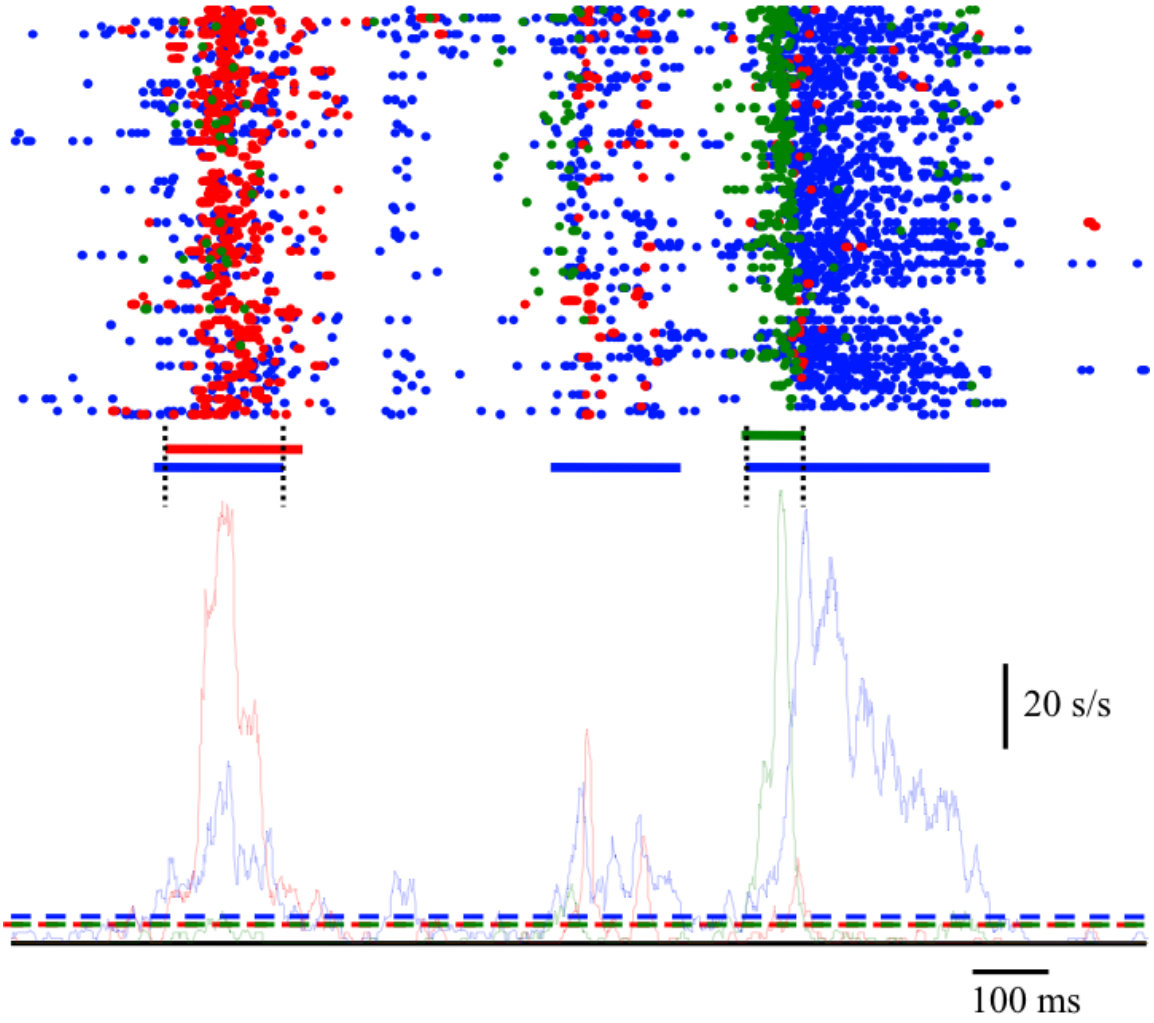

Figure 2.3.11 Detection of response events. A short epoch of data (1.5 sec) shows 100 superimposed spike rasters (top) and PSTHs (bottom) of 3 cells (blue, red, green) recorded from a single tetrode in response to a movie. The dashed horizontal lines indicate the thresholds for event detection (i.e. the 75th percentile of each cell's firing rate distribution). The colored horizontal lines above the PSTHs show the elapsed time of the events in each cell (blue, red, green). Some threshold crossings are not labeled as events, because they did not have a minimum of 1 spike on 33% of the trials. Joint events are marked by the vertical dashed lines. In this short epoch, there were joint events only between cells 1 (blue) and 2 (red) and cells 1 and 3 (green) but not between cells 2 and 3.

probability and duration distributions for all intra-group and inter-group cell pairs were computed (*see Figure 2.3.12*). The median probability of joint events for the intra-group

(0.0026) and inter-group (0.0035) pairs was roughly 5.8% and 7.8%, respectively, of the median probability of individual events. The median duration of joint events was 39 and 49 ms respectively for intra-group and inter-group pairs. Joint events were significantly less probable and shorter in duration than the events from single cells (KS-test for both probability and duration returned $p<0.001$ for both intra-group and inter-group cell pairs), again indicating that nearby cells tended to respond differently to the same stimulus. Therefore, if coactivity in response to the movies was observed, it was very rare and very brief. Interestingly, while there was no significant difference in the probabilities of joint events among intra-group and inter-group cell-pairs (KS-test $p=0.6$), joint events in intra-group cell-pairs were significantly shorter in duration than inter-group cell-pairs (KS-test $p=0.0056$). These findings further indicate that the heterogeneity in response properties among adjacent cells is similar to, if not higher than, that for cells approximately 150 μm apart, when using this method of analysis. To compare the joint event probability in a cell pair to the event probabilities of the individual cells, a measure refer to as the similarity index (SI) (see Section 2.2.10) was employed. This measure takes the difference between the observed and expected joint event probabilities for each pair of cells and normalizes each value on a scale ranging from -1 to 1. A value of 0 indicates that joint events occur with a probability expected of two independent responses. Positive and negative values indicate joint events occurring more or less often than expected by chance, respectively. Values of 1 or -1 indicate that joint events occur as often as possible, or not at all. Figure 2.3.13 shows the distributions of SI for cell pairs recorded on the same (A) and different (B) tetrodes. For both distributions, the SI values tended to be positive, indicating some

overlap in the responses of cell pairs to the movies. There were, however, a number of cell pairs with negative SI values (27/95 intra-group; 39/140 inter-group), indicating that joint events occurred less often than expected by chance. Most of the cell-pairs with negative intra-group SIs had values of -1, indicating that their response events to the movies were completely non-overlapping. Both distributions were non-Gaussian (Lilliefors test) and were not significantly different from one another (p=0.66, KS-test).

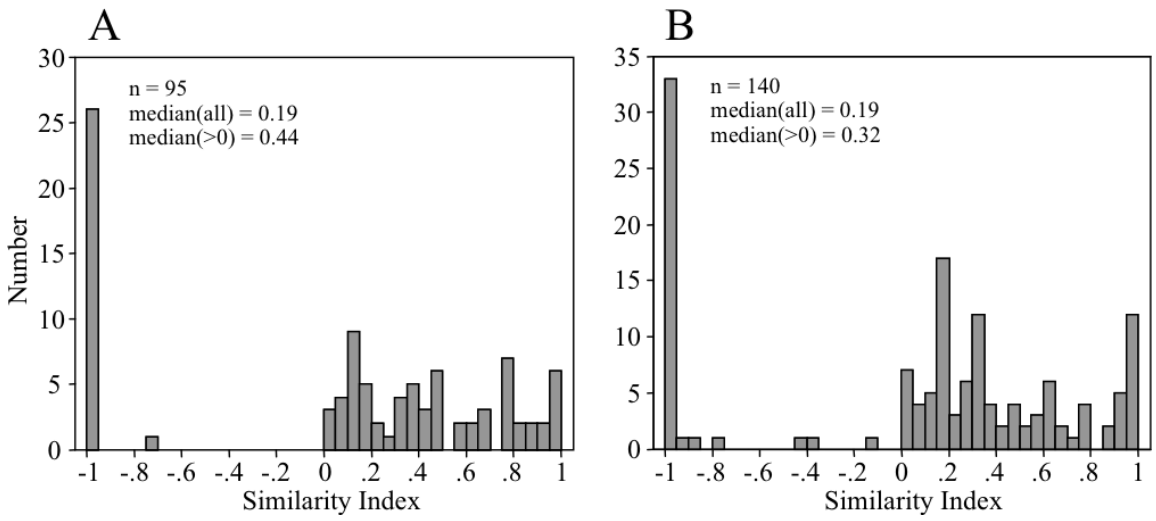

Figure 2.3.12 Histograms of the similarity index for cell pairs recorded on the same (A) and different (B) tetrodes.

2.4 Discussion

2.4.1 Summary of Main Results

When stimulated with time-varying natural scenes, striate cortical neurons exhibit responses that are rare and brief and that display both high lifetime and population sparseness, consistent with the concept of a dispersed code. Response events occurred ~5% of the time and had durations lasting 50-60 ms on average. The peak firing rates of

cells were widely distributed across the sample dataset, ranging from a low of ~1 spike/sec to a high of >200 spikes/sec. When comparing the activity of simultaneously recorded cells, a striking degree of response heterogeneity, even among cells recorded on the same tetrode is observed. The signal correlations and joint response probabilities were low and differences in the peak instantaneous firing rates were found to be close to the maximum expected for independent responses. It was common to observe response epochs in which one neuron was firing at its peak rate, while a neighboring neuron was effectively silent. The response heterogeneity of adjacent cortical neurons (recorded on the same tetrode) was similar to that observed between neurons separated by an average of 150 μm (recorded on different tetrodes). These findings demonstrate a high degree of local response heterogeneity and indicate that adjacent cortical neurons exhibit greater variations in stimulus preferences than previously thought. Before discussing the implications of these findings, it is important to rule out alternative explanations that may have come from the methodology.

2.4.2 Methodological Issues

One possible source of error in measurement could be due to one or more forms of sampling bias. Like any other neurophysiological study, this study contains sampling biases, some of which are known, and others that are more difficult to quantify. For instance, recordings were only conducted from sites where isolate single unit activity could be stability obtained. There were a number of instances where vigorous multiunit activity was sampled, but not evaluated, because the individual units could not be isolated. If, for example, the silicon probes were biased towards activity from large cells,

then it's possible small interneurons and possibly stellate cells in layer 4 were missed. This is an issue that could be resolved in future studies using probes with higher contact numbers (Blanche et al., 2005). Movie scenes that elicited strong responses from the single units were used and additional movie scenes could have been used were not. This could have biased the resulting sample database towards vigorously responding cells. However, because spike sorting was performed off-line, this bias was partially avoided, so that excluding unresponsive or weakly responsive cells during the experiment did not occur. Nonetheless, the resulting database may have been skewed towards those recording sites in which at least one neuron responded vigorously to the movie scenes selected.

A second possible source of error could result from misclassifications in spike sorting. Instabilities in the recording could easily have lead to changes in spike waveforms across the four channels of a tetrode that might have been interpreted as coming from distinct cells. This potential confound is well known (Gray et al. 1995) and several precautions were used to avoid this type of error (see Methods). In spite of these precautions, additional problems in sorting might have arisen due to efforts to recover superimposed waveforms. For example, a pair of cells may have appeared to fire at different times because the periods of joint firing were characterized by the overlap algorithm as belonging to a third cell. This possibility is highly unlikely for several reasons. First, overlapping spikes tend to occur with a distribution of relative phases, making these waveforms very different from one another, thereby avoiding the problem of consistently assigning them to a third cell. Second, participating waveforms were

required to be well isolated and to display little or no evidence of instability in shape or amplitude. This issue was made easier by detecting overlapping waveforms when utilizing the 4 channels of data, because spike voltages tended to add linearly. Finally, the output of the superposition algorithm was carefully inspected and any overlapping waveforms that clearly did not match the requisite templates were manually removed. Because of these various precautions and the extensive experience with the sources of error, spike sorting errors can be largely excluded as a factor contributing significantly to the results.

2.4.3 Response Heterogeneity within Cortical Columns

How then might one account for the striking heterogeneity of responses among nearby neurons? The most straightforward interpretation is that there are greater variations in the spatiotemporal receptive field (STRF) properties among adjacent clusters of neurons than have been previously identified. This interpretation runs counter to the classical notion that cells with similar response properties are clustered together and is inconsistent with the abundant evidence for columnar organization (Hubel and Wiesel 1962; Singer 1981; Hubener et al. 1997; Ohki et al. 2005). However, at least three lines of evidence lend support to this conclusion. First, there is increasing evidence for heterogeneous response properties among nearby cortical neurons. Multi-neuron recordings have revealed substantial variations of receptive field properties among adjacent striate neurons (Gray et al. 1995; Maldonado and Gray 1996; Maldonado et al. 1997; DeAngelis et al. 1999; Hetherington and Swindale 1999; Mechler et al. 2002;

Reich et al. 2001). While part of this effect could be due to the sampling of activity from pinwheel centers in the orientation map (Maldonado et al. 1997), it is unlikely to account for the majority of the findings. In the recordings conducted in this study, most sites displayed a broad range of signal correlations, suggesting that the observed heterogeneity was not simply due to recordings from orientation domains and pinwheel centers. Chance placement of the probes into these areas is very low given the area of striate cortex. In a related manner, heterogeneity in receptive field types has long been known to exist, with some cortical layers containing a mixture of simple and complex cell types (Martin and Whitteridge 1984; Martinez et al. 2005). The differences in RF properties could potentially account for a substantial fraction of the response heterogeneity to natural scenes. Figure 2.4.1 lends evidence to the notion that neighboring units may exhibit similar RF properties yet respond to natural scenes in markedly different ways. Below are the responses of three well-isolated single units recorded on a single tetrode and a subset of the population where clear RF kernels were obtained using a binary m-sequence stimulus (Reid et al., 1997).

A second line of evidence relates to the multidimensional tuning of cortical neurons. It is well known that striate neurons exhibit selectivity to multiple stimulus parameters, with some that are inter-dependent (De Valois et al. 1979; Skottun et al. 1994; Geisler et al. 2001). With such high dimensional spaces, many neurons with different tuning would be required to provide effective coverage of the entire stimulus space in a local population. However, these differences in high-dimensional space may not be apparent when probed with simple stimuli that vary in only one or two stimulus

parameters. Neighboring neurons may appear to exhibit very little response heterogeneity under tightly controlled conditions, simply because the full range of stimulus dimensions is not being implemented. Perhaps, only when probed with rich spatio-temporal visual stimuli, as is the case with natural movies, will the true heterogeneity of the local population be revealed?

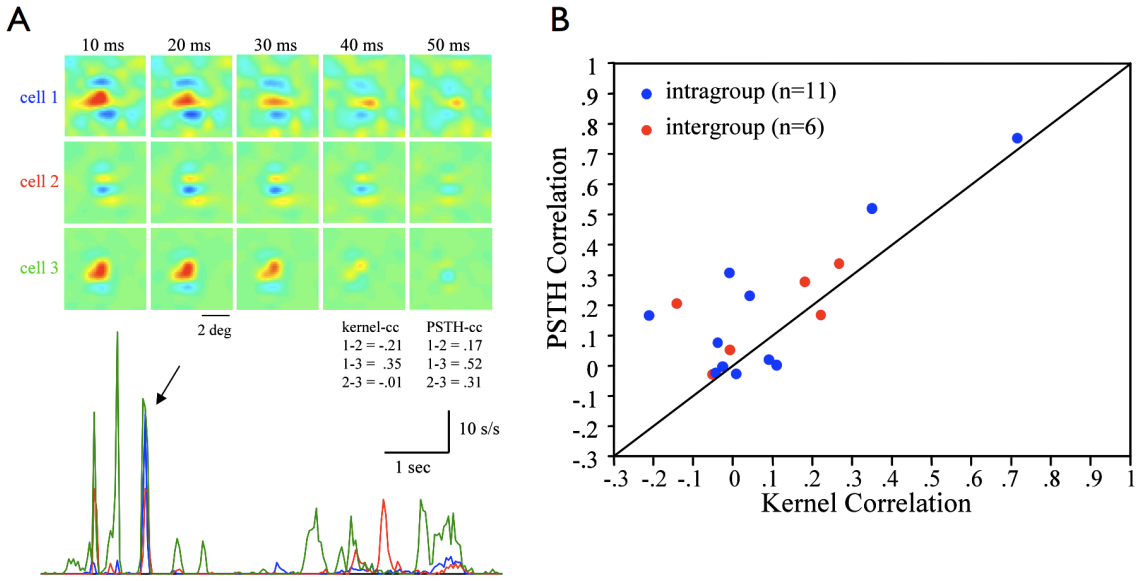

Figure 2.4.1 Relationship between the cellular responses to natural scenes and their corresponding spatiotemporal receptive fields (STRF) profiles. (A) The set upper left images are the 2D spatiotemporal receptive field maps calculated from 3 well-isolated single units recorded on a single tetrode. The bottom left plot shows the PSTH response of the same 3 cells during a short 7-second segment of the movie. Note the similarities between the STRF kernels and heterogeneity among their responses to the movie. (B) The scatter plot on the right is of the correlation coefficients computed on the PSTH responses of pairs of cells to the movie and the correlation coefficient of the STRF profiles, all simultaneously recorded pairs of cells are shown. Cell pairs recorded within a tetrode (intragroup) and between tetrodes (intergroup) clustered together.

A third line of evidence supporting the existence of functional heterogeneity comes from studies of cortical microcircuitry and cellular neurophysiology. Neocortex

contains a wide variety of both excitatory and inhibitory cell types that differ in morphology, laminar position, synaptic connectivity, and intrinsic electrophysiological properties (Thomson and Bannister 2003; Beierlein et al. 2003; Nowak et al. 2003; Markram et al. 2004, Binzegger et al. 2004; Karube et al. 2004; Yoshimura et al. 2005). This organization gives rise to a variety of sub-networks with distinct functional and dynamic properties. Thus, cells intermingled within the same column might be expected to display a continuum of response properties due to their selective anatomical connections and intrinsic electrophysiological properties. This notion was recently examined using dynamic fluorescent calcium imaging in mouse visual cortex under simple and natural scene stimulation, confirming the linkage between fine sub-network connectivity and functional heterogeneity (Ko el al., 2011).

Finally, another important factor that might have contributed to the observed response heterogeneity was the use of full-field movies. These stimuli extended well beyond the boundaries of the classical receptive fields of the cells recorded and because of their rich spatiotemporal structure would likely have had a variety of nonlinear modulatory influences, both suppressive and facilitatory (Sillito et al. 1995; Walker et al. 1999; Vinje and Gallant 2000; Jones et al. 2001; Yao and Li 2002; Webb et al. 2003; Cavanaugh et al. 2002). Such non-uniform stimulation of the receptive field surround may have had a pronounced influence on the response heterogeneity to natural scenes, particularly given the evidence that surround influences are spatially asymmetric. Such effects have been demonstrated indirectly in the study of Vinje and Gallant (2000).

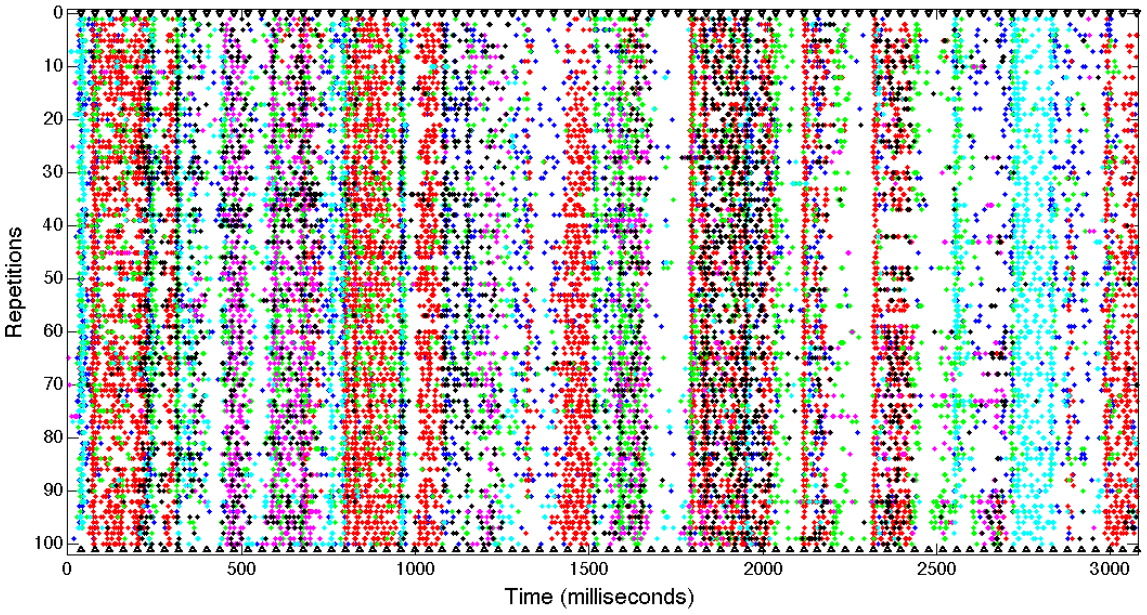

Figure 2.4.2 Heterogeneous responses during a jittering grating stimulus. Displayed are the spike rasters for 6 simultaneously recorded single units, each plotted in a different color, from a silicon tetrode probe. The drifting sinewave grating was optimally tuned for the preferred orientation, direction and spatial frequency. Note the striking level of heterogeneity among this small set of neurons to a rather simplistic stimulus.

These authors showed that signal correlations between pairs of nearby neurons were significantly reduced when the size of the movie patches presented to the cells was increased. These effects were interpreted as evidence for an active, nonlinear process of decorrelation, expected to increase the coding efficiency of cortex by reducing response redundancy (Barlow 1961; Olshausen and Field 1996, 2004; Dimitrov and Cowan 1998). However, a handful of experiments were conducted where the responses of multiple single units were recorded to optimally tuned drifting sinewave gratings that jittered in time and an example can be seen in Figure 2.4.2. In this example, heterogeneous responses among neighboring neurons were elicited while using a more classical stimulus. This raises the question of where does the heterogeneity originate, from the

statistics of the stimulus used, the inherent cellular properties, or a combination of the two? A study in anesthetized cat striate cortex has shown that non-classical receptive field stimulation, using full field natural scenes, enhances sparseness, reliability and spike precision within excitatory pyramidal cells, due to enhanced inhibitory inputs (Haider et al., 2010). In another recent study conducted in anesthetized cat striate cortex (Martin and Schroder, 2013), heterogeneity among neighboring neurons was demonstrated during drifting grating, sparse noise and natural scene stimulation, confirming the results in this chapter (see Figure 2.4.3). A related study conducted in primary visual cortex of awake macaques has shown that neighboring neurons share little or no correlated variability in their responses to drifting gratings and natural scenes (Ecker et al., 2010) and the distribution of signal correlations was tightly centered at zero, significantly lower than the average correlation of 0.2 reported in this chapter and the commonly reported range of 0.1-0.3 in other studies in visual cortex (Zohary et al., 1994; Reich et al., 2001; Kohn and Smith, 2005; 2008). This raises the potential that the observed levels of signal correlation may significantly drop during unanaesthetised preparations, however several technical issues have been raised in the Ecker et al. study which may bias the results to lower than expected correlations.

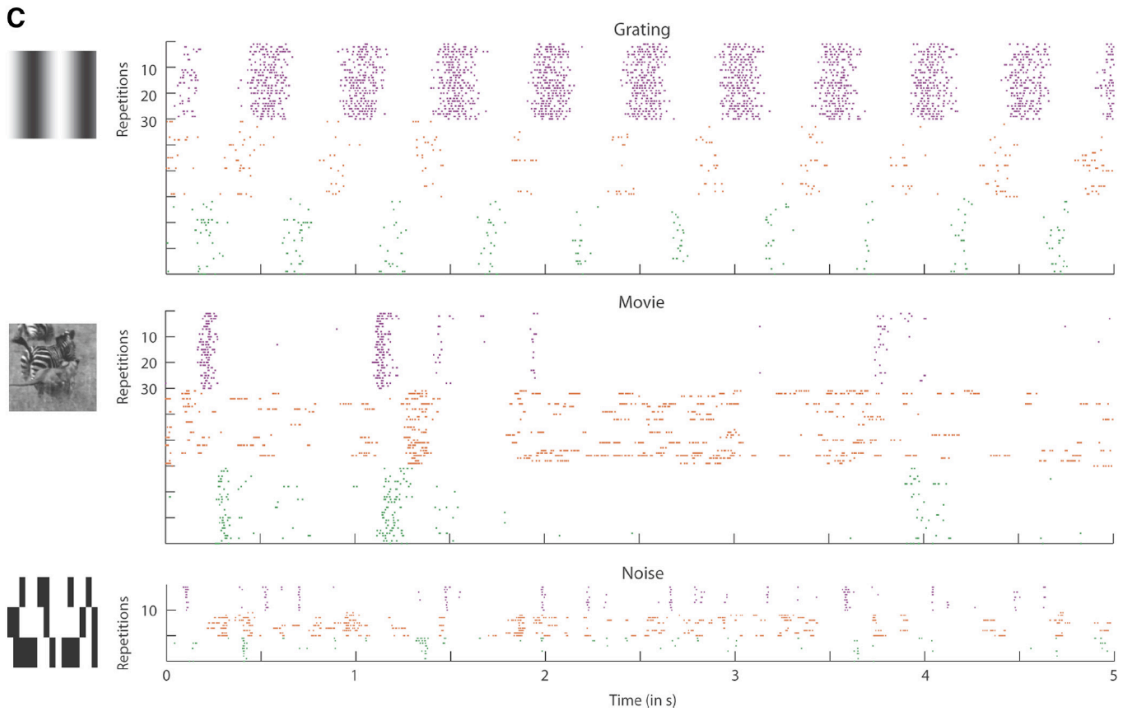

Figure 2.4.3 Raster plots depicting the spike times of the three simultaneously recorded neurons from a single microelectrode during 5 seconds of a drifting sinusoidal grating, a natural movie scene, and a noise stimulus, respectively. The colors of the raster's represent the same neurons across the three stimulus classes. The small images on the left of each raster are example frames from each stimulus class. The gratings and the movies were presented 30 times and the visual noise stimulus was presented 10 times. (This figure is reproduced from Figure 1, part C in Martin and Schroder, 2013).

2.4.4 Implications for Pooling

Models of Visual Cortex

It is clear from the presented results that the traditional concept of averaging the responses of neighboring neurons to produce a more reliable signal is problematic. Neighboring neurons in this study were seldom simultaneously active. There was little evidence that the responses of neighboring neurons could be effectively averaged without losing information, assuming downstream targets utilize the temporal information present and is consistent with the conclusions of an earlier study that quantified the information

present in spike trains responding to m-sequence stimuli (Reich et al. 2001). Averaging of neuronal responses could still be useful if knowledge about one particular stimulus parameter is all that is needed. In that case, information from all the other stimulus dimensions could be averaged out and only the relevant stimulus dimension would remain. However, it seems unlikely to us that such reductions in stimulus dimensions would be the primary output of striate cortex and this seems as a highly inefficient strategy, in terms of cortical computation and energy requirements (Attwell and Laughlin, 2001; Lennie, 2003).

Large differences in the peak firing rates of neighboring neurons were observed in the given dataset. Although it is reasonable to suspect that the neurons with low firing rates might not have been activated by their preferred stimuli, it is also quite possible that neighboring neurons, perhaps those with different intrinsic properties (Connors and Gutnick 1990; Gray and McCormick 1996; Nowak et al. 2003), may have very different peak rates. This possibility, which is well known to physiologists but has seldom been analyzed, especially with respect to responses to natural scenes, raises some interesting problems for downstream neurons. Is the activity of downstream neurons predominantly determined by upstream neurons with high firing rates? Or do the individual neurons contribute equally regardless of their absolute rates, perhaps through some form of synaptic plasticity or through their unique anatomical connectivity? These issues raise additional difficulties with the notion of averaging the responses of neighboring neurons to obtain a consensus signal.

2.4.5 Sparse Coding

Several recent studies have looked at the issue of sparse coding in visual cortex (see Olshausen and Field, 2004, for a review) yet only one preliminary study has described the population sparseness of multiple, simultaneously recorded single neurons (Blanche et al., 2006). While the database consisted of recordings with small numbers of cells, the results add an important dimension to the growing consensus that cortical activity is sparse. The advent of newer recording techniques have now made it possible to record simultaneously from much larger numbers of single neurons (Blanche et al., 2005) and it appears that these results do in fact scale to larger populations of neurons (Blanche et al., 2006).

It has been argued that a distinction could be made between a compact code (e.g. principal component analysis) and a sparse-dispersed code (e.g. Field, 1994) on the basis of dispersal. Although relatively few cells are active at one time in both codes (i.e. both codes are sparse), the same few cells are constantly active when representing different images in a compact code (e.g. cells representing the first few principal components), while different cells are active in a sparse-dispersed code (Willmore et al., 2000). The results shown in this chapter suggest that cortical activity is in fact dispersed, but again, due to the relatively small numbers of cells, it remains to be seen if studies with larger numbers of single neurons will show similar dispersal.

2.4.6 Outstanding Issues

One outstanding issue in the present work is whether the heterogeneity described is due to the use of natural movies, or if artificial stimuli with the appropriate spatio-

temporal characteristics (i.e. 1/f or white noise) would be sufficient to elicit similar heterogeneous responses. To properly address this issue, one would have to record the responses to different classes of artificial stimuli, each with different spatial and/or temporal characteristics. Unfortunately, an adequate dataset is not available to address this issue, primarily due the goal of this study, which was record and analyze striate responses to natural scenes. A preliminary analysis (seen in Figure 2.4.2) suggests that 'jittering' drifting sinewave gratings can elicit similar levels of heterogeneity, suggesting that spatiotemporal stimulus patterns that possess 1/f temporal characteristics can have the same effect in eliciting heterogeneous responses from cat striate cortex.

Another outstanding question is whether the sparsity of unit responses is a result of network interactions or if it arises from the sharpness of the spatial-temporal tuning of the cells recorded, even though this former may result from the later. This issue could be partially resolved by convolving the space-time receptive fields of the recorded neurons with the natural movies in order to compare the predicted outputs with the responses of actual neurons. A preliminary attempt was made with the current database and the attempt has highlighted the difficulties in obtaining space-time receptive fields that are of sufficient quality to make proper comparisons, and the specific transformations to convert the output of the convolution to a form appropriate for comparisons with the neuronal responses is difficult (Olshausen et al., 2004).

2.4.7 Natural Scenes

Finally, these findings lend support to the notion that the use of natural scene stimulation is highly informative in the study of vision (Kayser et al, 2004; Felsen and

Dan, 2005; also see Rust and Movshon, 2005 for a counter argument). The use of time varying natural images these experiments have shed light on the sparseness of the neural representation in primary visual cortex, and revealed that local response heterogeneity in striate cortex is substantial. Overall, the findings raise questions regarding the functional significance of columnar organization (Horton and Adams 2005), and highlight the potential loss of information that would result from the averaging of neighboring responses to obtain a consensus signal (Reich et al. 2001).

CHAPTER THREE

DYNAMICS OF SPIKING AND LOCAL FIELD POTENTIAL ACTIVITY IN CAT STRIATE CORTEX DURING NATURAL SCENE STIMULATION

3.1 Background and Introduction

Oscillatory activity is a hallmark of interconnected neuronal networks and has been observed in species ranging from insects to humans (Buzsaki, 2004; 2007). In the mammalian brain, oscillatory activity recorded within neurophysiological potentials exhibits a broad range of amplitudes and frequencies that have been historically parsed into quasi-consistent frequency ranges or 'bands' containing the greatest power fluctuations within a range from 1 Hz up to 250 Hz (Buzsaki, 2004). These field potentials can be recorded extracellularlly from the surface of the scalp, termed electroencephalography (EEG), form the dural and/or cortical surface, termed electrocorticography (ECoG), or more directly from within large neural populations in the cortex using macro and microelectrodes, termed local field potentials or LFP. The power spectral density of the LFP within the mammalian cortex generally exhibits an inverse relationship, proportional to the frequency (Pesaran et al., 2002; Buzsaki, 2004). This *1/f* power relationship has been attributed to the physical architecture of the cortex, which is limited by axon conduction speeds and synaptic delays or may result from the resistive and capacitive properties of the brain (Nunez, 2006; Logothetis and Kayser, 2007). In the mammalian neocortex, the vast majority of synaptic connections made between neurons are in fact local and theoretically confine the higher frequency

oscillations to more local neural populations, whereas slower oscillations typically engage much larger expanses of the cortex, as observed during deeper stages of sleep (Steriade et al. 1993; 2001). The biophysically nature of the LFP is complex and thought to reflect population synaptic potentials (Mitzdorf, 1985, 1987; Juergens et al., 1996) and intracortical processing within a cortical area, which includes voltage-dependent membrane oscillations (Kamondi et al., 1998), spike afterpotentials and back propagating action potentials (Buzsaki and Kandel, 1998) and slow varying field potentials, which relate well to subthreshold integrative processes in areas such as dendrites that are otherwise inaccessible to microelectrode recordings (Pesaran, 2009; Rasch et al., 2009). It is a well-established fact that the brain uses electricity, in the form of ionic conductances, for the processing of information and communication, therefore any type of current within the brain could and likely contributes to the LFP. Even thought the actual spatial spread of the LFP is not known and still debated (Buzsaki et al., 2012), it has been estimated to range between several hundred micrometers to several millimeters (Mitzdorf, 1985; Engel et al., 1990; Liu and Newsome, 2006; Kreiman et al., 2006; Berens et al., 2008). Recent studies within cat (Katzner et. al., 2009) and monkey (Xing et al., 2009) striate cortex have estimated the LFP to reflect activity within ~200-400um of the recording electrode, however the debate concerning the spatial scale of the LFP continues (Kajikawa and Schroeder, 2011; Linden et al., 2011; Buzsaki et al., 2012). Regardless of the actual spatial extent of the LFP, it can be used as an index of local network processing and its relationship to output spiking activity can be quantified. One of the primary experimental goals in this chapter was to measure these low frequency

potentials and spiking activity, along the entire length of the striate cortical microcircuit and quantify and relationships observed between the two signals during natural scene stimulation.

In the striate cortex, response properties of individual units have been explored extensively over the past 60 years under a variety of stimulus conditions, however investigations focused on recording and characterizing local field potentials, in relationship to spiking activity, have only recently increased in the past decade. From these studies, it has been shown that power within certain frequencies of the LFP are most prevalent during visual stimulation, specifically the so-called 'gamma' frequency band, generally ranging from 25-90Hz. Gamma-band synchronization among unit activity was first observed in cat striate cortex using moving light bars and gratings (Gray et al. 1989; Gray & Singer 1989). This seminal result was expanded to extrastriate regions (Engel et al. 1991a, b, c) and later demonstrated in awake preparations (Frien et al. 1994, 2000; Kreiter and Singer 1996; Fries et al. 1997; Gray & Di Prisco 1997; Friedman-Hill et al. 2000; Maldonado et al. 2000; Fries et al. 2001, 2002, 2008b; Bichot et al. 2005; Taylor et al. 2005; Womelsdorf et al. 2006, 2007). Gamma-band synchronization has been well documented over the past 20 years (reviewed in Fries 2009) and observed in many brain regions and under a variety of stimulus and behavioral conditions. The mechanistic role of gamma frequency band oscillatory activity has moved beyond its initial proposed role in stimulus feature binding in the visual system (Singer and Gray, 1995) to include a wider range of cognitive and executive processes as well as in the pathophysiology of certain psychiatric conditions (Uhlhaas and Singer,

2006; 2010). As stated above, the large-scale measurement and quantification of significant interactions between spiking activity and power fluctuations within the LFP, specifically in the gamma frequency band (25-90Hz), was a primary experimental goal in this chapter. Accessing the level of interaction between these two signals during natural scene stimulation would enable a better understanding of stimulus processing within the striate cortical microcircuit.

In recent years, there has been a rapid expansion in the number of studies investigating relationships between the spiking activity and the local field potential, focusing on sensory coding, perception, attentional and working memory within striate, association and motor cortices (Frien et al, 2000a,b; Fries et al., 2001; Pesaran et al., 2002; Siegel and Konig, 2003; Gail et al., 2004; Kayser and Konig, 2004; Henrie and Shapley, 2005; Rickert et al., 2005; Scherberger et al., 2005; Taylor et al., 2005; Womelsdorf et al., 2006; Liu and Newsome, 2006; Van Der Werf et al., 2008). Most of these studies have reported significant links between enhanced gamma frequency band activity and spiking activity, while comparing the 'tuning' of these responses in relation to the stimulus properties or the behavioral task. When the experiments discussed in this chapter began, the relationship between spiking and local field potential activity during the presentation of time-varying natural scenes, i.e. movies, within the striate cortex was unknown. However, in the past several years, a small set of studies has examined the tuning properties of spiking and LFP activity during natural scene stimulation in both cat (Kayser et al., 2003; 2004) and monkey (Montemurro et al., 2008; Belitski et al., 2008; 2010) striate cortex. In addition, an elegant extra- and intracellular study was conducted

in cat striate cortex under natural scene stimulation, reporting on MUA, SUA and membrane potential fluctuations (Haider et al., 2010). Results from these studies have shown that spiking and LFP activity are strongly influenced by natural scene stimulation in variety of ways, including significant co-engagements between spiking and gamma frequency band activity. Results in this chapter extend these findings by reporting on the dynamics of spiking and gamma frequency band activity throughout the layers of striate cortex during natural scene stimulation.

The issues discussed above were further explored by recording large-scale spiking and LFP activity across all layers of cat striate cortex during natural scene stimulation in order to investigate a series of questions concerning the prevalence and proposed role of spiking activity and gamma oscillations in sensory processing and representation. In addition, individual spiking responses, in terms of sparsity, reliability and heterogeneity were also investigated under natural scene stimulation to extend the findings reported in chapter two. Below are the set of questions and hypotheses that were investigated in this chapter.

In terms of spiking activity, how sparse and reliable is the unit activity across the layers of striate cortex during repeated presentations of both short and long movies? Additionally, how heterogeneous is multi single unit activity across the layers of cortex during both short and long movie presentations and can diversity within the classical spatial temporal receptive field profiles of the unit responses account for any of the observed heterogeneity during natural scene stimulation? Based on previous studies and

results in chapter two, spiking activity will be sparse, reliable and neighboring units will respond heterogeneously to both short and long movies.

Are the firing rate dynamics observed in unit activity under time varying natural scene stimulation significantly correlated with ongoing power fluctuations of specific frequency bands within the local field potential and if so, do the dynamics significantly differ across the layers of striate cortex? Based on previous studies spiking activity will significantly couple, in terms of timing and amplitude, with gamma frequency band fluctuations throughout the movie presentations and will significantly vary across the cortical layers.

To investigate these questions, broadband signals were recorded using multicontact silicon probes, i.e. polytrodes, within the striate cortex of anesthetized and paralyzed cats while presenting both short and long movie segments along with a set of more classical visual stimuli, including sparse spots and bars and drifting sinewave gratings. In general, unit activity during the movie presentations was sparse and reliable, however the level of heterogeneity was difficult to access. In the majority of recording locations, significant elevations of power within the gamma frequency band of LFP were present throughout the movie presentations. These robust fluctuations in gamma frequency band activity were well correlated with ongoing spiking activity fluctuations, which occasionally localized to specific regions within the striate cortical microcircuit. These findings extend and expand our understanding of sensory processing within the mammalian visual system.

3.2 Materials and Methods

3.2.1 Surgery

All experiments were conducted in anesthetized and paralyzed adult male cats weighing 2.5-5.5kg. Details concerning the induction and maintenance of anesthesia, along with the surgery and electrophysiology methods can be found in section 2.2.1. This protocol was approved by the Institutional Animal Care and Use Committee at Montana State University and conforms to the guidelines recommended in Preparation and Maintenance of Higher Mammals During Neuroscience Experiments, NIH publication No. 91-3207 (National Institutes of Heath, Bethesda, MD, 1991).

3.2.2 Electrophysiology

Recordings were made from a total of 31 individual probe penetrations within the striate cortices of four male adult cats using either a 16-contact silicon tetrode probe (*see Figure 2.2.1 and Section 2.2.2 for details*) or a 54-contact laminar silicon polytrode (*see below 3.2.3 Silicon Polytrodes*) provided by the Center for Neural Communication Technology (CNCT) at the University of Michigan and NeuroNexus. The impedance of each contact for both probe types ranged from 0.3-1.5 MΩ measured at 1 kHz (Bak Instruments). Broadband signals (0.001-10kHz) were amplified 5000 times using a combination of 10X preamplifiers (MPA32I) and a 64-channel programmable gain amplifier (PGA64) (Multi Channel Systems, MCS GMBH), that were then digitized (14-bit) and recorded at a sampling rate of 30 kHz per channel using a custom configured data acquisition board (United Electronics Industries, Canton, MA) running custom-

written functions built on Matlab's data acquisition toolbox routines. All signals were streamed to a custom configured PC running Microsoft Windows XP and stored for offline analysis. Once stable unit signals were obtained, the borders of the aggregate receptive fields, the preferred stimulus orientation, and the dominant eye for each recording site were determined using mouse-controlled light bars and sinewave gratings. All subsequent stimuli were displayed to the eye that dominated cellular responses at the majority of recording sites (*see below 3.3.7-9 Visual Stimulation*), while temporarily occluding the non-dominant eye.

3.2.3 Silicon Polytrodes

Laminar recordings were performed using 54-channel silicon probes (Blanche et al., 2005) provided by NeuroNexus (Ann Arbor, Michigan). Each silicon polytrode probe was ultrasonically bonded to an in house custom designed printed circuit board (PCB), that enabled the manipulation and fine insertion of the probe, along with a rigid mount for the two 32-Channel MultiChannel Systems preamplifiers (MPA32I). Unused and/or dead channels (infinite or high impedance) were grounded to reduce 60Hz line noise contamination. Each polytrode consisted of two staggered columns of 27 contacts, with a horizontal separation between the columns of contacts of 56μm, and a vertical separation between the rows of contacts of 65μm (see Figure 3.3.1). This arrangement spans a distance of ~1.7mm from the upper to the lower contacts, and was therefore well suited to record neuronal activity from all layers of cat striate cortex simultaneously (Peters and Payne, 2002). The small separation between contacts, both horizontal and vertical, enabled the extracellular recording of action potential waveforms from a number of

adjacent and contiguous contacts. This arrangement could in principle dramatically improved the separation of spike waveforms from different cells, and could in theory enable the identification of different cell types on the basis of the signal distribution across the array (Buzsaki and Kandel, 1998; Henze et al., 2000; Blanche et al., 2005). In practice, extracting and sorting individual spike waveforms from the data recorded proved difficult due to instabilities in the recording quality over each recording session and across sessions and animals. (*see Section 3.2.6 for details*).

For each polytrode and tetrode insertion, the goal was to implant the probes normal to the cortical surface and within 5° of the representation of the area centralis (Tusa et al., 1978). The alignment of the polytrode in both the mediolateral and anteroposterior axes would in theory allow for the sampling of neuronal activity uniformly from all of the layers of the cortex within a single or most likely multiple, putative microcolumn(s) of intraconnected neurons (Peters and Payne, 2002). In practice this proved quite difficult and near perfect alignment in all orientations was likely never achieved. Dimpling of the cortex and pia matter during the insertion was partially dealt with by cutting the pia and surrounding the probe in agar and mineral oil. However, the original trajectory of the probe deviated from normal in nearly all penetrations. Several methods were used in order to determine the final alignment of the polytrodes within the cortical layers (*see Section 3.2.4 for details*).

3.2.4 Histology

In order to reconstruct each silicon probe location, combination of several well-established fluorescent staining techniques was used (DiCarlo et al., 1996; Alonso and

Martinez, 1998; Blanche et al., 2005; Naselaris et al., 2005). These methods provided an independent validation of the experimental recording depths determined from micromanipulator readings and full-field black to while flashed stimuli and subsequent current source density (CSD) measurements. Prior to cortical implantation, the backside of the silicon tetrodes and/or polytrodes were painted with the fluorescent dye DiI (1,1'-dioctadecyl-3,3,3',3'-tetramethylindocarbocyanine perchlorate), dissolved in 10% ethanol, and prepared using standard protocols (Molecular Probes, Eugene OR). DiI uniformly labels neurons via lateral diffusion in the plasma membrane (6mm per day, in vivo) and is thus taken up into neurons adjacent to the polytrode. Through a trial and error process, using fresh mouse cortex and the use of thin and thick layers of DiI, a uniform layering method was developed to reliably coat and then identify the probes position within the cat visual cortex postmortem.

Experiments were terminated through the intravenous injection of a lethal bolus of pentobarbital. The animals was then quickly perfused, transcardially, with a non-standard fixative (1.25% paraformaledeyde, 0% glutaraldehyde in phosphate buffer, pH 7.4). Glutaraldehyde is a standard part of fixative, but it was not used due to its known auto-florescent properties, which would have washed out the DiI and fluorescent Nissl stain fluorescence in the confocal microscope. After perfusion, the head was removed from the body, fixed into the stereotaxic frame and the overlying skull was removed. A large region of area 17, containing all probe penetrations was blocked in situ, removed from the brain, and bathed in chilled (4°C) phosphate buffered saline (PBS) and then placed in a 4% paraformaldehyde / 10% sucrose overnight. Cryosections (50μm) were

prepared using standard protocols and placed onto gelatin coated glass slides. The tissue slices were then counterstained with a Green fluorescent Nissl stain (NeuroTrace 500/525, Molecular Probes) using standard protocols and coverslipped. Each probe track was visualized and digitally photographed using standard wide field fluorescent microscopy. The final position of the polytrode and tetrode tips were identified in about half of the penetrations and calibrated to the micromanipulator readings with the goal of determining layer information. Small electrolytic lesions were attempted in the first polytrode experiment, however locating and then identifying these lesions was ambiguous at best and so the approach was abandoned.

3.2.5 Silicon Tetrode Probe Spike Sorting

Spike waveforms were extracted from the broadband signals on each channel of the recording probes using a multi-step procedure. Details concerning the extraction and clustering of single unit activity (SUA) from each of the tetrode recording sessions can be found in Section 2.3.3. A subset of recording sessions yielded poor signal to noise quality, therefore multi unit activity (MUA) waveform clusters were generated using the same extraction and clustering methods for the SUA with an additional step. All putative spike waveforms were extracted using a threshold of 6 times the SNR ratio. This microvoltage level ensured that only unit activity was extracted. Mechanical and electrical artifacts were excluded for the MUA clusters by comparing waveform extraction times across the array of channels. Artifacts typically consisted of a very sharp positive or negative going peak in the voltage, simultaneously recorded along the array, and were easy to exclude. Waveforms lagging behind another spike waveform within an

inter-waveform interval of less than 1ms were also excluded from the MUA clusters. Even though multiunit clusters typically contain inter-spike intervals of less than 1ms, due to the near simultaneous activity of two or more cells, this step ensured that double extractions of the same complex waveform were excluded. It is possible that the final estimation of the MUA firing rates were lower than the actual MUA firing rates.

3.2.6 Silicon Polytrode Spike Sorting

Spike waveforms were extracted from the broadband signals on each channel of the polytrode using a multi-step procedure. Details concerning the extraction of the waveforms can be found in Section 2.3.3. The spike extraction and spike waveform sorting algorithm was developed by Roger Herikstad in the lab of Dr. Shih-Cheng Yen in order to handle the polytrode data. For a detailed description and application of this sorting algorithm, see Herikstad et al., 2012. Briefly, the extracted waveforms from each polytrode penetration site and for each recording session were concatenated to ensure a consistent waveform across the individual stimulus sets. These extracted and concatenated spike waveforms were divided into spike ‘complexes’ which consisted of a contiguous group of waveforms observed on neighboring polytrode contacts. Several amplitude and timing criterion were empirically established to include and excluded putative waveforms into these spike ‘complexes’. In addition, a spiking neuron model that incorporated a decay function, 1/r, r being set to a given distance between the model cell and the electrode contact, and was used to identify spike ‘complexes’ containing slight drifts in the timing of the spike ‘complexes’ across the array, which may indicate back propagating action potentials (Stuart and Sakmann, 1994). Mismatches in the

impedance levels among the polytrode contacts were also factored into the algorithm. An initial set of spike 'complexes' were deemed single unit or multiunit, based on ISI distributions and then merged if they satisfied a set of criterion using a hierarchical clustering algorithm and then the final resulting set of template clusters were used to extract the final spike times, based on correlation coefficient criterion, which were then saved and designated SUA and MUA for subsequent analysis.

3.2.7 Visual Stimulation using Natural Scenes

High contrast monochromatic movie sequences, digitized from a DVD movie (World of House Cats) covering a wide range of natural and man-made scenes, were presented monocularly to the dominant eye, while occluding the non-dominant eye, at a distance of 57 cm, using a 20″ CRT monitor (Viewsonic P810) with a screen resolution of 800 x 600 pixels. Movie frames had dimensions of 640 x 480 pixels and were positioned at the center of the screen, occupying 32º x 24º of visual angle (0.05º/pixel). The luminance distribution of the monitor (3-80 cd/m2) was gamma-corrected so that luminance values were set on linear scale and the transition between pixel intensity values, ranging 0-255, were uniform. Individual movie frames were first de-interlaced from the standard 3-2 pull down, recombined and then presented at a rate of 25 Hz (6 refreshes per frame at 150 Hz refresh rate). Individual movie clips (30-40 seconds) were repeated 100 times and following each repetition, a uniform gray screen of mean luminance (38 cd/m2) was presented for 2-5 seconds. This type of movie stimulus is referred to as 'Short Movie' in this chapter. Each short movie session lasted from 58.33 to 70 minutes in total duration. For most recording sites, the entire length of the movie

(9000 frames, 6 minutes) was repeated 5-10 times with a 10 second period of uniform gray following each repetition. This movie stimulus is referred to as 'Long Movie' in this chapter. Each long movie session lasted from 30.83 to 62 minutes in total duration. The blank uniform gray screen allowed for the collection and assessment of spontaneous neural activity levels between subsequent movie repetitions. Power fluctuations in the local field potentials recorded within these 'spontaneous activity' periods were used as a baseline for the subsequent analysis of power fluctuations in the LFP during the movie presentation (*see Sections 3.2.10-11 for details*).

3.2.8 Visual Stimulation with Sinewave Gratings

High contrast drifting sinusoidal gratings, presented for 2 seconds and consisting of 24 directions (0° - 345°, in 15° steps), 5 spatial frequencies (0.25, 0.44, 0.63, 0.83 and 1.0 cycles/degree) and 5 temporal frequencies (1.0, 2.2, 3.5, 4.7 and 6.0 cycles/second) were presented in a pseudo-random order. The spatial dimension of gratings matched the movie dimensions of 640 by 480 pixels (32º x 24º of visual angle). A total of 600 different gratings were presented and the set of 600 gratings were presented 5 times in total. Following each block of the 600 grating stimuli, a uniform gray screen of mean luminance (38 cd/m^2) was displayed for 10 seconds to collect spontaneous neural activity. Each grating session lasted a total of 100.83 minutes in duration.

3.2.9 Visual Stimulation with Black and White Spots and Bars

High contrast black (3 cd/m2) and white (80 cd/m2) spots (0.5°) and elongated bars (0.5° x 2°) of light were presented on a uniform gray screen (38 cd/m2) in a pseudo-

random order and within a 10 x 10 point grid extending 3-5° beyond the aggregate hand-mapped receptive-fields. Each spot or bar was presented for a total of 40ms (6 repeated refreshes at 150Hz video refresh rate). Bars orientations spanned 360° at 15° intervals. Standard spike-triggered reverse correlation analysis was conducted in order to generate space-time receptive field maps of the cells (Ringach 2004).

3.2.10 Local Field Potential

Local field potentials (LFP) were extracted from the broadband signals by bandpass filtering the raw signals from 1 to 100 Hz using a multistep procedure. First, the broadband signals were down-sampled by a factor of 30 from 30kHz to 1kHz, using the 'resample' function provided in the signal processing toolbox in MATLAB. A window of +/- 5 seconds, including each movie repetition was extracted and then filtered to reduce edge effects of the filter. Padding in the time domain with the correct voltage value, instead of zeros, maintains the original power spectrum of the signal, otherwise an artificial sharp transition can result, thereby contaminating the power across all frequency bands. The down-sampled signal was then low-pass filtered, using a fourth-order Butterworth 'butter' filter (3 dB/octave), in both directions using the noncausal 'filtfilt' function in MATLAB, which resulted in a zero phase shifted low-pass signal. The resulting lowpass filtered signal was then processed to remove any residual 60 Hz line noise using the Chronux toolbox function 'rmlinesc', which uses an F-statistic to identify and then subtract out the quasi-regular sinusoidal line noise signal without removing power from neurogenic signals. Most of the recordings contained a minimal amount of power line noise, yet several required the removal of the line noise to effectively uncover

the neurogenic frequencies of interest, specifically the gamma band 25-90Hz. Even after removing the line noise from the downsampled and filtered signal, line noise power could still be observed, as seen in Figure 3.2.1 To reduce or eliminate the potential for 'spiking activity' to directly affect power within the LFP signal, all extracted waveforms were subtracted from the broadband signal prior to low-pass filtering as described in Pesaran et al., 2002. This preliminary step was conducted to reduce the small bias spiking activity may contribute to the overall power within the LFP.

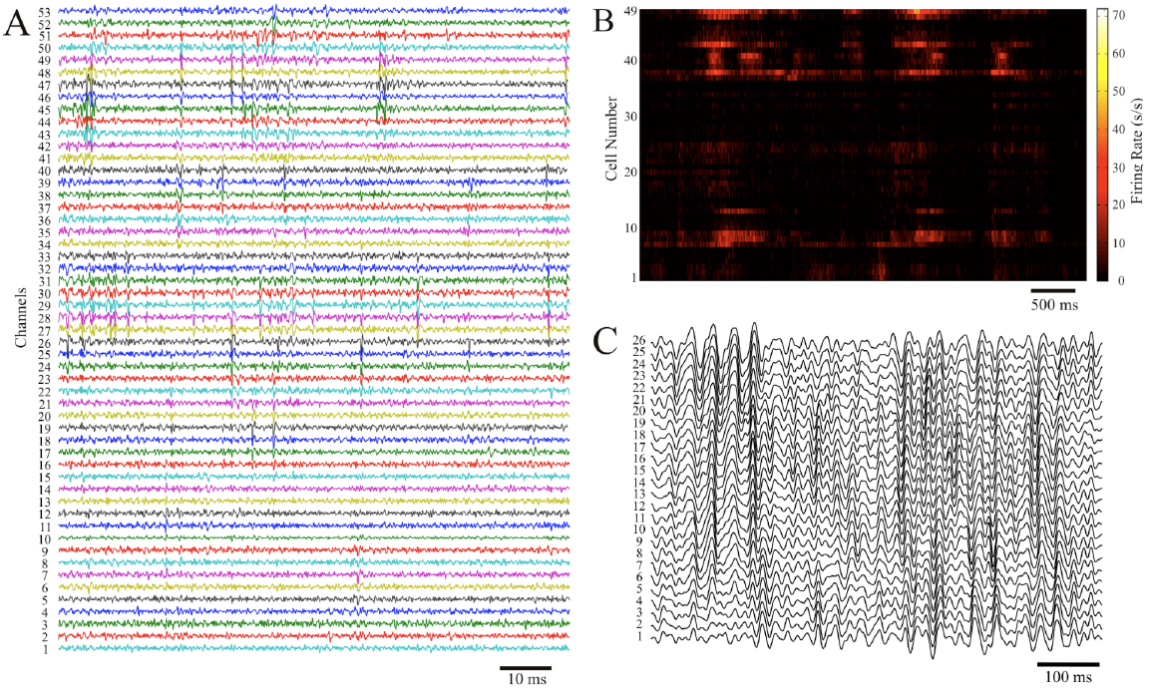

Figure 3.2.1 Several examples of neural activity recorded from the polytrode probes, recorded across all layers of cat striate cortex during natural scene stimulation. (A) Neural activity recorded across 53 of 54 contacts on the polytrode. The broadband signals (0.5-10KHz) were filtered (500-10KHz) for spike extraction and sorting into both single and multiple unit clusters (*see Section 3.2.6 for details*). (B) The average firing rates for 49 isolated units recorded along the entire length of polytrode during a Short movie session. (C) Broadband neural activity was lowpass filtered (1-100Hz) and then standard multi-taper spectral analysis routines were employed to estimate the power spectral density and relate power fluctuations within specific frequency bands to the stimuli presented (*see Sections 3.2.10-17 for details*).

Even though 'sharp' spike waveforms and high firing rates affect power in frequencies above 100 Hz (Ray and Maunsell, 2011), the spike afterpotentials (AHP) produced by spiking neurons have been shown to influence LFP power below 100Hz in rate barrel cortex (Einevoll et al., 2007). This step further removed the potential for spurious correlations between spiking activity and the LFP (Zanos et al., 2011) and power within frequencies near the upper limit of gamma band (*see Figure 1 in Zanos et al., 2012*). These sanity measures were employed to ensure that correlations and coherences between the spiking activity and the LFP were not cross contaminating each other and thereby lead to invalid conclusions regarding any relationships between spiking activity and particular frequencies within the LFP.

3.2.11 Multitaper Spectral Analysis

In order to characterize the power dynamics within the LFP signals and to correlate the estimated dynamics to the simultaneously recorded spiking activity, standard multitaper power spectral density analyses were performed (Pesaran et al., 2002). The power spectrum of the LFP signal is a measure of the variance within the LFP as a function of frequency and is related to the original time domain signal through the Fourier transform of the auto-correlation function. The frequency bands of interest in this chapter and all subsequent spectral analysis were excluded to the 'gamma' band (25-90Hz) and the 'sub-gamma' band (1-15Hz). Following Pesaran et al. (2002), the frequency range of 25–90 Hz was set as the gamma band. All power spectrum analyses were implemented in Matlab (The MathWorks, Inc., Natick, MA) using custom-written software routines built on functions within the Chronux 2.0 toolbox (Chronux.org). The

local field potentials recorded in these experiments typically displayed the characteristic "1/f" power spectrum, yet exceptions were observed during the movie presentations, where marked increases in power within the gamma frequency range (25-90Hz) were observed (see Figures 3.3.8 and 3.3.9). The spectrum were calculated using the multitaper method in order to detect subtle changes within the frequencies of interest, with improved sensitivity to nonstationarities in power and to calculate jackknife confidence intervals (Jarvis and Mitra, 2001). Multitaper spectral analysis performs an estimate of the spectrum by multiplying the time series with a set of unique windowing functions called tapers, also known as 'Slepian' sequences or discrete prolate spheroidal sequences (Thomson, 1982; Percival, 1993; Jarvis and Mitra, 2001). These tapers are distinguished from each other by their orthogonality and therefore each taper provides an independent estimate of the spectrum and the final quality of the estimate depends on the number of tapers used. The number of tapers, K, determines the frequency resolution, 2W, given by the equation 2NW-1=K. The tapers have maximally concentrated energy in the frequency interval [-W, W]. Multiplying the de-trended ('detrend' function in Matlab) LFP by each taper provides the spectral estimate. The frequency resolution of the spectral analysis is inversely proportional to the temporal duration of the window used, therefore a ±250 ms window (500ms temporal window) was used in all subsequent analysis and moved across the LFP signals in steps of 50 ms. The use of 5 tapers in this study resulted in a spectral concentrations with 5 Hz resolution. The sliding window method is well established and has been applied to LFP and spike train data in a number of studies (Pesaran et al., 2002; 2008; Womelsdorf et al., 2006). The same window method was used for all movie

repetitions, both short and long. Temporal windows of ±125, ±150, and ±500ms were also used and the general results were not significantly altered. The power spectrum of the spontaneous periods, where the visual display was set to a mean gray luminance, essentially displayed the expected "1/f" power spectrum. During the movie presentation, there was a broad increase in the higher frequency range and when inspected more closely, this broad range contained discrete epochs where the peak within the gamma band was in fact constrained to a tighter sub-band, which dynamically changed across space and time during the stimulus. The enhancement of this sub-band was also unique to the laminar position of the recording (*see Figure 3.3.10 and 3.3.11*). Consistently identifying and tracking these sub-band dynamics became nearly impossible across recording sessions and animals using the statistical methods provided by the multi taper approach. Additional methods were employed in order to capture and quantify these epochs, however those methods also failed. In the end, power estimates within the wider gamma frequency band (25-90Hz) were investigated as a whole.

3.2.12 *Z*-transformed Multitaper Spectral Analysis

In order to characterize and quantify significant epochs of enhanced spectral power within the gamma (25-90Hz) and sub-gamma (1-15Hz) bands during the movie presentations, the absolute power within each spectrum was converted to a unit-less Z-score and is referred to as the 'Z spectra'. Since all movie repetitions were followed by a uniform mean luminance for several seconds, these periods were used to assess power fluctuations within the neural signals during these 'spontaneous' activity periods. The Z-

transform was accomplished by calculating the mean and standard deviation of the power spectra within all spontaneous activity periods, 100 periods for the Short movie, 5-10 periods for the Long movie, minus the first 500ms of each period to account for the offset of the movie stimulus and the resulting visually evoked potentials, due to the abrupt transition in global luminance (see Figure 3.3.11 for an example and Figure 3.3.19 for a summary). The windowed spectra calculated during the movie periods were then Z-transformed by subtracting the mean power of the spontaneous activity period and dividing by the standard deviation of the power within the spontaneous periods. Generally Z-scores > 2 would indicate power fluctuations exceeding the baseline spontaneous activity levels by 2 standard deviations, i.e. the 95th percentile. Yet all frequency windows within the power spectra during the spontaneous periods were never uniformly distributed, typically skewed leftward, so a hard threshold of 2 was not considered valid for nearly all data sets. Therefore an empirically derived threshold of the 95^{th} percentile was calculated for each frequency window within the power spectra across all spontaneous periods. In addition, the time-frequency Z-spectrum for each movie repetition was averaged across all stimulus repetitions in order to account non-stationarities in the signals and to enable comparison across all signals recorded simultaneously and across experiments and animals. These smoothly varying estimates of enhanced spectral power, as shown in Figure 3.3.11, were to be used in all subsequent analysis, however the variability in the Z-spectra was too great across experiments and animals, precluding a simple summary of the data collected (*see Section 3.2.13 for details*).

3.2.13 Z-Spectra Events

One of the analysis goals in this chapter was to quantify the spatial and temporal dynamics of significant gamma and sub-gamma frequency band activity during the movies, in order to correlate the dynamics of these 'events' to the cortical microcircuitry and eventually relate the events to the stimulus properties within the aggregate hand mapped receptive fields. To quantify the duration and frequency of significant 'Z-Spectra Events', defined as contiguous points in both time (50ms resolution) and frequency (5Hz resolution) of elevated spectral activity, an empirically derived Z-score threshold, based on the 95th percentile of the power calculated during the spontaneous periods was used. Spurious 'Z-Spectra Events' occurring shorter than an arbitrary criterion of 250ms, were combined with neighboring events if separated by less than 100ms, or disregarded as false positive events and removed from further analysis. Continuity of these putative 'events' across frequency windows was much more difficult to access, given the wider range of frequency bins in the gamma band. Therefore the average values within the gamma and sub-gamma frequency bands were used to combine or separate events. This approach was initially successful in capturing 'events' within select short movie sessions, however when applied across the database of all short and long movie sessions, it became clear that this approach was flawed, difficult to interpret and likely resulted in a high number of false positives. Discontinuity in the frequency bins, mostly within the gamma frequency range (25-90Hz), made it difficult to combine events beyond the frequency resolution and in addition to the fact that the peak frequency within the gamma band displayed various non-stationarities. These non-stationarities took several forms,

including shifts in the peak frequency during a single movie repetitions and worse across repetitions of the movie. Given these issues, this approach was abandoned.

A secondary method, using an ROI (Region-Of-Interest) analysis was attempted in order to identify and capture these 'Z-Spectra Events' by taking into account the temporal dynamics of the spectral power as it crossed frequency windows within the two frequency bands of interest. A combination of built-in Matlab functions: 'roicolor', 'roifilt2', 'roipoly' and 'bwlabel', were used to extract and then analyzed statistically significant regions within the Z-Spectrograms. The assumption that continuity in the time-frequency plane reflected continuity in the waveform of the LFP signal had to be made in order to validate the method. Numerous attempts were made to first implement this approach on the higher quality data sets and generalize the analysis across the entire dataset, yet this approach was also abandoned due to high variability in the outcomes and likely contamination due to spurious, yet real neurogenic events within the LFP. Even when electrical and mechanical artifacts were identified and excluded, the reproducibility across datasets was difficult to achieve. Statistical significance was also an issue of concern, however the false discovery rate (FDR) could have been applied across the spectrograms. Perhaps a more statistically sound variant of ROI, like those employed in the analysis of fMRI data or a bootstrapping and re-sampling methods could be adopted to capture the rich spatial-temporal dynamics that are clearly observed during natural scene stimulation as seen in Figure 3.3.11.

A recently developed method for the detection of "ripple" (140-200Hz) and "fast-gamma" activity within large-scale broadband recordings within the hippocampus

(Sullivan et al., 2011) could in principle be employed to identify sub-gamma and gamma events within the LFP data recorded. To implement this method on the movie data, band-limited power, 1-15Hz and 25-90Hz, would be extracted from the LFP, then rectified, smoothed through integration and then z-score normalized. As in Sullivan et al., 2011, potential 'events' would be aligned to a CSD signal and a minimum of 100ms would separate candidate events. Multitaper spectral analysis could be conducted to exclude false positives by comparing the power within the candidate event to power within the spontaneous periods. If power within the frequency range exceeded 2 standard deviations of the spontaneous period or the empirically derived 95% threshold, the candidate 'event' would be allowed to pass and combined with neighboring 'events' to exclude double counting. This method should in principle more reliably identify events and allow one to better quantify the duration and frequency of events during the movie presentations. Also by using the band-limited power, the issue of determining significance across frequency bins is largely eliminated is one assumes a normally distributed range of powers within the frequency band. Given non-uniform spread of power within the gamma and sub-gamma bands, this assumption would be invalid. This method would allow for the quantification of the spread of an event across the recording array in both space and time, thereby achieving the original analysis goal of the chapter, which was to characterize gamma and sub-gamma frequency band events and correlate the dynamics of these events to the spiking activity, in the hope of eventually related these interactions to the cortical microcircuit and the processing of the visual content being displayed to the animal.

3.2.14 Correlation between Z-spectra and Spiking Activity

To assess the time-varying relationship between SUA and MUA with ongoing power fluctuations in the simultaneously recorded LFP, the Pearson's correlation coefficient was calculated between the average firing rate profiles of the unit activity (PSTH) and the Z-Spectrum of the LFP. In addition, correlation coefficients were calculated for each movie repetition and the values were Fisher Z-transformed (Fisher 1921) to create a near Gaussian distribution. This step corrected for smaller sample sizes used in the short and long movie sessions. As discussed in section 2.2.9, this measure was used to quantify the temporal similarity of the responses (i.e. signal correlation) between the two signals of interest, independent of absolute amplitudes in those individual signals (Reich et al. 2001). In this section of the analysis, the degree of correlation between only the average spiking activity (PSTH) and the LFP was considered, however the calculation between all possible LFP combinations could be conducted. Correlation coefficient values were computed using identical temporal windows (500ms) for each signal type (SUA, MUA, LFP) and the average Z-Spectrum within the gamma (25-90Hz) and sub-gamma (1-15Hz) frequency bands were considered separately. Z-Spectrum values within the frequency range of 55 and 65Hz were removed to eliminate potential biases due to line noise (60Hz) contamination. Since both signal types were estimated using the same temporal window of 500ms and moved in 50ms steps, the resulting signals were relatively smooth estimates. Several temporal windows were used (50-500ms) and the relative differences in the distribution of correlation coefficient values for the gamma and

sub-gamma bands were conserved and the statistically significant differences between the two distributions were also conserved.

3.2.15 Spike-LFP Coherence

To better estimate the degree of correlation between simultaneously recorded spiking activity and the local field potentials, standard multi-taper spike-LFP coherence analysis was conducted (Jarvis and Mitra, 2001; Pesaran et al., 2002). SUA, MUA and LFP spectra were all calculated with a 500 ms window, convolved with 5 Slepian data tapers, that slide across the movie segments at 50ms intervals to obtain a relatively smooth estimate of spike-LFP coherence across time. For each segment of SUA, MUA and/or LFP data, the signal was first multiplied by one of the 5 Slepian tapers and the Fourier transform was calculated.

For continuous data the windowed Fourier transform is:

$$\tilde{x}_k(f) = \sum_{t=1}^{N} w_k(t) x_t e^{-j2\pi ft} ,$$

where x_t $(t=1,\ldots,N)$ is the time series of the signal and w_k $(k=1,\ldots,K)$ are the set of K orthogonal taper functions with appropriate properties.

For point process data (SUA and MUA), the windowed Fourier transform is:

$$\tilde{x}_k(f) = \sum_{j=1}^{N} w_k(t_j) e^{-j2\pi ft} - \frac{N}{T} \tilde{w}_k(0) ,$$

where t_j $(j=1,\ldots,N)$ is the sequence of spike events in the time interval of 0-T and N is the total number of spikes in that time window. $\sim wk(0)$ is the Fourier transform of the data taper at zero frequency.

The multitaper spectral estimate of one time series, $S_x(f)$, is defined as:

$$S_x(f) = \frac{1}{K}\sum_{k=1}^{K}\left|\tilde{x}_k(f)\right|^2 ,$$

and the cross spectrum of the two time-series, x and y, $S_{xy}(f)$, is defined as:

$$S_{xy}(f) = \frac{1}{K}\sum_{k=1}^{K}\tilde{y}_k(f)\tilde{x}_k^*(f) .$$

Finally, given the two time-series, x and y, the multi-taper coherence function, $C_{xy}(f)$, is defined as:

$$C_{xy}(f) = \frac{S_{xy}(f)}{\sqrt{S_x(f)S_y(f)}} .$$

Coherence is a unit-less complex quantity whose magnitude is a function of frequency with values between 0 and 1, and represents the fraction of common variance present between the two time series x and y. A value of 1 reflects correlation between the two signals and 0 reflects no correlation. Coherograms are typically used to illustrate the coherence values and color-coded on a 2-D plot. The band-limited coherogram shown in Figure 3.3.16 represents the coherency between the spiking activity and the LFP on a 2-D grid with integrated coherence values on the ordinate and time on the abscissa. The

frequency grid, 2W is determined by the number of tapers (K) and the data points (N) by the equation 2NW – 1 = K. 95% confidence intervals were calculated using an empirical leave-one-out jackknife estimate of the coherence for each tile, across all tapers and trials (Thomson and Chave, 1991). Specifically, this procedure generates a Z-score by calculating the expected standard deviation of the coherence given the number of degrees of freedom (ν = number of repetitions multiplied by the number of tapers) and transforms the measured coherence so that, under the null hypothesis that the coherence is zero, the transformed coherence is distributed normally with a variance equal to 1 (see Jarvis and Mitra, 2001 and Pesaran et al. 2008 for more details). In addition, the false discovery rate (FDR) was used to correct for multiple comparisons and type 1-error rates within the coherograms (Benjamini and Hochberg, 1995). Tiles within the 95% jackknifed confidence limits and below the FDR cutoffs were excluded from further analysis and summary plots. The LFP signal used to calculate the spike-field coherence was chosen based on the polytrode and tetrode channel containing the maximal amplitude waveform for each spike. The spike-LFP coherence measure described above is however biased by the level of spiking activity, where periods of high firing rate lead to increased coherence, while periods of low firing rate lead to decreased coherence values. Although not explicitly dealt with in this chapter, the issue could be dealt with by generating 1000 Poisson distributed spike trains within a given temporal window while matching the ongoing fluctuations in the actual firing rate to empirically derive a 95% confidence threshold which would account for the firing rate bias in the coherence. However, most this bias is removed by using the combined methods discussed above.

3.2.16 Additional Spiking and LFP Analysis

Spike-triggered spectral analysis, utilizing the identical multi-taper methods described above, was conducted in order to measure the relationship between spiking activity and the putative synaptic inputs (i.e. LFP), and more importantly to investigate potential spike-phase relationships. The rationale for conducting such an analysis was to estimate the potential locking of spike-LFP relationships across the layers of striate cortex and to test the cortical circuit hypothesis of information processing, where the putative flow of information follows the timing of unit activity within the microcircuit (Douglas and Martin, 2004). The result of this analysis was not obvious, even when compared to the randomization of spike times (1000 times), which conserved the spike rates yet abolished spike-LFP phase relationships. In the end it provided little insight into the phase relationship between spiking activity and the LFP that also contains biases induced by the overall firing rates of the units and the underlying assumptions of the circular statistics used (Okun et al., 2010; Vinck et al., 2010). In general, spiking activity in this dataset occurred predominantly around the negative going phase of the LFP, which has been reported by countless studies and can be seen in Figure 3.3.19. More advanced and statistically rigorous methods do exist for such spike-phase analysis (Vinck et al., 2010) and these methods could be employed to potentially gain insights into the circuit level mechanisms of complex sensory processing and enable the tracking of the information flow through the microcircuit. However, given the level of jitter in the spiking output to repeated presentations of natural scenes (Herikstad, et al., 2011), and

the level of heterogeneity observed among neighboring units (Yen et al., 2007), it will be difficult to track the flow of information in the face of such variability.

Multi-taper spectral coherence was also conducted between all LFP signals recorded simultaneously, yet due to the near identical phase structure within simultaneously recorded signals (*see Figure 3.2.1*), this analysis provided marginal utility and just confirmed the expected results, that neighboring contacts contained nearly identical phase and amplitude structure, resulting in average coherence values near 1. There were however notable shifts in coherence within a subset of the polytrode recordings. Common mode averaging, which subtracts the average LFP signal from each individual LFP signal was conducted in order to drop the high level of coherence, yet this approach was abandoned due to computation time and memory limitations, making the approach prohibitive and not feasible given the available resources. Dedicated multi-core processor machines running parallel computations with expanded memory recourses could handle such computations. However, in the end, what would be gained from such analysis is not obvious, since the LFP generally reflects the integration of potentials from a sphere of 300-500um (Buzsaki et al., 2012), and the separation distances between contacts was 25-65um, therefore the initial profiles collected were more or less expected and contributed little to the questions being addressed in this chapter. If the spatial spread of LFP power for particular frequencies were being addressed in this chapter, it would likely be consistent with known striate cortex power spread functions (Leopold et al., 2003).

3.2.17 Global Scene Transitions

As discussed in Section 2.2.4, scene transitions within the movie were a concern and each transition was documented. The largest global changes in screen luminance occurred during the transitions between the movie repetitions and the mean luminance periods, known as the spontaneous activity period, that flanked each movie repetition. These global transitions evoked robust LFP and spiking responses in all four experiments and the average scene transition evoked responses are shown in Figure 3.3.19. Based on the average SUA, MUA and LFP profiles observed during these transitions, a conservative 1000ms of data centered at the onset and offset of the movie presentations, for SUA, MUA and LFP data were excluded from all analysis. Even though robust and reliable activity was evoked during these periods, the transient responses were removed in order to better characterize sustained activity levels during the movie presentations. Scene transitions that occurred during the movie, as described in Section 2.2.4, were not excluded from the data analysis and the average scene transition evoked responses are shown in Figure 3.3.19.

3.3 Results

3.3.1 Summary of Data Collected

Broadband multichannel electrophysiological data was collected from the striate cortices of four adult male cats (2.5-5.5kg), who were anaesthetized and paralyzed, while visually presented with a set of simple and more complex stimuli, including flashed full-field black to white screen transitions, sparse black and white spots, sparse black and

white oriented light bars, drifting sine-wave gratings, and time-varying natural scenes. A total of 21 polytrode (*see Section 3.2.3 for details*) and 20 tetrode (*see Section 2.2.2 for details*) penetrations were conducted across the four animals. Only 10 polytrode and 11 tetrode recordings provided quality unit and local field potential data. Half of all penetrations resulted in unit activity with low signal-to-noise ratio or neural "hash", which consisted of high frequency noise elevations during visual stimulation. Following these "hash" penetrations, the cortical surface and probe were inspected, and in the majority of these penetrations, either excess blood or fluid had accumulated at the penetration sit or the delicate silicon probe had bent or was broken, most likely due to a thicker than expected layer of pia matter. These penetrations were noted and then abandoned for new recording locations. The resulting 21 combined polytrode and tetrode recording locations yielded high-quality broadband signals and single-unit (SUA), multi-unit (MUA) and LFP responses were then analyzed from 22 short movie sessions, (30-40 second segments, repeated 100 times) and 15 long movie sessions, (6 minute segments, repeated 5-10 times). Although not the focus of this chapter, broadband signals were collected during the presentation of drifting sine-wave gratings (*see Section 3.2.8*) and sparse spots and/or light bars (*see Section 3.2.9*) at most recordings sites, in addition to the natural scenes, however analysis conducted on the responses to these stimuli will not be included in this chapter. The quality of the neurophysiological recordings, in terms of the unit signal-to-noise ratio, LFP amplitudes, 60Hz line noise, and overall unit responsiveness to the natural scenes varied greatly within and across recording sites. As in Chapter two, a conservative responsiveness threshold level (*see Section 2.2.7 for*

details) of 20 was used to exclude unreliable and/or unresponsive unit activity from the movie dataset. This resulted in a population of 110 single and 193 multi units recorded during the short movies and 170 single and 122 multi units recorded during the long movies. This subset of unit activity was used in all subsequent analyses. The discrepancy between the total units collected, 303 (SUA/MUA) for the short movies and 292 (SUA/MUA) long movies reflects the lack of stability in several recording sites and/or the use of multiple short movie segments at several recording sites and lack of use of the long movies at several recording sites.

As stated before, the primary experimental goal of this chapter was to densely sample spiking and local field potential activity across all layers of cat striate cortex during controlled visual stimulation in order to obtain a better understanding of the neurobiological significance of heterogeneous unit activity and its relationship to power fluctuations in specific frequency bands recording within the local field potentials and to characterized these relationships across all layers of the striate cortical microcircuit. The primary analytical goal of this chapter was to characterize population activity and to look for relationships, in terms of co-occurrences and strength, between the larger population of spiking neurons and specifically power fluctuations within gamma frequency band (25-90Hz), relative to the cortical microcircuit. However, several experimental and analytical limitations precluded these goals. Regardless of the limitations, novel results discussed in this chapter do originate from the analysis of population activity occurring within the cat striate cortex during repeated presentations of both short and long segments of time varying natural scenes.

In general, significant elevations in spiking activity, SUA and MUA, tended to co-occur and co-vary during enhancements of gamma frequency band (25-90Hz) power recorded within local field potentials. This enhancement predominantly occurred within the upper layers of the striate cortex, consistent with past investigations (Gray and McCormick, 1997), but was not exclusive to the upper layers. There was a high degree of variability in this general trend when surveyed across the dataset, and several recording locations exhibited enhanced spiking and LFP power fluctuations within the sub-gamma band (1-15Hz), counter to the expected result and general observation. Yet overall, significant enhancements in spiking activity and LFP power within the gamma band co-occurred and co-varied within the cat striate cortex during the presentation of time-varying natural scenes. Qualitatively, these patterns of spike-LFP coactivity varied greatly across the cortical microcircuit and throughout the movie presentations. To demonstrate the recording preparations used in this chapter, Figure 3.3.1 portrays several schematics of the silicon polytrode and tetrode probe types used and the ideal positioning of the polytrode within the cat striate cortex, based on histological confirmation (see Section 3.2.4 for details). Note the number of recording contacts on each probe type and the fixed spacing between contacts, ranging from 25 to 56um. Compared to the tetrode probes, the overall length of the polytrode was scaled to span all layers of cat striate cortex (Payne and Peters, 2002). In principle, the polytrodes would provide a denser sampling of activity with a fixed geometry between recording contacts and result in the simultaneous capture of spiking activity from multiple single and multi-units along the parallel arrays of contacts, as well as an oversampling of the local field potentials as

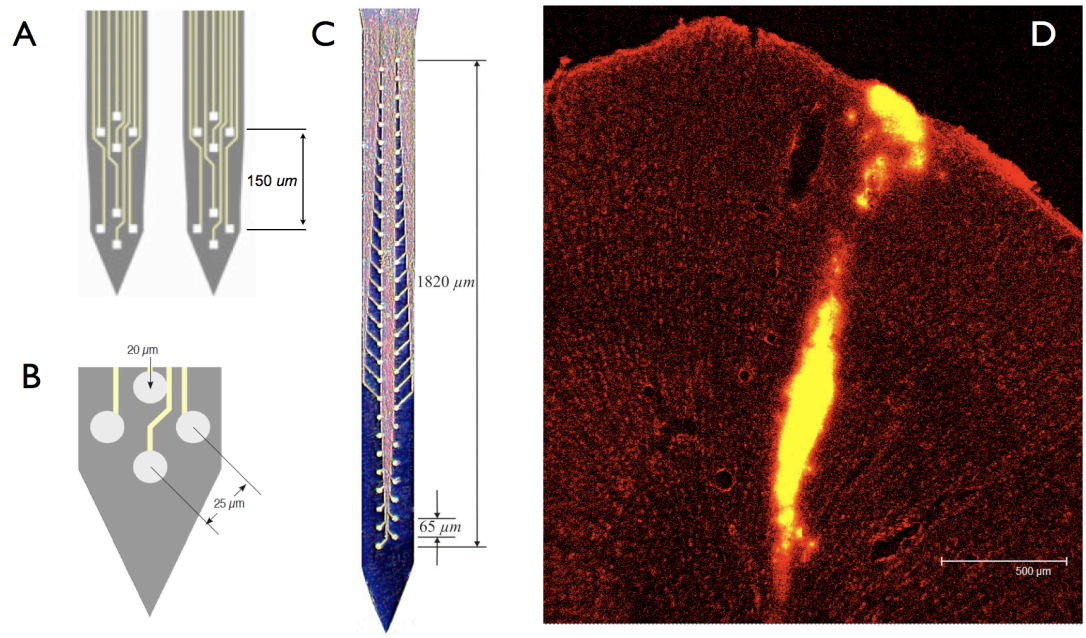

Figure 3.3.1 Schematics A-C illustrate the multicontact silicon probes used in this chapter. The upper image (A) is of the 16 contact 2x2 'tetrode' probe and the lower image (B) illustrates the tetrode arrangement of four contacts and their spatial arrangement. The middle image (C) is of the 54 contact 'polytrode' probe. Note the parallel and staggered arrangement of the contacts and the relative difference in scale between the tetrode and polytrode probes. Individual contact impedances on both probe types ranged from 0.1 to 1.5MOhms. (D) The confocal image illustrates the optimal position of the polytrode probe in relationship to the striate cortex in one of the recovered recording sites.

shown in figure 3.2.2 and 3.3.11. The oversampling of spike waveforms and resulting overlap of near synchronous firing of simultaneously recorded units posed a significant problem for conventional multicontact spike sorting routines, which was only partially solved (see Section 3.2.6 for details). However, single unit activity extracted and sorted from the polytrode recordings were well isolated and only units passing strict interspike interval and cross-correlation criterion were included in this dataset. Numerous multiunit activity clusters were also included in the datasets containing single units. Several polytrode recording sites yielded high SNR spike waveforms and responsive spiking and

LFP activity, yet the final isolation of single units became problematic when employing the currently available methods. These recordings were deemed entirely multiunit (*see Section 3.2.5*) and likely resulted in the oversampling of unit activity, which will skew the population results. However, when MUA was excluded from the final dataset, the general overall findings and results were not changed.

3.3.2 Spiking Activity during Natural Scene Stimulation

Unit activity recorded with the polytrode and tetrode probes in this chapter displayed similar response profiles, in terms of responsiveness, sparsity and heterogeneity, compared to the population dataset presented in chapter 2. The majority of unit activity consisted of sparse, brief epochs of reliable increases in firing rate that punctuated the low baseline firing rate that usually persisted throughout the time coarse of both the short and long movies presented. Several well-isolated single units simultaneously recorded from two separate polytrode recording sites are shown in Figure 3.3.2, to illustrate the reliability and sparsity of the spiking activity among closely spaced units. In addition, the level of heterogeneity, in terms of maximal firing rates and timing, is quite high and remarkably similar to the data presented in chapter 2. Yet the similarity in neighboring unit activity, along the length of the polytrode, tended to be significantly higher than the level of heterogeneity for neighboring units reported in chapter 2 (*see Figure 2.2.7 for a comparison*). The polytrode recordings oversampled unit activity and attempts were made to sort individual units from these recordings (*see Section 3.2.5 and 3.2.6 for details*), however, due to instability in the recordings, uncontrolled fluctuations

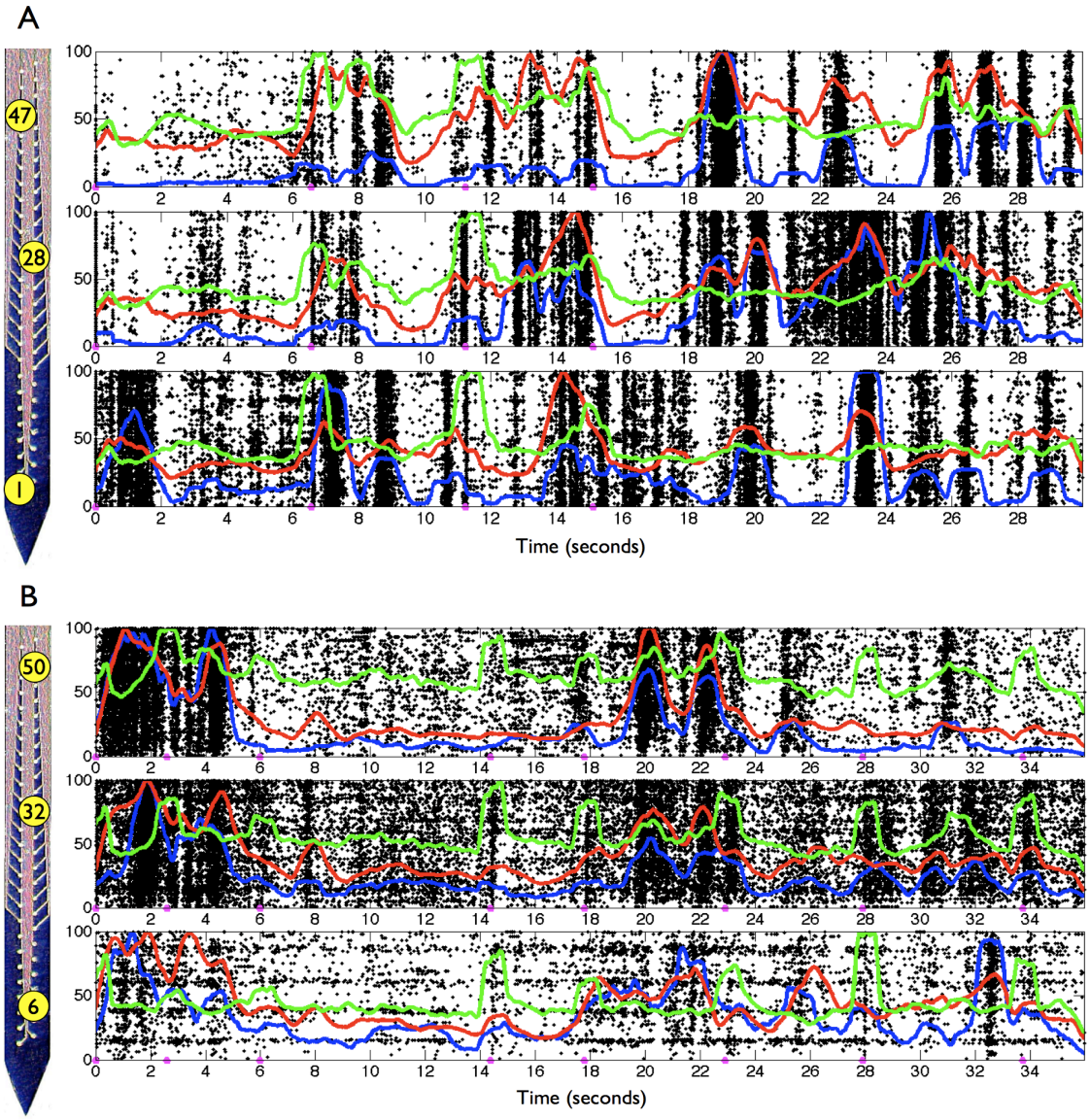

Figure 3.3.2 Single unit activity recorded in cat striate cortex using silicon 'polytrode' probes during two short movie presentations. (A) Rastergrams of 3 single units recorded from channels 1, 28 and 47 of the polytrode during a 30 second short movie scene repeated 100 times. PSTHs of the corresponding single units are shown in blue and the average integrated power with in the gamma (25-90Hz) and sub-gamma (1-15Hz) bands are shown in red and green respectively. A single sliding temporal window (500ms, 50ms steps) was used to construct each of the three traces and all three are normalized to better illustrate the dynamic nature of each. (B) Rastergrams of 3 single units recorded from channels 6, 32 and 50 of the polytrode during a 36 second short movie scene repeated 100 times. Activity in B was recorded from a separate animal. Scene transitions within the movie are marked with small magenta triangles along the time axis.

in the anesthesia level and the attempted application of existing spike sorting techniques to extract well-isolated units from the polytrode signals; each of these issues at some level precluded reliable unit separation and therefore conclusions resulting from the spiking activity recorded from the polytrode data contain this caveat and should be interpreted appropriately. Given these issues, it was not possible to thoroughly study the level of heterogeneity among neighboring units, as a function of cortical layer. As a primer, the integrated power within the simultaneously recorded LFP, for both the gamma (25-90Hz) and sub-gamma (1-15Hz) bands are displayed atop the spiking activity to visually illustrate the degree of co-variation among the spiking and LFP signals. Note the degree of correlation between the PSTH and the two LFP frequency bands. The dynamic relationship between theses two signals is further explored and quantified in Section 3.3.4. Scene transitions within the movie segments are also marked throughout this chapter in order to highlight the transiently evoked responses, in both spiking and LFP activity, to each scene transition. Average evoked responses to these scene transitions are elaborated on in Section 3.3.5. Overall, unit activity was robust modulated throughout the movie presentations, exhibited periods of significant elevations in firing rate, which punctuated the low baseline firing rates for most units recorded. These bursts of activity were, for the majority of recording sites, reproducible in amplitude and timing across repeated presentations of the movies. These findings are all consistent with the firing rate profiles of unit activity reported in chapter two, figure 2.3.9.

The reproducibility of unit responses to both the short and long movies was quantified using the same responsiveness criterion established in chapter two, section

2.2.7. A wider range of responsiveness values was observed in this dataset (*for the comparison, see Figure 2.2.3*) and the spread is skewed to both the ends of the spectrum for units recorded during the short movies, although the skew to higher responsiveness values for the long movies is consistent with the data presented in see Figure 2.2.3. The larger proportion of low responsiveness values in the short movie distribution was due to the higher number of MUA units included in the initial dataset. A conservative responsiveness threshold of 20 was used to eliminate a subset of the low responsive units and all other analysis was conducted with the residual dataset. The distributions of responsiveness values for both the short and long movies demonstrate that a large number of units were selective in their response to the movies presented.

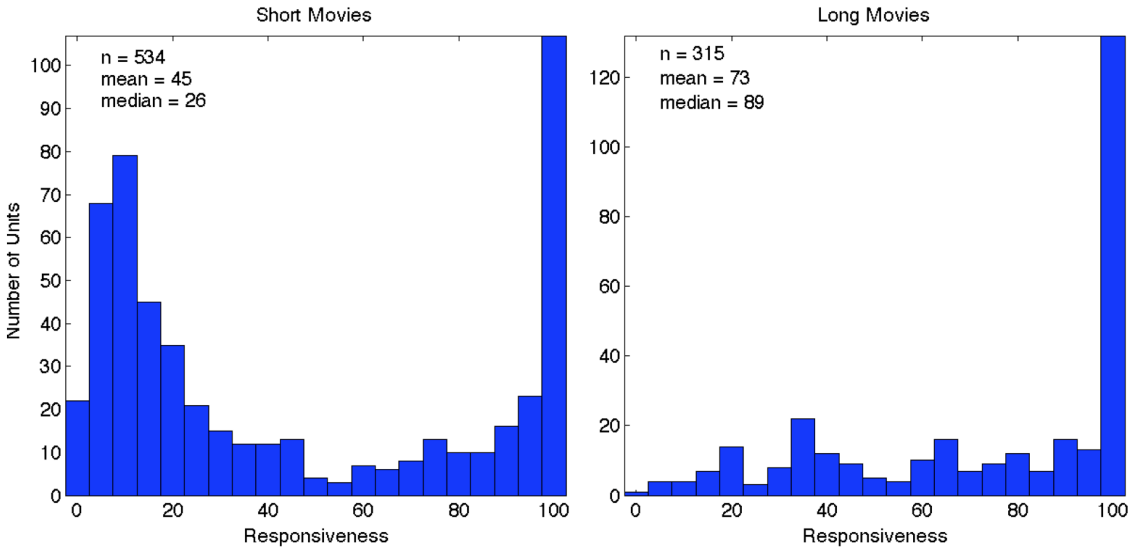

Figure 3.3.3 Distribution of the responsiveness values for all unit activity collected during the short and long movies. A conservative responsiveness threshold of 20 was used to exclude low responsive units from the final dataset, resulting in 303 SUA and MUA short movie responses and 292 SUA and MUA long movie responses.

The selectivity of the responsive units was quantified using the same sparsity (*S*) measure applied in chapter two, section 2.2.8. The distribution of sparsity values for both the short and long movies are presented in Figure 3.3.4 and based on the rightward skew of the distributions, these data, in addition to the data presented in chapter two, Figure 2.2.5, is evidence that directly supports the principles of the sparse coding hypothesis (Olshausen and Field, 2004) where individual unit activity is highly selective in terms of firing rate responses when presented with time-varying natural scenes. Not only were a majority of the units responsive to the movies presented, they were also highly selective in their responses to particular sub-sections of the movies. A mean sparsity of 66 and median of 73 for the short movie distribution is slightly lower than the mean of 88 reported in chapter 2. This is due to the addition of MUA in the dataset that contain a mixture of potentially heterogeneous unit activities, which would result in overall increased firing rates, durations and lower selectivity. A mean sparsity of 77 and median of 88 for the long movie distribution is significantly higher (2-sample KS test, p=4.4e-08) than the short movie distribution and likely due to the fact that the long movies were 12 times the duration of the short movies. As reported in Chapter 2, significant elevations in firing rate during the movies were brief and rare for a majority of the units examined. These firing rate 'events' were also brief and rare during both the short and long movie presentations when using the same criterion in Section 2.2.10. The average 'event' length during the short movie sessions was 92ms, ranging from 10 to 2105ms in duration and the average probability of observing these events during the short movies was 0.12, ranging from 0.01 to 0.44.

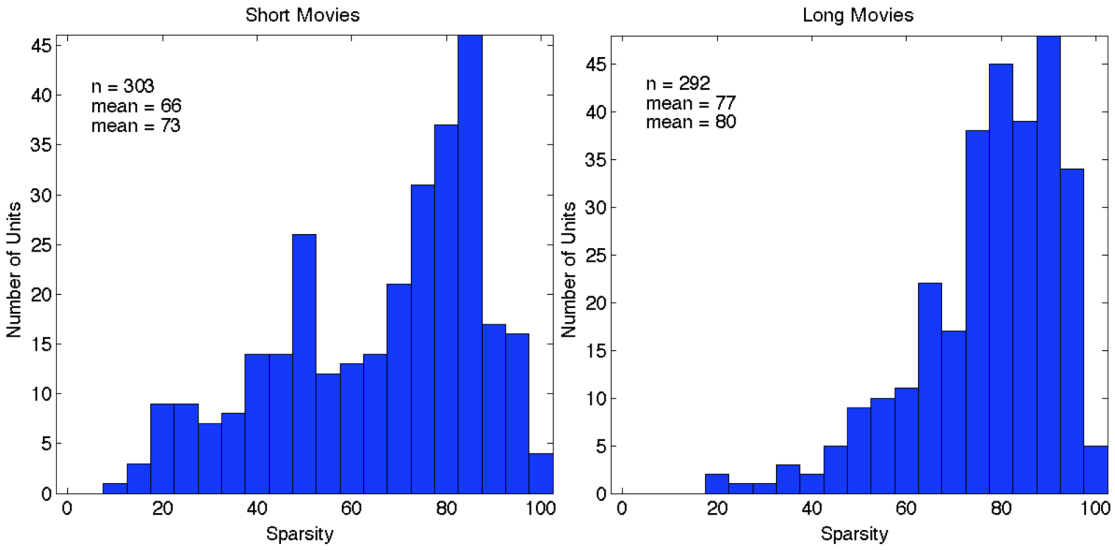

Figure 3.3.4 Distribution sparsity values for all responsive unit activity recorded to both the short and long movie presentations. Note the rightward skew in both distributions.

The average 'event' length during long movie sessions was 27ms, ranging 10 to 915ms in duration and the average probability of observing these events during the long movies was 0.06, ranging from 0.005 to 0.40. The distribution of short and long movie 'event' lengths and probabilities were significantly different (two sample kstest, $p<0.01$). However, the lower probability of observing events during the long movies was expected, given the sparsity and selectivity of unit activity in the striate cortex during natural scenes. Overall the majority of unit responses were reliable across stimulus repetitions and significant firing 'events' were brief and sparse during both the short and long movies.

In addition to the paucity of firing and high degree of response selectivity exhibited by individual units, neighboring units within the striate cortex often displayed large differences in terms of response amplitudes, timing and firing rate profiles during

natural scene stimulation (*see Figures 2.2.7-10*). In order to assess the level of similarity among simultaneously recorded units, as was done in chapter 2, signal correlation (Reich et al. 2001) analysis was computed at the pair wise level on the PSTH signal for all simultaneously recorded responsive units. The resulting distributions for both short and long movie responses are shown in Figure 3.3.5. Both distributions are skewed more to the right than those reported in chapter 2, and both have higher mean signal correlations, 0.32 and 0.25, compared to ~0.2 for the units in chapter 2, see Figure 2.2.7 for a direct comparison. This somewhat contradictory result is most likely due to the inclusion of multiunit activity into the dataset and secondly due to the denser sampling of unit activity in the polytrode recordings. In addition, the inclusion of multiunit activity into the dataset does contribute to the increase. Each distribution was significantly different from a normal distribution (Lillifores test), yet the distributions were significantly different from each other (2-sample KS test $p<0.01$). Interestingly, the distribution of signal correlations during the long movies more closely resembles the distribution of units to the short movies shown in Figure 2.2.7, while the short movie distribution in this dataset was significantly skewed to higher values. This result may be confounded by the correlation metric used, given the duration of the long movies (5 minutes) compared to the short movies (30-40 seconds). Alternatively, response correlation among simultaneously recorded units may naturally decrease as the response space, in terms of firing rate distribution and timing, is explored during the increased exposure to lengthier natural scene segments.

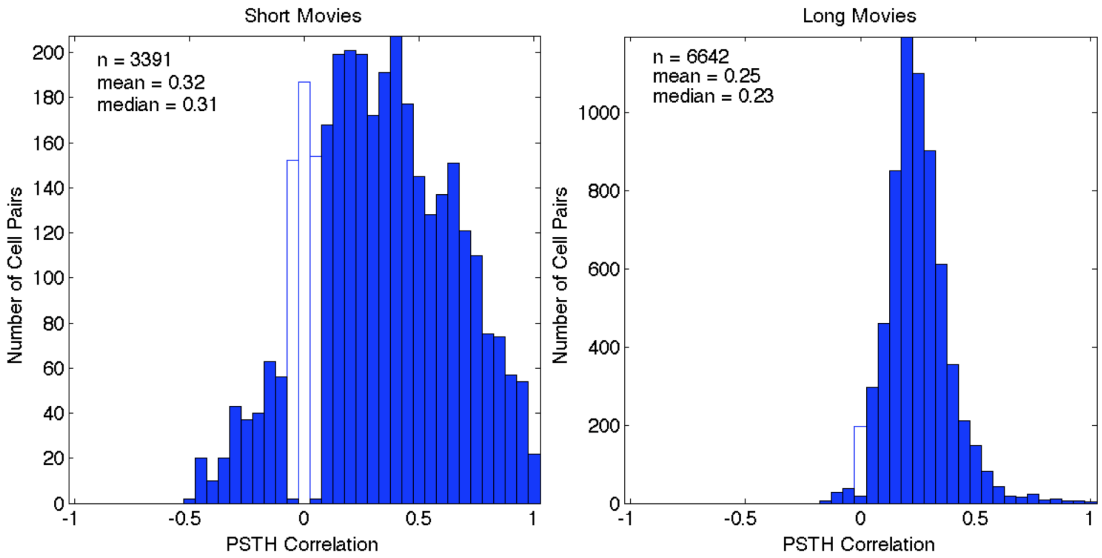

Figure 3.3.5 Distribution of pair-wise PSTH correlation values for all responsive units recorded during the short and long movie presentations. Significant correlation values ($p>.05$) are shown as filled bars in the histograms. Note the number of pair-wise comparisons in both distributions, 3391 in the short and 6642 in the long movies.

To appreciate the contribution of the polytrode data to the higher average signal correlations in both the short and long movies, the signal correlations for the responsive units recorded at each polytrode recording site are shown in Figures 3.3.6 and 3.3.7 for both the short and long movie sessions, respectively. Pair wise signal correlations were calculated for all possible unit pairings and are plotted relative to the location of the polytrode contacts, where values plotted at the top left corners represent the uppermost contacts of the polytrode and values plotted at the bottom right corners represent the lowest contacts. Each polytrode penetration sampled activity along the length of the probe, however not all polytrode recording sites afforded quality unit activity at all active contacts, hence the uneven number of responsive units displayed for each recording site. In addition, multiunit activity was collected along with single unit activity, therefore

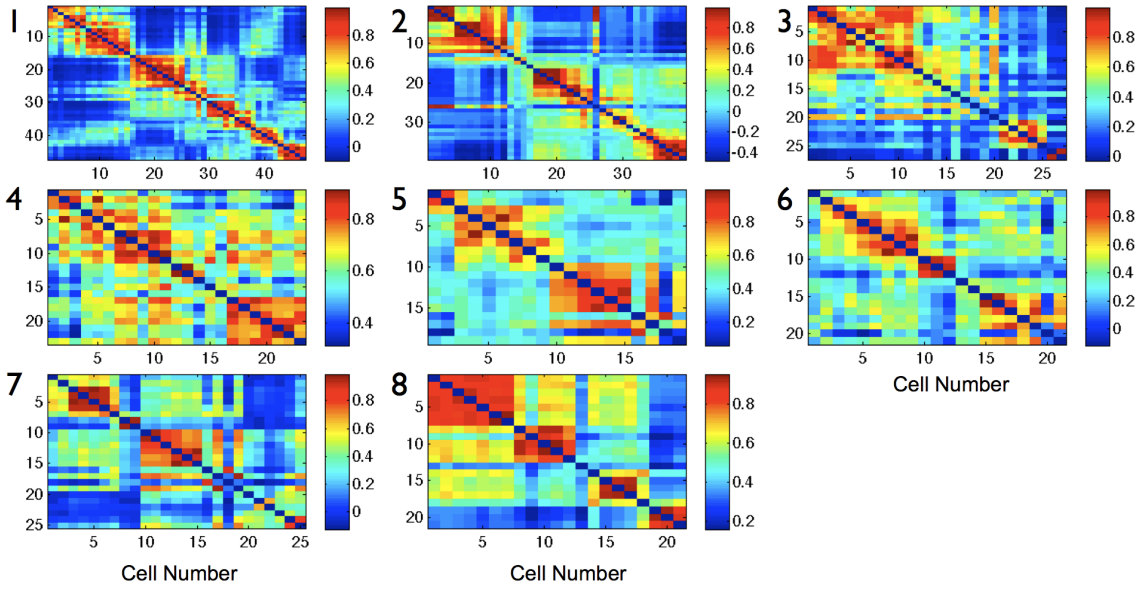

Figure 3.3.6 Pair-wise PSTH correlation values for all responsive units recorded at each polytrode recording site during the short movie sessions. The color-coded bar to the right of each plot indicates the level of signal correlation. Unit activity sampled from the upper contact of the polytrode is shown in the upper left corner and unit activity sampled from the lower contact is shown in the bottom right corner of each plot.

oversampling of activity becomes a potential confound. However, given the level on inconsistencies among recording sites, there are several notable consistencies among the short and long movies. Neighboring units recorded along the length of the polytrode had very similar response profiles, illustrated by the high signal correlations along the diagonals in each plot, most notably in sites 1, 2 and 4 in Figure 3.3.6. Nearly all sites contained small clusters of units that had similar response profiles to the movies presented, with the only exceptions being sites 2 and 3 in Figure 3.3.7, which exhibit a higher degree of heterogeneity, with the addition of unexplainable strip patterns. The clustering of high signal correlations among neighboring units is most likely due to the oversampling of unit activity across the large array of polytrode contacts and the

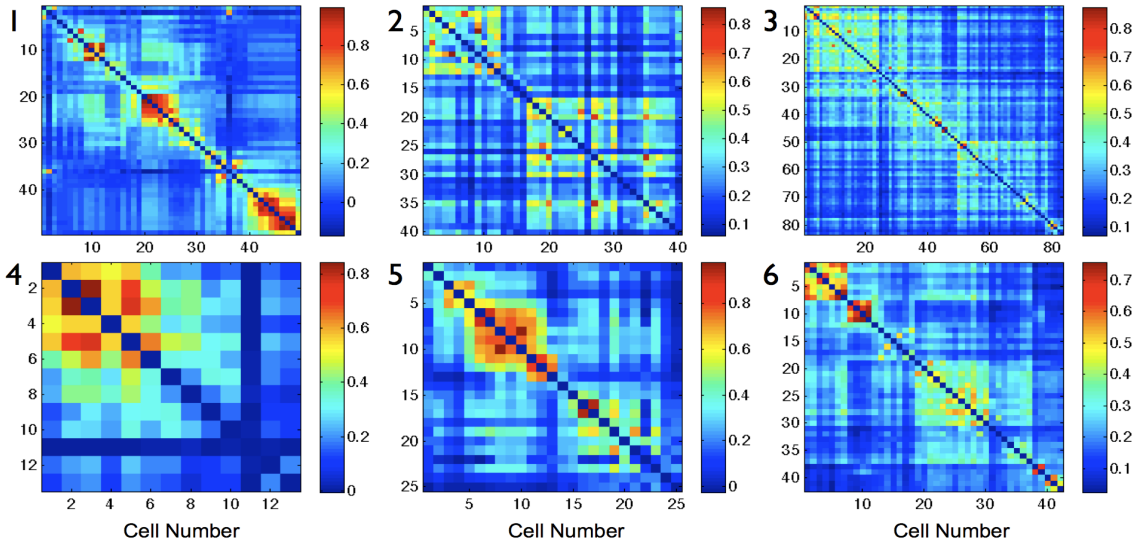

Figure 3.3.7 Pair wise PSTH correlation values for all responsive units recorded at each polytrode recording site during the Long movie sessions. The color-coded bar to the right of each plot indicates the level of signal correlation. Unit activity sampled from the upper contact of the polytrode is shown in the upper left corner and unit activity sampled from the lower contact is shown in the bottom right corner of each plot.

subsequent inclusion of a greater number of multiple units. This also raises concerns regarding the spike sorting methods employed to deal with the high-dimensionality of the polytrode data (see Section 3.2.6). However, these clusters of cells exhibiting similar firing profiles tend to occur more often in the uppermost contacts of the polytrode, which corresponds to activity recorded from with the upper layers of striate cortex. Histology confirmed a near normal penetration angle for polytrode sites 2, 3, 6 and 8 (Figure 3.3.6) and sites 3 - 6 (Figure 3.3.7). Even though the majority of these polytrode recordings sites contain a large degree of correlated activity among the units recorded by the upper contacts, there are exceptions to this general observation, where clustering also occurred in the lower contacts. Interestingly, there are several examples, in both the short and long movies, of high signal correlation far off the diagonal, indicating correlated activity

across the layers of cortex. The vast majority of pair wise signal correlations between neighboring units recorded from the polytrode sites are inconsistent with the data presented in Chapter 2, however there are many examples of heterogeneous firing profiles among neighboring units. Perhaps if more stringent spike sorting methods were employed and/or higher quality activity is acquired in future experiments, the underlying question of response heterogeneity and how it tracks across the striate cortical microcircuit could be better addressed.

3.3.3 Local Field Potential Activity during Natural Scene Stimulation

A systematic characterization of the local field potentials recorded during both the short and long movie presentations, along with the spontaneous activity periods that following each movie segment (measured in the absence of visual stimulation), were conducted using standard multi-taper methods. The average power spectrum for each active channel and recording session was calculated (*see Section 3.2.10-11 for details*). Figures 3.3.8 and 3.3.9 show the average power spectrums for the 22 short movie and 15 long movie sessions, respectively. The majority of short and long movie sessions contain a significant increase in the overall power at frequencies ranging 20 to 100Hz, during the movie (blue traces) periods compared to the spontaneous periods (red traces). The average power spectra for all active probe channels are shown. Short movie sessions 6 and 7 and long movie sessions 3 and possibly 9, are exceptions to this general trend. The separation in power between 20 and 100Hz was not uniform for all recording sites and not all active channels exhibit this separation.

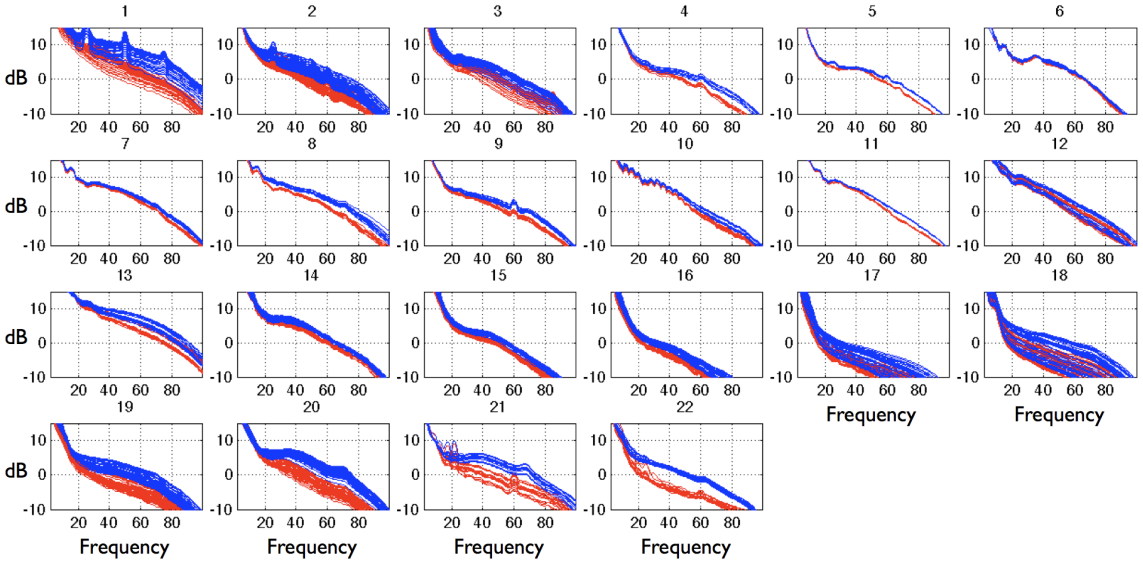

Figure 3.3.8 The average log power spectra of the local field potential for all active channels recorded during the short movie presentation shown in blue. The average log power spectra of the corresponding spontaneous activity periods are shown in red. All 22 recording sessions are displayed. A residual spectral peak at 60Hz corresponds to powerline artifact. The large spectral peak at 25Hz in sessions 1 and 2 correspond to LFP locking to the movie frame rate of 25 frames per second. The dB axis has been truncated to better visualize the separation in spectral power at the higher frequencies.

Short movie sessions 1, 2, 3, 12 13, 17, 18, 19 and 20 exhibit larger variability in the overall power (5-10dB) within the gamma frequency range during the movie presentation compared to the spontaneous period (Figure 3.3.8). This 5-10dB spread in spectral power within the gamma frequency range is also present within long movie sessions 1, 12, 13 and 14 (Figure 3.3.9). This spread of spectral power among closely space contacts is even more prominent throughout the movie session and is not well captured in these averages of power. In addition, the peak power within the gamma frequency range varied considerably across the recording sessions and more interestingly throughout the movie presentations. Peak gamma frequency power during the short movies ranged from 25 to 67Hz with a mean of 38Hz and during the long movies it ranged from 25 to 72Hz with a

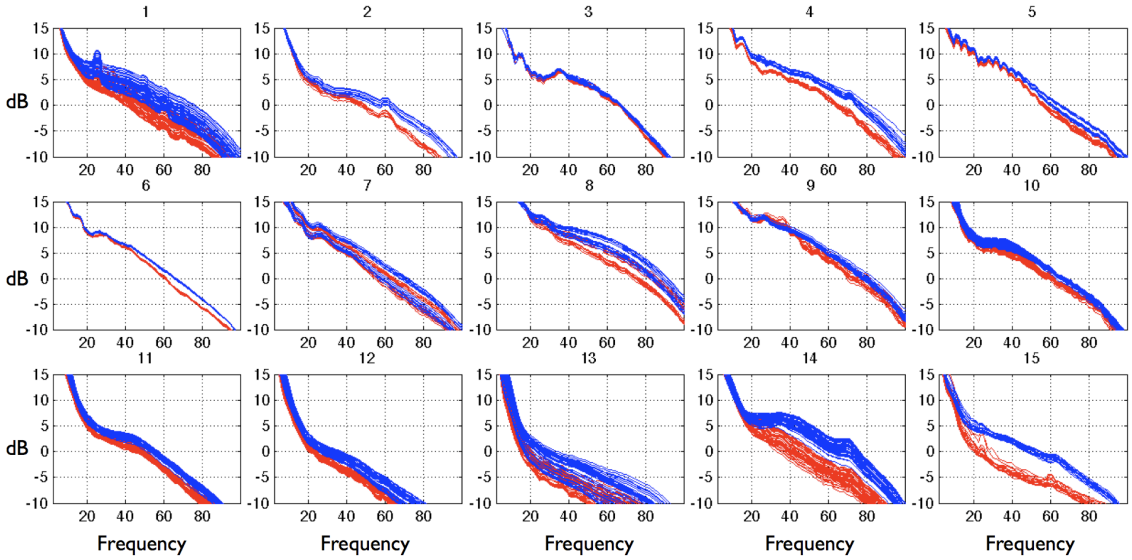

Figure 3.3.9 The average log spectra of the local field potential for all active channels recorded during the long movie presentations (n=15) are shown in blue. The average log spectra for the corresponding spontaneous activity periods are shown in red. A residual spectral peak at 60Hz corresponds to powerline artifact.

mean of 34Hz. Interestingly, the distribution of peak power was heavily skewed toward 25Hz, identically to the frame rate of the movies presented. Spectral power within the lower frequency range of 1-15Hz significantly overlapped between the movie and spontaneous periods in all recording sites. These general profiles of LFP power are consistent with previous studies (Frien et al., 2000; Henrie and Shapley, 2005; Belitski et. al., 2008) where LFP power within the gamma frequency band has been shown to be significantly higher during periods of visual stimulation compared to spontaneous activity periods. In order to quantify the observed separation in LFP power during the movie and spontaneous periods, the Z-transform of the LFP was calculated (see section 3.2.12 for details). When Z-transformed, the separation is most prominent within the gamma frequency band compared to the sub-gamma frequency band and Figure 3.3.10 illustrates

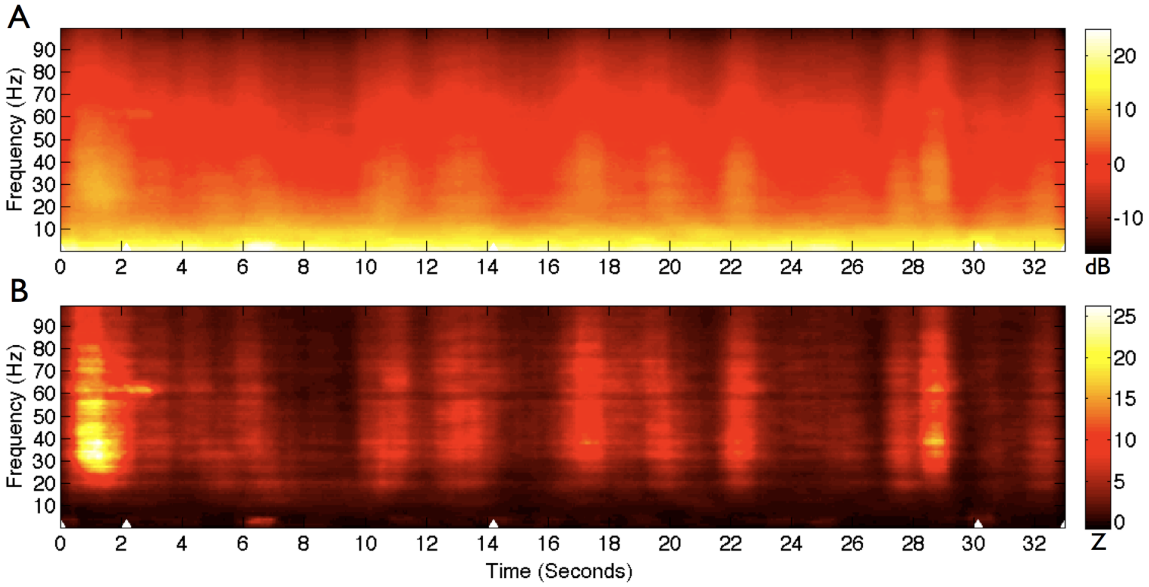

Figure 3.3.10 (A) Average spectrogram of LFP power for all active tetrode contacts during the presentation of a 33 second short movie, repeated 100 times. The colorbar to the right of the figure indicates the power level in dB. (B) Average Z-transformed spectrogram of the data shown in A. The colorbar to the right of the figure indicates the normalized Z score of the dB power shown above in A. Note the enhanced separation in the higher frequencies ranging from 20 to 100Hz. The continuous horizontal band of lower Z values at 60Hz corresponds to residual powerline noise. White triangles plotted along the lower axis indicate scene transitions within the movie.

the dynamics of this separation during the movie presentation. Large power fluctuations within the gamma frequency range (10-15 dB) are observed throughout the movie presentation and become most visible when converted to a Z-score (Figure 3.3.10B). Compared to the gamma band, power within the sub-gamma frequency range (1-15Hz) was quite stable throughout the movie presentation. Significant increases in the sub-gamma band power during scene transitions in this example short movie session were quite low compared to other recording sessions (see Figure 3.3.11B). The absolute level of separation (Z scores > 25) between the sub-gamma and gamma bands within this example session (data from Figure 3.3.8, session 22) is not representative of the entire

dataset, yet it does illustrate the overall trend across movie sessions, where power within the gamma band fluctuates significantly throughout the movie presentation. The range of maximum average Z-scores within the gamma band during the short movies (n=22) was 0.5 to 35 (mean = 7.5) and within the sub-gamma band the range of average Z-scores was 0.2 to 10.6 (mean = 2.6). The range of maximum average Z-scores within the gamma band during the long movies (n=15) was 1.7 to 50.8 (mean = 13) and within the sub-gamma band the range of average Z-scores was 0.15 to 22.6 (mean = 6). The wider range and higher average Z-scores for the long movies likely results from a lower number of stimulus repetitions. However, the distribution of peak and average Z-scores within the gamma band, for both short and long movies, is significantly greater than those in the sub-gamma band. The range of average Z-scores not only varied across recording sessions but also between probe channels recorded simultaneously. Figure 3.3.11 illustrates this variability by illustration the average Z-scores for both the gamma band (shown in subplot A) and sub-gamma band (shown in subplot B) during a short movie session where the polytrode sampled activity uniformly across the layers of cortex and was placed normal to the cortical surface. The range of maximum average Z-scores across the polytrode was 18.6 to 35 in the gamma band and 1.2 to 2.6 in the sub gamma band. The larger spread in Z-scores within the gamma band highlights the greater dynamics present within this frequency range and illustrates the variability across the layers of cortex, as clearly seen at time points 1-5 seconds and 20-22 seconds in Figure 3.3.11A. Interestingly, there is a clear separation in the gamma power across the layers,

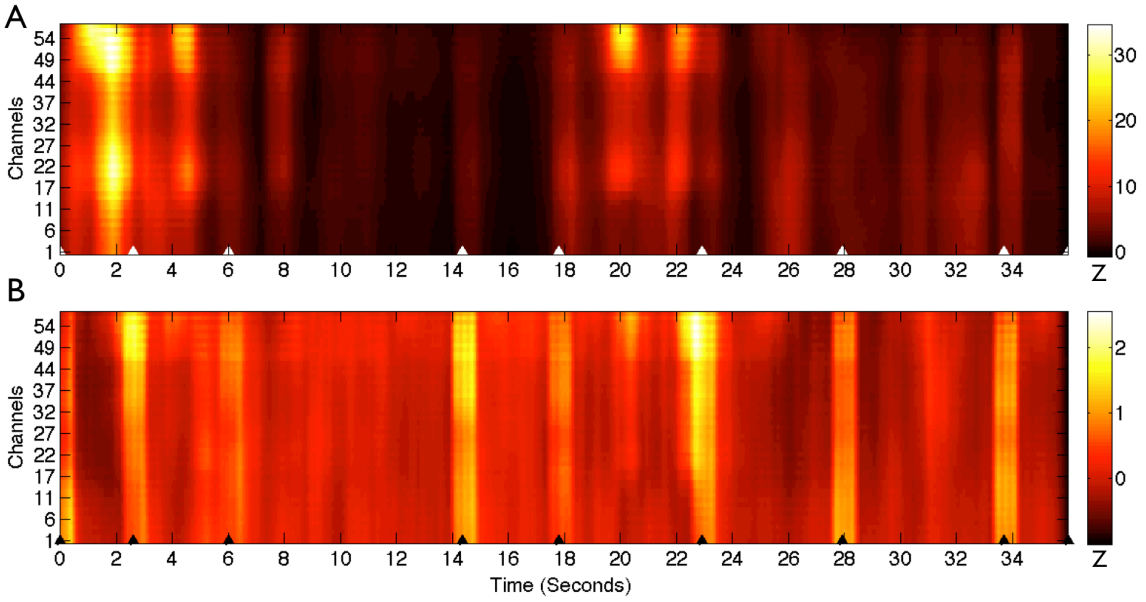

Figure 3.3.11 (A) Average Z-transformed spectrogram, within the gamma frequency range (25-90Hz) for all active polytrode contacts during the presentation of a 30 second short movie, repeated 100 times. The colorbar to the right of the figure indicates the Z score. White triangles along the time axis indicate scene transitions. (B) Average Z-transformed spectrogram, within the sub-gamma frequency range (1-15Hz) for all active polytrode contacts during the same short movie. Note the range of Z scores between A and B. Black triangles along the time axis indicate scene transitions.

which loosely corresponds to the input layer 4 of striate cortex, although the spread of LFP power is considered to be quite broad, ranging 300 to 500um (Buzsaki et al., 2012). The higher spatial spread in the sub-gamma band Z-scores indicates a more uniform spread of low frequency power and the range of Z-scores within the sub-gamma band indicates lower variability throughout the movie and across the layers of cortex. As eluded to before and which is quite appreciable in this example, the upper layers do exhibit the highest power fluctuations within the sub-gamma band that tended to co-occur with scene transitions in the movie, indicated by black triangles along the time axis (Figure 3.3.11B). Across the entire dataset, during both short and long movie sessions,

the spread of average Z-scores was significantly greater in the gamma frequency band and displayed a lesser degree of uniformity among the probe contacts when compared to the sub-gamma band. Several attempts were made to track the dynamics of these two bands across both space and time using the Z-score as a metric (*see Section 3.2.11-12*), but due to variability among recording sessions and adequate statistical rigor, only descriptive statistics are given in this chapter. The above example highlights this failed attempt. If a Z-score of 2 is used as the threshold for significance in elevated gamma band power, then the entire space time plot in Figure 3.3.11A would be considered significant, in contrast only a select number of periods within the sub-gamma band would be considered significant in Figure 3.3.11B. However, new methods (Sullivan et al., 2011, *see Section 3.2.13 for a description*) could be employed to better capture the spatial and temporal dynamics of gamma frequency power as it fluctuates during the movie presentation. In general, significant elevations in both frequency bands were observed during the movie presentations, however the greatest variability, in terms of power fluctuations across space and time was observed within the gamma frequency band.

3.3.4 Dynamics of Spiking and Local Field Potential Activity

One of the goals in this chapter was to investigate the dynamics between spiking activity (SUA and MUA) and the concurrent power fluctuations within the local field potentials (LFP) recorded simultaneously within the cat striate cortex during the presentation of time-varying natural scenes. Since both signals exhibited a large degree of variability in terms of amplitude (i.e. firing rates and power) and temporal dynamics

throughout the movie presentation is quantifying the level of co-engagement between the two signals was done by first calculating the Fisher corrected Pearson correlation coefficients between the average responses (PSTH and band limited average) for both signals (*see Section 3.2.14 for details*) and second through spike-LFP coherence analysis to estimate finer temporal relationships between the timing of individual spikes and specific frequencies within the LFP (*see Section 3.2.15 for details*). Figure 3.3.2 displays several examples of single units recorded across the polytrode for two recording sites, along with the average firing rates (PSTH) and integrated power within the gamma (25-90Hz) and sub-gamma (1-15Hz) frequency bands. Through careful inspection, the firing rate profiles for each unit exhibited a higher degree of correlation, in terms of temporal modulations in amplitudes, with power fluctuations in the gamma band compared to sub-gamma band.

A Fisher corrected Pearson correlation coefficient calculation was used to quantify these observations across the entire dataset, between responsive units and their corresponding LFP, for both short and long movie presentations. The distribution of those correlations calculated between the PSTH and the average power within the gamma (blue distributions) and sub-gamma (red distributions) frequency bands during the short movie sessions are shown in Figure 3.3.12 and during the long movie sessions in Figure 3.3.13. The average correlation between the PSTH and gamma frequency band was 0.37 for the short and 0.32 for the long movie sessions while the average correlation for sub-gamma frequency band was 0.1 for the short and 0.11 for the long movie sessions. The distributions of correlations in the gamma band, for both the short and long movie

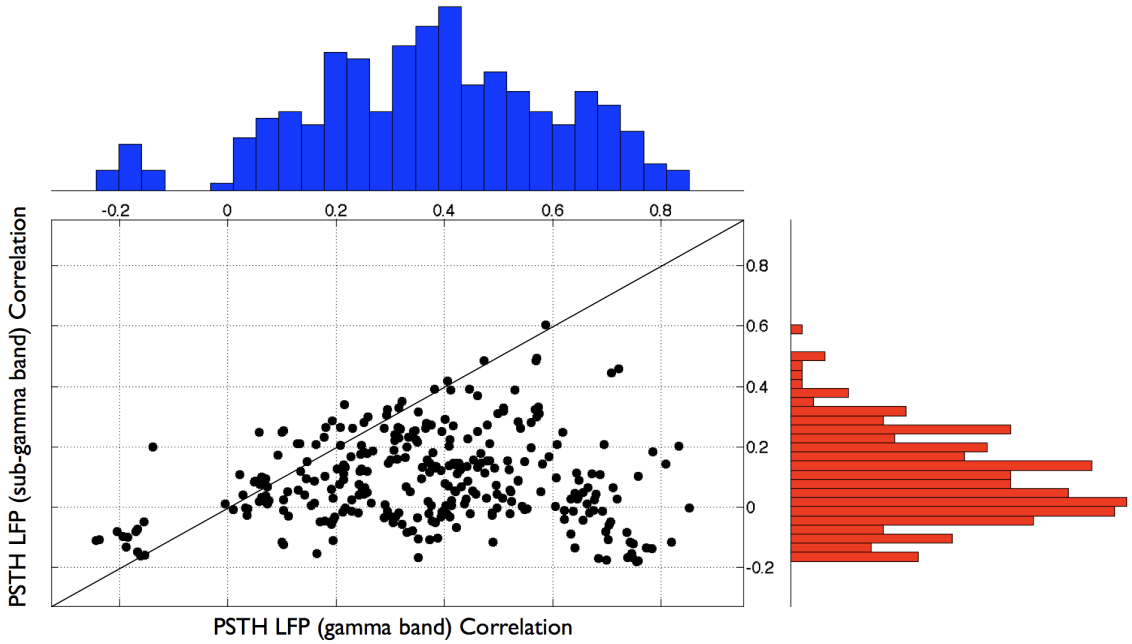

Figure 3.3.12 Scatterplot and histograms of Fisher correlation coefficients calculated between the spiking activity (PSTH) and the sub-gamma (red distribution) and gamma (blue distribution) frequency band power for all Short movie sessions.

sessions are significantly higher than both the sub-gamma frequency band (two sample ttest, p=3.7e-04) while the signal correlations within the sub-gamma band were not significantly different (two sample t-test, p=0.14). The range of signal correlations for both the short and long movies was much broader for the gamma band compared to the sub-gamma band, indicating a higher degree of variability across the units recorded during the short movie sessions. The level of variability in the correlations, when observed across repetitions of the movie and between simultaneously recorded unit activity, sampled along the cortical microcircuit, was significant in both short (Figure 3.3.14) and long (Figure 3.3.15) movie sessions. The PSTH and gamma (blue distributions) and sub-gamma (red distributions) frequency band correlations are significantly separated for the majority of units recorded across the layers of cortex.

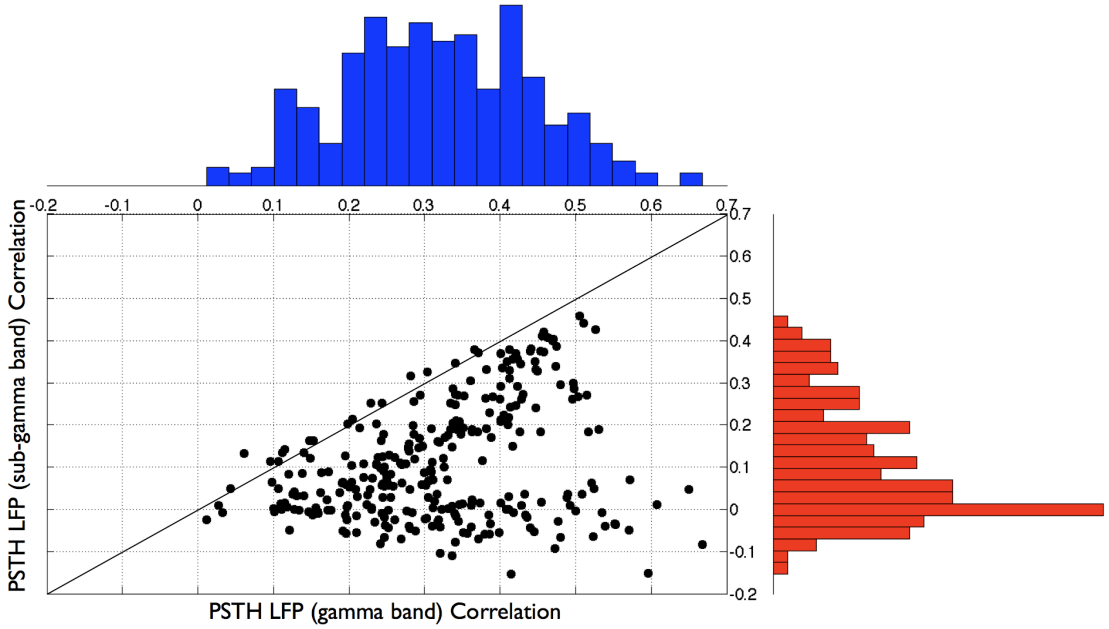

Figure 3.3.13 Scatterplot and histograms of Fisher correlation coefficients calculated between the spiking activity (PSTH) and the sub-gamma (red distribution) and gamma (blue distribution) frequency band power for all Long movie sessions.

Exceptions to this trend can be seen in upper units in short movie session 2 and in the mid layer units in long movie session 1. Extensive variability in correlation strength is observed in both short and long movie sessions 1 and 3. The variety of PSTH/LFP correlation profiles recorded across sessions and animals underlies the level of variability encountered in the dataset and in general the dynamics of the microcircuit under natural scene stimulation. Yet overall, there were significantly higher correlations between unit activity and power within the gamma frequency band compared to sub-gamma band power throughout the time course of both short and long movies. Given the degree of variability observed within the correlations during the movie sessions, could this variability be partially accounted for by the level of response reliability in the population of units? When comparing the responsiveness of the unit activity during the short movie

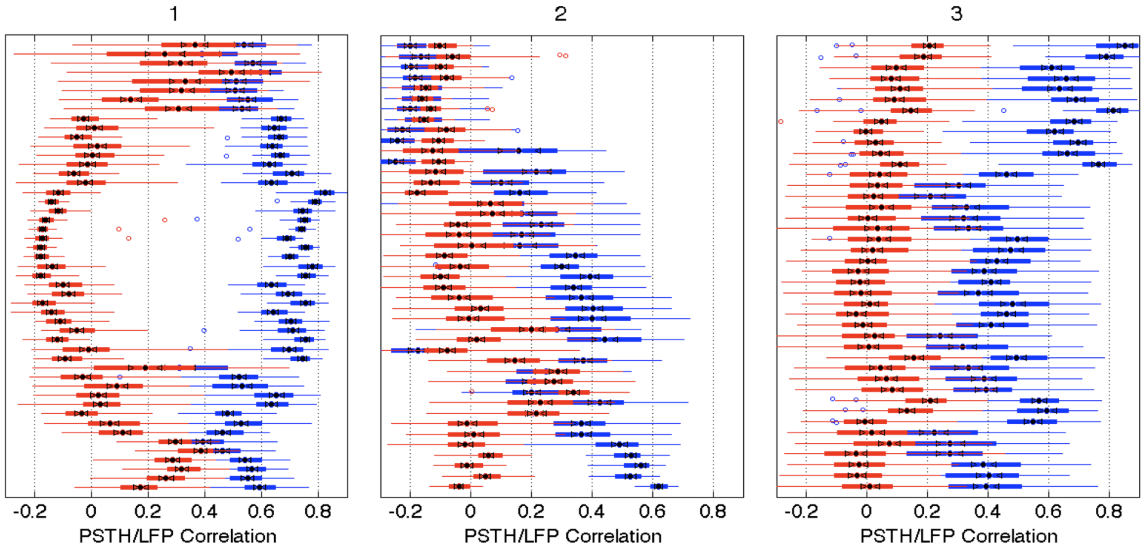

Figure 3.3.14 Laminar profile of signal correlations between the average spiking activity (PSTH) and sub-gamma (red) and gamma (blue) frequency band LFP activity during three Short movie sessions where the polytrode was used to collect the signals. Session 1 was recorded in the first animal. Sessions 2 and 3 were recorded in second animal and but from different locations.

sessions to the measured strength of correlation between the integrated gamma and sub-gamma frequency LFP power, there indeed was a significantly positive correlation for the gamma frequency band (Pearson $r = 0.30$, $p<0.01$) and significant negative correlation for the sub-gamma band (Pearson $r = -0.15$, $p=0.0125$). This indicates that units responding more reliably to repeated presentations of the movie also had a tighter association with the ongoing power fluctuations within the gamma frequency power in the LFP. In contrast, less reliable unit activity was more correlated with the ongoing power fluctuations in the sub-gamma frequency band of the LFP. This trend was also present in the long movie sessions, where the more reliable the unit activity was more positively correlated with ongoing power fluctuations in the gamma frequency band (Pearson r =

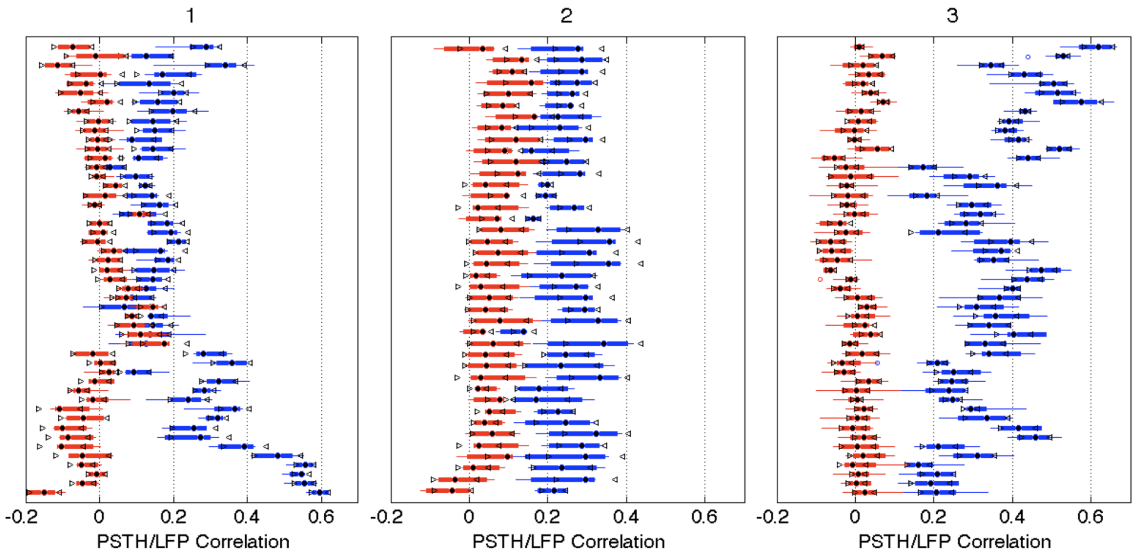

Figure 3.3.15 Laminar profile of signal correlations between the average spiking activity (PSTH) and sub-gamma (red) and gamma (blue) frequency band LFP activity during three separate Long movie sessions where the polytrode was used to collect the signals. Sessions 1 and 2 were recorded in the same animal but in different locations. Session 3 was recorded in a separate animal.

0.34, $p<0.01$) however in contrast, the negative correlation for the sub-gamma band was not significant (Pearson $r = -0.07$, $p=0.23$). To further examine the relationship between spiking activity and the LFP, the estimated spike-LFP coherence was performed between all units and the LFP (see Section 3.3.15 for details). Coherence is typically used to measure synchrony, specifically between two oscillatory processes, for example between the local field potentials recorded from two separate electrodes, and is quantified as a function of the oscillation frequency and then normalized by the amplitudes of the two signals, resulting in unit less range of values from 0 to 1. In this chapter, spike-LFP coherence was used to investigate the timing relationship of spiking activity to the relative phase of all oscillation frequencies between 1 and 100Hz, with a 5Hz resolution.

Therefore, significantly high coherence values indicate that the timing of action potentials is well correlated with ongoing fluctuations in the LFP, at a particular phase of a specific oscillation frequency. Figure 3.3.15 illustrates the spatial and temporal profile of the peak significant spike-LFP coherence values for all responsive units recorded during one short movie session where the polytrode probe was used. The upper rows and lower rows represent unit activity recorded from the upper and lower layers of striate cortex, respectively. In this example short movie session, 49 responsive SUA and MUA were significantly correlated with the ongoing fluctuations in both the sub-gamma and gamma frequency bands, however there were striking differences in the spike-LFP coherence across the layers of cortex. In addition, the spike-LFP coherence in both frequency bands varied greatly throughout the movie presentation. Qualitatively, significant spike-LFP coherence among the units shown in Figure 3.3.16 exhibit large shifts in both space and time, where a majority of units are coherent with the sub-gamma band and then rapidly shifted into significant coherence with the gamma frequency band. Several analysis routines were employed in an attempt to capture these significant spike-LFP interactions as a function of both space and time. However aggregating these dynamics across datasets became problematic due to the variability in the recording quality from session to session and most likely due to the analysis routines used (*see Section 3.3.13*). It is however likely that employing a bootstrapping method, where the randomization of spike times in relationship to the ongoing LFP or shifting entire spiketrains across repetitions, while conserving inter-spike interval relationships, would allow for the generation of a statistical threshold, derived empirically for each movie session.

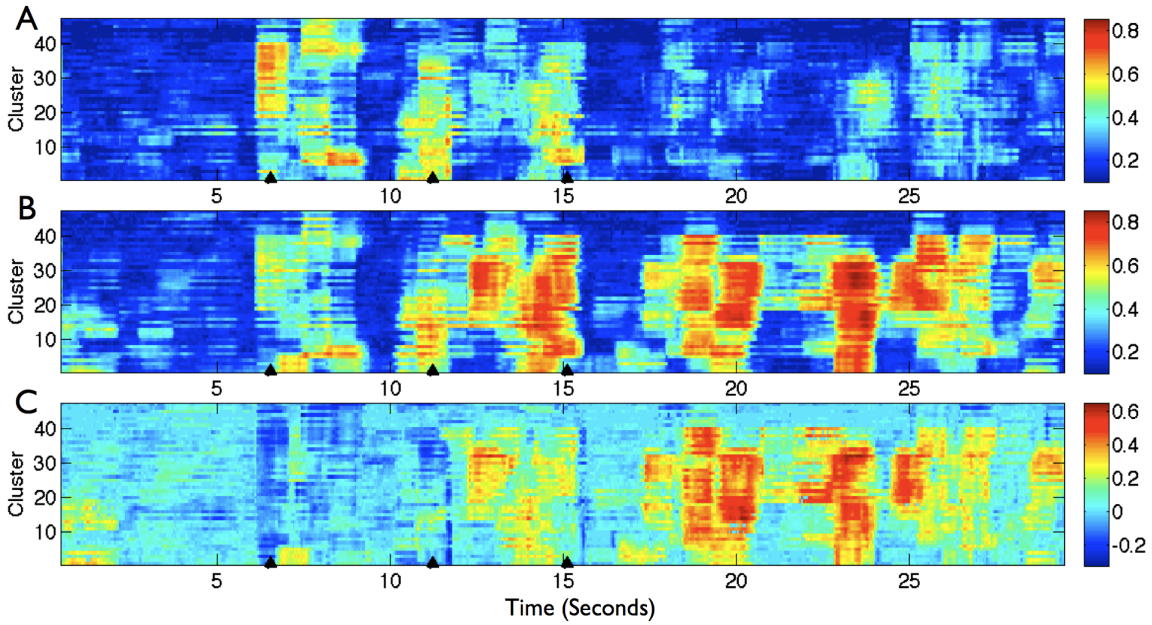

Figure 3.3.16 Spatial and temporal profile of maximum spike-LFP coherence values during a Short movie session where activity was uniformly collected across the layers of striate cortex using the silicon polytrode. (A) Peak spike-LFP coherence values within the sub-gamma band (1-15Hz). (B) Peak spike-LFP coherence values within the gamma band (25-90Hz). Note the non-uniform spread and temporal dynamics of significant peak coherence values during the movie presentation. (C) Difference between A and B, positive values indicate higher coherence in the gamma band and negative values indicate higher coherence in the sub-gamma band. Black triangles plotted along the lower axis indicate scene transitions within the movie.

This empirically derived threshold could then be used to segment significant spike-LFP coherence across both space and time, thereby enabling the characterization of spike-LFP 'events' in order to relate them to the cortical microcircuit and the processing of the natural scenes being presented. The 95% confidence intervals and FDR correction of the spike-LFP coherences shown in Figure 3.3.16 does not allow for this segregation of 'events', because there exists a continuous line, in both space and time, of significant spike-LFP coherence for both the sub-gamma and gamma frequency bands.

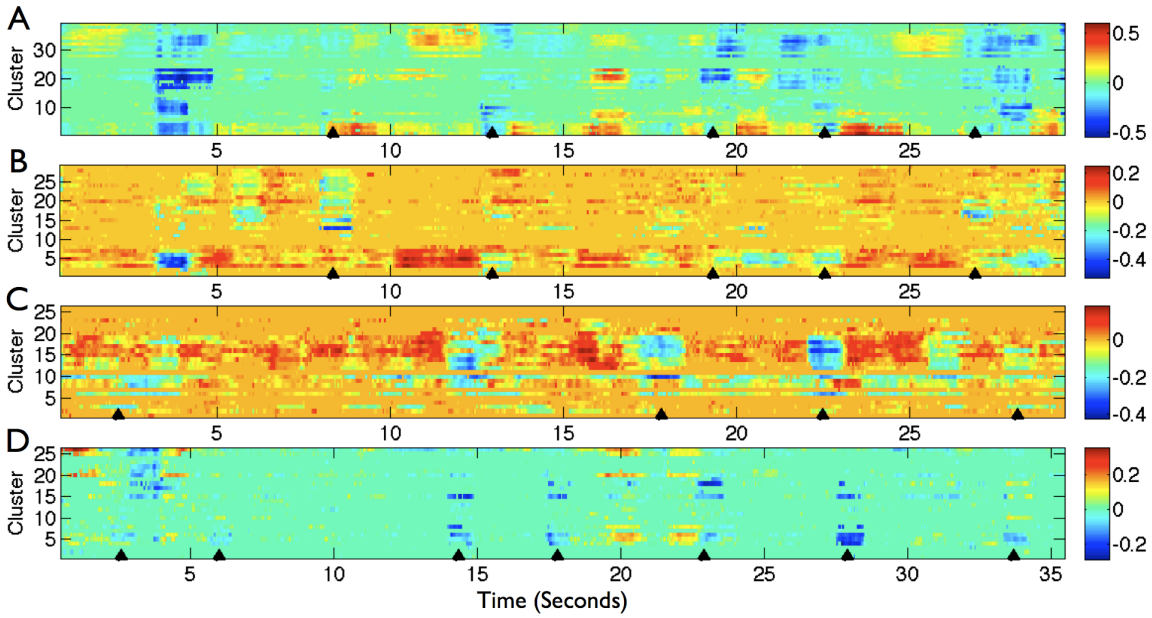

Figure 3.3.17 The spatial and temporal profile of the relative differences between peak gamma and sub-gamma spike-LFP coherence values during four individual short movie sessions. The data were recorded in two separate animals where activity was uniformly collected across all layers of striate cortex using the silicon polytrode probes. Positive values indicate higher spike-LFP coherence in the gamma frequency band and negative values indicate higher spike-LFP coherence in the sub-gamma frequency band. Note that the color scales for each plot have a different absolute range, which also indicates the level variability across sessions. Black triangles plotted along the time axis denote scene transitions within the movie. The duration of the movie segments in A, B and C are 30 seconds and 35 seconds in D. Even though unit activity was uniformly sampled across the polytrode array in all experiments, only unit activity with responsiveness indexes > 20 (*see Figure 3.3.3*) were included, resulting in a variable number of units.

In contrast to PSTH-LFP signal correlation measure, where unit activity was consistently related to power fluctuations within the gamma band, the relationship between the relative phases of spiking was consistently correlated to both the sub-gamma and gamma bands, and this relationship was greater for the sub-gamma band for a majority of the units (*see Figure 3.3.18A*). Since the PSTH-LFP signal correlation distills these spike-LFP relationships between the two signals into a single value, a Pearson

correlation, it does not fully capture periods of significant spike-LFP phase relationships, as seen in Figures 3.3.16 and 3.3.17. For example, the average and peak spike-LFP coherence values for the gamma and sub-gamma frequency bands were not significantly different (two sample kstest, $p=0.1$ and $p=0.06$), however the distribution of PSTH-LFP signal correlations for the gamma and sub-gamma frequency bands were significantly different (two sample kstest, $p<0.01$). When investigating absolute differences between peak spike-LFP coherences across all units within both the short and long movie session, the average difference is nearly zero for both, yet a large range (-0.58 to 0.65) of peak spike-LFP coherence differences exists. These absolute differences are shown in subplot C of Figure 3.3.16 and in Figure 3.3.17 for four separate short movie sessions. As observed in these examples, significant differences in spike-LFP coherence exhibit a wide variety of spatial and temporal profiles, where neighboring clusters of units peak in their spike-LFP relationships throughout the movie presentation. In addition, these clusters of enhanced spike-LFP coherence also co-occur in time with relatively distant clusters of units within the cortical microcircuit, which are presumably processing the same visual information. Although not possible in this dataset, ascribing layer information to these spike-LFP coherence dynamics could be possible with better histological confirmation. One final observation is the co-occurrence of enhanced spike-LFP coherence within the sub-gamma band and the scene transitions, marked with black triangles in Figures 3.3.16 and 3.3.17. This relativity consistent result is further discussed in section 3.3.5.

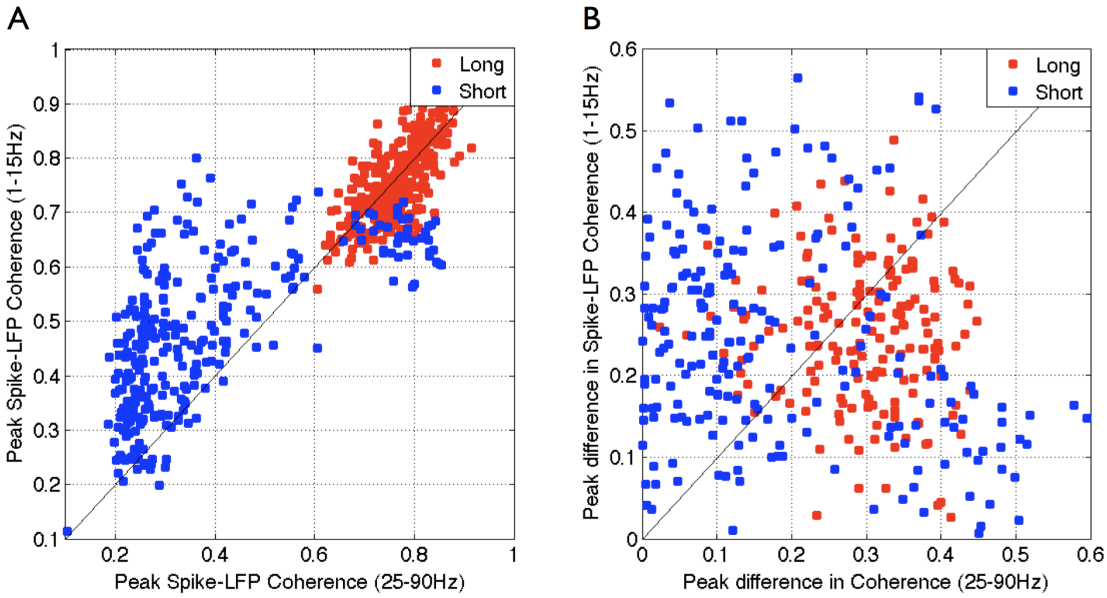

Figure 3.3.18 (A) Scatterplot of peak spike-LFP coherence values in the sub-gamma (y-axis) and gamma (x-axis) frequency bands during all Short (blue points, n=303) and Long (red points, n=292) movie sessions. (B) Scatterplot of the absolute differences in the peak spike-LFP coherence values in the sub-gamma (y-axis) and gamma (x-axis) frequency bands during all Short (blue points) and Long (red points) movie sessions.

Overall, the relationship between spiking activity and ongoing fluctuations within the LFP are robust and they dynamically shift in both space and time throughout the movie presentations. In light of these interesting dynamics, the quantification of their durations and spatial scales were not pursued, however the individual peak spike-LFP coherence values for both sub-gamma and gamma frequency bands were plotted in Figure 3.3.18A and the absolute difference between peak spike-LFP coherences for both the sub-gamma and gamma frequency bands are plotted in Figure 3.3.18B, in order to illustrate the wide range of coherence values encountered during both the short and long movie sessions. Significant coherence values within the gamma frequency band ranged from 0.11 to 0.86 with a mean of 0.38 +/- 0.19 during the short movie sessions. This

distribution displayed a U shape and was significantly skewed toward lower values (Lilliefors test, p=1.0e-3), highlighting the variability across the unit activity recorded across experimental sessions, which can be seen in Figure 3.3.18A. However, significant peak spike-LFP coherence values within the sub-gamma frequency band ranged from 0.12 to 0.80 with a mean of 0.48 +/- 0.14 during the short movie sessions. In contrast to the skew within the gamma band, the distribution of peak coherence values within the sub-gamma frequency band was more normally distributed (Lilliefors test, p=0.03) and centered at a significantly higher peak spike-LFP coherence value. This result indicates that spiking timing was more tightly correlated with the sub-gamma frequency range compared to the gamma frequency range for a majority of the units. Significant peak spike-LFP coherence values within the gamma frequency band ranged from 0.55 to 0.92 with a mean of 0.74 +/- 0.07 and within the sub-gamma frequency band the range was 0.55 to 0.92 with a mean of 0.74 +/- 0.07 during the long movie sessions. Both of these distributions of were both normal in their distribution (Lillifors test, $p<0.01$) and significantly shifted toward higher coherence values compared to the short movie sessions. This baseline shift is clearly seen in Figure 3.3.18, subplot A, when comparing the short (blue points) and long (red points) movie sessions. The shift is due to the lower number of long movie repetitions, 5 or 10 repetitions, compared to the short movie repetition number of 100. Therefore, the non-significant difference between the gamma and sub-gamma frequency band spike-LFP coherence values for the long movies should be interpreted in context of the low number of movie repetitions. Interestingly, the absolute differences between peak gamma and sub-gamma spike-LFP coherence were not

significantly different (two sampled ttest and kstest, $p<0.01$), for both short and long movie sessions, indicating that the level of variance in peak coherence, between the two frequency bands, was conserved across movie sessions. However, as observed and discussed above, there is not only considerable variability in the spike-LFP coherence within all movie sessions, there is also a considerable point spread in absolute differences, as seen relative to the unity line in Figure 3.3.18B.

3.3.5 Evoked Responses during Scene Transitions within the Movies

Scene transitions within the movies displayed to the animals contained global changes in luminance and contrast between subsequent movie frames, which were artificially introduced during the initial construction of the movies. These scene transitions tended to generate large evoked potentials with the LFP and induced reliable spiking activity across the repetitions of the movie (*see Figure 3.3.19*). Transitions between movie repetitions were also present, but excluded from any analysis. In addition, increased peak spike-LFP coherence within both the sub-gamma and gamma frequency bands were observed. These peaks in spike-LFP coherence tended to occur at different times relative to a scene transition, where peak spike-LFP coherence in the sub-gamma band occurred prior to the gamma band, although this relationship was not consistent and therefore not analyzed further, however several examples can be seen in Figures 3.3.16 and 3.3.17. During scene transitions within the short movie sessions (n=105), the average peak spike-LFP coherence within the sub-gamma band was 0.31 +/- 0.13, significantly higher than the gamma band, at 0.14 +/- 0.13 (two sample, one-sided, kstest, $p<0.01$).

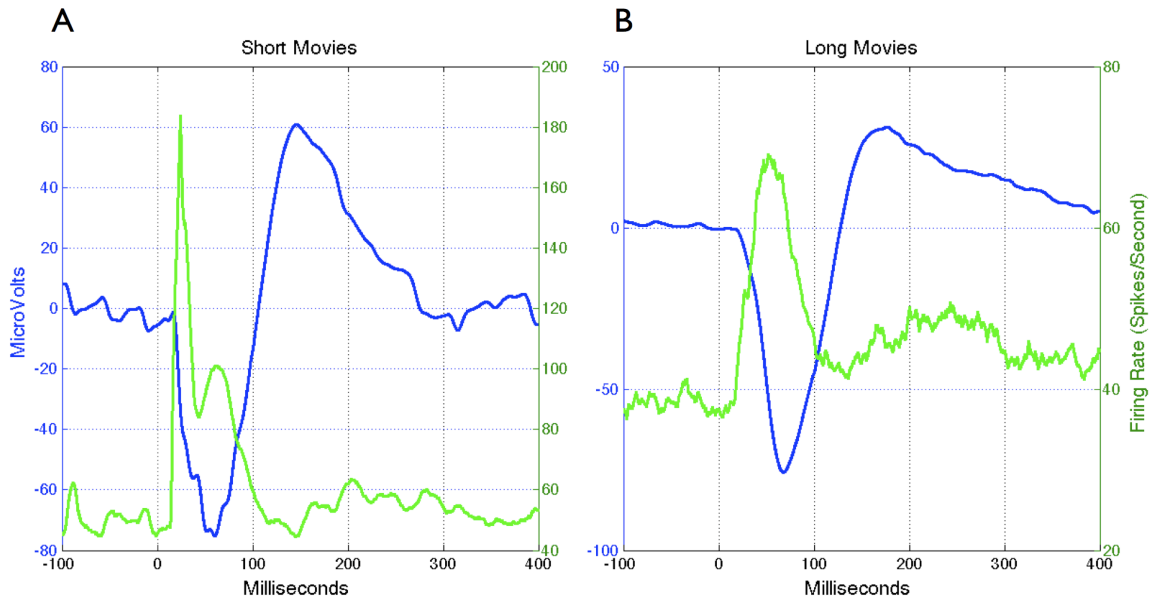

Figure 3.3.19 Profiles of the average spiking and local field potential (0.1-100Hz) activity aligned to the scene transitions in the (A) Short movie sessions and (B) Long movie sessions. The average spiking activity (SUA and MUA) is shown in green trace and the average LFP is shown in the blue trace.

During scene transitions within the Long movie sessions (n=885), the average peak spike-LFP coherence within the sub-gamma band was 0.50 +/- 0.10, significantly higher than the gamma band, at 0.38 +/- 0.10 (two sample, one-sided, kstest, $p<0.01$). Even though the spike-LFP coherence values were consistently higher in the long movie sessions, the trend was consistent with the short movie sessions, where scene transitions evoke significantly higher spike-LFP coherence in the sub-gamma compared to the gamma band.

The onset of the movie and the offset of the movie, flanked by the uniform gray screen periods also induced a similar profile in both the LFP and spiking activity. Figure 3.3.19 illustrates the average scene change evoked potentials in the spiking and LFP activity during both the short and long movies, excluding the onset and offset of the

movie. Elevated spiking activity occurred just prior to the low point within the voltage potential of the LFP during both short and long movies. The sharp spike ~25ms in the scene change evoked spiking response during the short movie segments corresponds to a subset of units that consistently responded with a 25ms latency to a scene transition, consistent with the lower bound of information transfer from retina to cortex The average peak negativity in the LFP occurred 70-75ms after the scene transition in both the short and long movies. The documentation of these scene transition phenomenon, observed in both the spiking and LFP activity, are relevant to our understanding of the processing of information within the natural scenes being presented and bring into question results from recent studies that have investigated striate responses to full-field flashed natural stimuli (Weiliky et al, 2003) and natural image 'movies' void of temporal correlations (Talebi and Baker, 2012). In addition, several studies investigating spiking and LFP relationships in striate cortex while using natural movie stimuli have reported higher than expected information rates in the lower LFP frequency ranges (Beliski et al., 2008) and tighter and more consistent spike-LFP phase relationships within the lower LFP frequency ranges (Montemurro et al., 2008) compared to the gamma frequency band. Both of these studies did not specifically discuss scene transitions or any significant luminance changes within the movies used.

3.3.6 Summary of Results and Main Findings

Large-scale spiking and local field potential activity was densely sampled and recorded simultaneously from all layers of striate cortex during the presentation of time-varying natural scenes, i.e. movies. For the dataset used in this chapter, the silicon

polytrode probes were successfully used in two of the four animals and the silicon tetrode probes were successfully used in three of the four animals. The results from these four experiments have been aggregated and are briefly summarized as follows: 1) Consistent with the main results presented in Chapter 2, spiking activity in cat striate cortex is indeed sparse, brief and reliable under both short and long movie presentations when using both probe types. 2) Heterogeneity among simultaneously recorded units was for the most part consistent with data presented in Chapter 2, although the inclusion of MUA from the polytrode recordings decreased the level of heterogeneity, as would be expected. 3) The majority of the average unit activity (PSTH) recorded under both short and long movie sessions was significantly correlated with ongoing power fluctuations within the gamma frequency range (25-90Hz) of the LFP, compared to the sub-gamma frequency range (1-15Hz). 4) The relative timing of spiking activity, in relation to the phase of the LFP, was significantly more correlated within the sub-gamma frequency band compared to the gamma frequency band. 5) The laminar profile of all the above results varied greatly across sessions and experiments and identifying a clear pattern, in the anticipation of correlating the results to the underlying cortical microcircuit was not possible with this dataset and the with the methods employed. 6) Scene transitions within both the short and long movies evoked robust and reliable spiking and LFP power responses.

It is quite apparent that both spiking and LFP activity display rich spatial and temporal dynamics across the striate cortical microcircuit in response to time-vary natural scenes. Further experimentation, using more reliable recording and histology techniques would allow for a better assessment of the cortical dynamics and perhaps provide a richer

understanding of information processing within the striate cortical microcircuit. The spiking and LFP patterns observed in these recordings and qualitatively described in this chapter will require more sophisticated analysis routines to better correlate the myriad of patterns observed to the underlying microcircuits that are responding to the natural scenes presented. The use of natural scenes to investigate information processing in the cat striate cortex has and will continue to aid in our collective goal of understanding general sensory processing within the mammalian cortex.

3.4 Discussion

3.4.1 Summary of Main Results

The results in this chapter illustrate the dynamic nature of both spiking (SUA and MUA) and local field potential (LFP) activity in the cat striate cortex during natural scene stimulation. Spiking activity tended to be sparse and significant epochs of activity were brief and reliable across repeated presentations of both short and long movie segments. These spiking results are in well agreement with those presented in chapter 2. However, neighboring unit activity, primarily recorded from the polytrode probes, exhibited higher than expected levels of response similarity during the movie presentations. This result is counter to the higher degree of response heterogeneity reported in chapter 2, even though many neighboring units did exhibit similar response heterogeneity, as seen in figures 3.3.6 and 3.3.7. In the majority of recordings, the brief, yet robust and reliable spiking activity significantly co-occurred and co-varied with power fluctuations in the gamma-band (25-90Hz) of the simultaneously recorded local field potentials. However, several

recording locations exhibited a markedly different pattern, where spike-LFP correlations within the sub-gamma band (1-15Hz) were significantly higher compared to the gamma-band. Significant PSTH-LFP correlations within the gamma-band were observed in 264 of 303 units in 22 of 22 short and in 287 of 294 units in 14 of 15 long movie sessions. Significant spike-LFP correlations within the sub-gamma band were observed in 131 of 303 units in 18 of 22 short and in 132 of 294 units in 6 of 15 long movie sessions. Periods of significant spike-LFP coherence within the gamma band were observed in all units recorded in both short and long movie sessions, in addition periods of significant spike-LFP coherence within the sub-gamma band were observed in all units and in both short and long movie sessions. However, periods of significant spike-LFP coherence within the sub-gamma band were three times more likely to occur during scene transitions within the movies presented. The primary experimental and analytical objectives of this chapter were to record large-scale neural activity within the cat striate cortex under natural scene stimulation and to characterize and quantify unit activity and to relate that activity to the local field potential patterns. The results of these experiments are further discussed below in the context of what is known about the representation of natural scenes and gamma-band activity within the striate cortex. Experimental deficiencies and solutions are discussed in the final section.

3.4.2 Natural Scenes in the Study of Striate Cortex

The primary visual cortex evolved under the constraints of a natural environment that is highly complex and dynamic in both space and time. The processing of visual

information within the natural environment occurs within networks of intricately connected neurons that exhibit highly complex and dynamic patterns of activity during the representation and transmission of information (Gilbert and Wiesel, 1983; Gilbert 1983, Douglas and Martin, 2004; 2007a,b). Historically, the classical experimental paradigm used in the study of the mammalian visual system has been to simplify the visual information presented and investigate response properties of individual neurons without explicit consideration of the underlying dynamics of the network, whose ongoing activity likely influences response properties (Arieli et al., 1996; Tsodyks et al., 1999). The use of moving light bars and gratings has resulted in a great wealth of knowledge concerning the receptive field properties of individual neurons (Hubel and Wiesel, 1962; Movshon et al, 1978; reviewed and defended in Rust and Movshon, 2005). However translating these response properties and receptive field models into the domain of more complex stimuli has more or less failed (David et al., 2004; Touryan et al., 2005; Felson et al., 2005; David and Gallant, 2005). Static natural images contain well-described statistical regularities, where correlations in luminance intensity and color are highest among neighboring locations in space and these pair wise correlations decrease with spatial distance (Field, 1987; Ruderman & Bialek, 1994; Simoncelli & Olshausen, 2001). These pair wise correlations possess a spatial frequency power spectrum that has a 1/f relationship, where the correlation power exponentially decreases as a function of frequency (Field, 1987). Time-varying natural scenes contain the third dimension of time, where spatially correlated objects and contours translate throughout the scene over time in a complex yet predictable and stereotypical fashion (Dong and Atick, 1995). Given the

unique statistical properties of the natural world, Horace Barlow (Barlow, 1961) proposed that a goal of early sensory systems was to exclude the statistical regularities and maximize the relevant information required for processing within the higher order areas of the brain. This 'efficient coding' hypothesis (reviewed in Barlow, 2001; Simoncelli and Olshausen, 2001) has gained support over the years from experimental findings conducted within the early visual system. One of the first studies to explicitly test this hypothesis was conducted in anesthetized cat LGN during time varying natural scene stimulation (Dan et al., 1996). This study showed that individual unit responses were well adapted for the 'efficient' coding of information in the natural scenes compared to the more classical control stimuli typically used Several studies conducted in the striate cortex of cats, ferrets and monkeys, have demonstrated that neuronal activity during natural scene stimulation is qualitatively and quantitatively different from activity recorded under more simple stimulus conditions (Vinje & Gallant, 2000; 2002; Ringach et al., 2002; Kayser et al., 2003; Weliky et al., 2003; David et al., 2004; Guo et al., 2005; Felson et al, 2005). In these studies, striate neurons tended to produce sparser responses under natural scene stimulation, consistent with predictions of the 'efficient' coding hypothesis. The sparsity of individual striate responses has been shown to increase as the visual stimulation size increases beyond the classical receptive field (Vinje and Gallant, 2002). In addition, the correlation among the responses within the population followed the same trend, where increased stimulus size led to decreased correlation. Since normal visual experience involves full-field stimulation, these results are likely to reflect the activity patterns generated under normal stimulus conditions. Within this 'efficient'

coding framework, increased reliability and decreased correlation within a population of striate neurons is thought improve the stimulus representation through enhancement of encoding capacity for each neuron in the population and by reducing the redundancy between the participating neurons. In addition to striate visual neurons, neurons at higher levels in the visual stream, for example, the inferotemporal cortex, also exhibit sparse responses under more naturalistic visual stimulation (Lamme, 1995; Baddeley et al., 1997). The main results discussed in this chapter and in chapter two provide additional experimental support for the 'efficient' coding hypothesis (Barlow, 1972; Olshausen and Field, 2004). Repeated short and long movie presentations resulted in reliable and sparse responses and neighboring neurons tended to respond at different points in time throughout the movies. However, many units displayed a high degree of redundancy (see Figures 3.3.5-7), which is most likely due to the inclusion of multi-unit activity and deficiencies in the spike sorting routines used to extract and isolate units from the polytrode probes.

3.4.3 The Origin and Spatial Scale of Local Field Potentials

The low frequency oscillatory activity readily observed in all extracellular recordings conducted within the central nervous system is generally thought to originate from coordinated activity among networks of interconnected neurons (Buzsaki, 2007). However the precise origin and scale of this low frequency potential (LFP) activity remains more or less a mystery (reviewed in Buzsaki et al., 2012). Post-synaptic currents are generally presumed as the primary generator of the LFP (Mitzdorf, 1985) and the

spatial scale of these currents, relative to the recording microelectrode, is generally accepted to range from 300 to 500 micrometers (Mitzdorf, 1985, Katzner et al., 2009; Xing et al., 2009; Linden et al., 2011), however the final spread of the LFP can be amplified by correlations among neurons with similar response properties (Linden et al., 2011) and may actually span several millimeters (Kajikawa and Schroeder, 2011) when several important technical issues are addressed. Regardless of the actual spread of LFP power in the cat striate cortex, the objective in this chapter was to characterize and quantify interactions between spiking activity and the LFP, and if possible, to relate any significant interactions to the known laminar structure of the cortical microcircuit (Gilbert, 1983; Payne and Peters, 2002). However, due to several methodological constraints and reproducibility across datasets, it was not possible to consistently record and then relate the observed spike-LFP interactions to the underlying cortical microcircuit. Qualitatively, the spatial spread of sub-gamma frequency band power was consistently higher than gamma frequency band power, which can be seen in Figure 3.3.11. Enhanced sub-gamma frequency band power and the higher spatial spread of that power was observed in all polytrode recording locations, whereas gamma frequency power tended to be less and more localized along the length of the polytrode. Instead of attempting to relate the spread of LFP power to the cortical microcircuit, amplitude fluctuations within the LFP, in the form of Z-transformed power, were used to index activity within the local cortical network, which enabled inferences to be made concerning the underlying representations of the natural scenes being presented. Across the dataset, this index dynamically fluctuated in both space and time during natural scene

presentations. Power within the gamma frequency band consistently co-varied with enhanced spiking activity compared to sub-gamma frequency oscillations. This result is consistent with the well-documented phenomenon of gamma frequency oscillations in the striate cortex and extends the potential role of gamma frequency band oscillations to the representation of information within time-varying natural scenes.

3.4.4 Gamma Frequency Band

Activity within the Striate Cortex

The first definitive study to demonstrate a functional relationship between gamma frequency band oscillatory activity and synchronous spiking activity was conducted within the anesthetized cat striate cortex (Gray et al., 1989). In this study, stimulus selective gamma frequency oscillations within the simultaneously recorded LFP and spiking activity was reported for the first time, which subsequently inspired countless studies within the visual cortex and beyond in order to elucidate the mechanisms and potential functional role that these stimulus-response properties may have in visual perception (Gray, 1994; Singer and Gray, 1995). This general finding was soon observed across the cortical hemispheres (Engel et al., 1991a) and within alert cats (Gray and Viana di Prisco, 1997). More recent studies have demonstrated robust stimulus selectivity within the gamma frequency band of the LFP, specifically for stimulus orientation (Frien et al., 2000; Siegel and Konig, 2003; Henrie and Shapley, 2005; Liu and Newsome, 2006), temporal frequency (Gray et al., 1990; Freidman-Hill et al., 2000; Kayser and Konig, 2004) and contrast (Henrie and Shapley, 2005; Ray and Maunsell, 2010). Since the above studies, as well as numerous others, report a large degree of variability in

gamma frequency band oscillations, in terms of power, peak frequency and timing, under a variety of experimental preparations, species and stimulus conditions, it was expected that gamma frequency band activity would be highly variable during natural scene stimulation. As discussed above, time-varying natural scenes contain special properties, including coherently moving elongated contours of various orientations, contrasts and speeds, therefore the resulting variability in gamma frequency power and timing discussed in this chapter is fairly consistent with the prediction made from what has been observed under more controlled and simple stimulus paradigms. However, several additional sources of variability in regards to gamma frequency power and timing can be partially explained by known cellular and network properties of striate cortex.

A unique type of superficial layer II/III pyramidal neuron termed 'chattering' cell was first identified in cat striate cortex (Gray and McCormick, 1996). These cells have intrinsic membrane potential oscillations and spiking responses that predominantly oscillate within the gamma frequency band during visual stimulation. Intrinsic membrane 'resonance' properties have been documented in several cortical neuron types (Llinas et al., 1991; Steriade et al, 1998; Hutcheon and Yarom, 2000; Izhikevich, 2001; Whittington and Traub, 2003; Cardin et al., 2005) and these intrinsic resonance properties are postulated as a potential mechanism for the enhancement and stabilization of cortical gamma frequency oscillations. In addition to cortical neurons, thalamocortical projection neurons exhibit membrane potential oscillations in the gamma frequency range (Pedroarena and Llinas 1997; reviewed in Llinas and Steriade, 2006) and these cells predominantly connect with cortical layer 4 excitatory as well as inhibitory neurons in the

visual cortex (Thompson et al., 2002; Thomson and Bannister, 2003). Two recent studies conducted in the juvenile rat whisker sensory system have elegantly explored thalamo-cortical interactions and have shown that the generation of gamma frequency band oscillatory activity is partly dependent on thalamocortical network interactions, involving both excitatory and inhibitory neurons (Minlebaev et al., 2011; Yang et al., 2012). The role of inhibitory interneurons in the generation and maintance of gamma frequency band oscillations has been studied and well documented (Bartos et al., 2007) and it has been proposed that the ephemeral nature of gamma frequency oscillations likely results from close interactions between excitatory glutamatergic neurons and inhibitory GABAergic interneurons (Whittington et al, 2000; Borgers and Kopell, 2003, Whittington et al., 2011). These so called PING (pyramidal inhibitory network gamma) models of cortex are composed of interconnected excitatory and inhibitory neurons that upon receiving temporally delayed thalamocortical inputs, result in enhanced synchronous activity that oscillates within the gamma frequency range. It has been recently demonstrated that GABAergic inhibitory interneurons play a causal role in the emergence of gamma oscillations within cortex (Hasenstaub et al., 2005; Sohal et al., 2009; Cardin et al., 2009), lending evidence to the PING models. Gamma oscillations have been shown to be most prominent within the superficial, rather than deep layers of cortex (Gray and McCormick, 1996; Buffalo et al, 2011), consistent with the anatomical arrangement of recurrent networks of excitatory and inhibitory neurons (Douglas and Martin, 2004; 2007). Qualitatively, recordings conducted within the upper layers of striate cortex exhibited a high degree of gamma frequency band power that was also well correlated

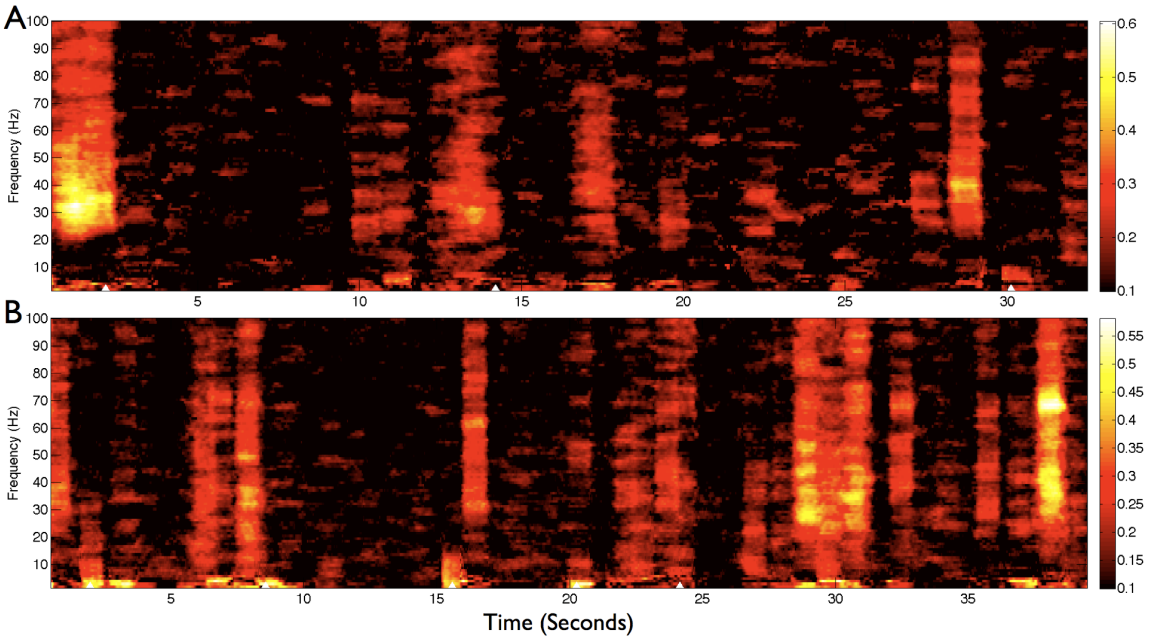

Figure 3.4.1 Average spike-LFP coherence for two independently recording single units during two short movie presentations. (A) The average spike-LFP coherence of a single unit recorded 250um below the cortical surface using a tetrode silicon probe. (B) The average spike-LFP coherence of single unit recorded 450um below the cortical surface using a tetrode silicon probe. The units were recorded from separate recording locations in the same animal and two different short movie segments, 32 and 40 seconds, respectively, were used. The colorbars to the right of each plot indicate the level of spike-LFP coherence. White triangles plotted along the time axes indicate scene transitions within the movies.

with the simultaneously recorded spiking activity. Figure 3.4.1 shows the spike-LFP coherence of two independently recording single units from two separate locations within the same animal. Both of these units were recorded from the upper layers of striate cortex (250um and 400um) and both exhibited significant spike-LFP coherence (peak coherence = 0.62 and 0.58) within the gamma frequency band. Their average spiking activity (PSTH) was significantly more correlated with power fluctuations in the gamma frequency band (r = 0.85 and 0.72) compared to the sub-gamma frequency band (r = 0.00 and 0.01). Overall, significant correlations between spiking activity and power

fluctuations within the gamma frequency band were observed in the majority of recording locations during natural scene stimulation (Figure 3.3.12 and 3.3.13). However, variability in the gamma frequency band, in terms of peak frequency, timing and spatial spread, was high across the dataset. The observed variability may just be inherent to the striate cortex under natural scene stimulation, since the mechanisms generating gamma oscillations are multifaceted and complex, as discussed above. The fact that individual striate neurons are embedded within a complex local microcircuit that receives direct inputs from a variety of local and more global regions, the 'state' of the larger network likely influences sensory processing. Visually induced gamma frequency oscillations within the striate cortex can be facilitated through electrical stimulation of the medial reticular formation (MRF) (Munk et al., 1996; Herculano-Houzel et al., 1999). Direct application of cholinergic agonists can induce gamma frequency oscillations in cortex and the enhancements can also be abolished by blocking muscarinic receptors within the striate cortex (Rodriguez et. al., 2004). Both cholinergic agonists and electrical stimulation of the MRF have been shown to stabilize power fluctuations within the gamma frequency band during visual stimulation and reduce spike count variance to repeated presentations of sinewave gratings (Rodriguez et al., 2010). In addition, electrical stimulation of the rat basal forebrain was shown to markedly change spiking activity in the visual cortex and the subsequent encoding of visual information during natural scene stimulation (Goard and Dan, 2009). These external interventions shift the 'state' of the cortex from high amplitude, low frequency dominated oscillations, to a more 'activated' state where low amplitude, high frequency oscillations predominate,

similar to the normal function of the reticular activation system during awake periods (Moruzzi and Magoun, 1949; Steriade et al., 1996). The mechanisms underlying these global shifts are still unknown. However, it has been shown that cells within the intralaminar nuclei of the cat, which broadly project onto and influence large areas of cortex, posses unique intrinsic firing patterns, characterized by high intraburst rates ranging from 800-1000Hz with interburst rates concentrated in the gamma frequency range (Steriade et al., 1993) which have been shown to synchronize with gamma oscillations in cortex (Steriade et al., 1996). Whatever the actual mechanisms causing this 'state' shift are, the resulting 'state' of the cortex has been shown to directly influence the receptive field properties of striate neurons (Worgotter et al., 1998, 2000), which presumably would alter response profiles of individual and larger groups of striate neurons during natural scene stimulation. Therefore, ongoing 'state' fluctuations within the striate cortex may be a source of considerable variance and explain in part, the variability observed in the spike-LFP correlation distributions.

3.4.5 Dynamics of Spiking and Gamma Band Activity during Natural Scene Stimulation

In this chapter, considerable variability in the frequency and power of gamma frequency band oscillations was observed during natural scene stimulation. This variability is most likely due to the rich spatiotemporal properties of the dynamic movies presented, where a continuum of spatial and temporal frequencies, contrasts, orientations and directions of motion are encountered, compared to more classical stimuli where individual parameters are systematically varied and controlled. As expected, robust

power within the gamma frequency band was observed and these power fluctuations were significantly correlated to the simultaneously recorded spiking activity and reproduced over repeated presentations of the movie. When these experiments were first conducted, very little was known about gamma band activity fluctuations during natural scene stimulation (Kayser et al. 2003), however recent studies have shown that modulations in local field potentials recorded in striate cortex during time varying naturalistic stimuli are substantial (Belitski et al. 2008; 2010; Montemurro et al. 2008; Kayser et al. 2009). Interestingly, these studies concluded that amplitude fluctuations below 10Hz were the most informative about the natural stimuli presented, in terms of information encoded into the dynamics of spiking and LFP activity. In this chapter, information calculations were not performed, however significant spike-LFP correlations were observed at frequencies below 10Hz, corresponding to scene transitions within the movie, which were not addressed in the above studies.

Several methods were developed in order to quantify and track the level of gamma frequency power fluctuations during the movie presentations (*see Section 3.2.14-3.2.16*), however given the dynamic and ephemeral nature of gamma activity, in terms of peak frequency and spatial and temporal evolution, these efforts were abandoned and qualitative descriptions have been used. Several studies conducted in striate cortex have shown that the magnitude and peak frequency of gamma oscillations is modulated by specific features of the stimulus presented, where contrast (Henrie and Shapley, 2005; Ray and Maunsell, 2010; Roberts et al., 2013), orientation (Berens et al., 2008; Jia et al., 2011) and spatial scale (Jia et al., 2011; Gieselmann and Thiele, 2008) all contribute to

the variability in the measured gamma frequency activity. The studies used more classical visual stimuli and parametrically varied individual stimulus features while holding others constant and still observed large fluctuations in peak gamma power and frequency. Peak gamma frequency has been shown to systematically increase with the drift speed of an optimally tuned grating in cat striate cortex (Gray et al., 1990). In addition, peak gamma frequencies recorded from within the anesthetized (Ray and Maunsel, 2011) and awake (Vinck et al., 2010; Roberts et al., 2013) non-human primate striate cortex has been shown to be highly variable across stimulus parameters and animals. Therefore, given the rich spatio-temporal dynamics of time-varying natural scenes, the variance in gamma power and frequency documented in this chapter could have been anticipated, however the coincidence of spiking activity with these fluctuations is notably high, given the level of sparsity in the spiking activity. The close temporal correlation of spiking and gamma oscillations during natural scene stimulation suggests their involvement in stimulus representation.

It has been proposed that gamma oscillations may provide a temporal framework for the firing of neurons, such that information about the stimulus is encoded in the timing of spikes relative to the ongoing gamma cycle and the level of cycling depends on the inhibitory network (Buzsaki and Chrobak, 1995; Buzsaki and Draguhn, 2004; Mann and Paulsen, 2007; Fries, 2007). If this turns out to be true, then information embedded within the timing of spikes would be more reliably transferred between cortical areas when those areas are coherently active as proposed in Fries et al., 2009. As discussed above in Section 3.4.3, the close coordination between excitatory and inhibitory activity,

where excitation is generally thought to lead inhibition during the gamma cycle (Hasenstaub et al., 2005; Fries, 2009) is thought to establish "windows of opportunity" for representing and transmitting stimulus information within and between cortical areas (Haider and McCormick, 2009). These proposed 'network' mechanisms for gamma oscillations rarely consider the role played by individual neurons in the striate cortex. Mechanistically, it has been shown *in vivo* that membrane potential fluctuations in cat striate neurons exhibit high orientation selectivity and gamma band fluctuations in the membrane potentials are significantly higher compared to sub-gamma band fluctuations (Gray and McCormick, 1996; Azouz and Gray, 2000; 2003). In addition, these studies showed that spiking activity was highly correlated to membrane potential fluctuations in the gamma frequency band compared to the sub-gamma frequency band, and that these faster membrane potential fluctuations resulted in an increased probability of action potential generation (Azouz and Gray, 2000; 2003). The mechanisms discovered in these intracellular studies are similar and related to observations made from LFP recordings conducted in the striate cortex of awake monkeys (Frien et al., 2000), where orientation tuning was greater for the gamma-band power compared to sub-gamma band power. Based on an expanding body of literature (Fries 2009), the basic phenomenon of gamma-band oscillations has been well established, however a consistent explanation of the functional role of gamma-band oscillations remains elusive. One of the first proposed functions of gamma-band oscillations was to coordinate spiking activity across spatially segregated regions in the striate cortex in order to functionally link the distributed spiking activity, considered as representing aspects of the visual stimuli, which included

orientation and direction of movement of bars of light (Gray et al., 1989). Within this framework, 'binding through synchrony" resulted from the coordination of spiking activity through rhythmic entrainment within the gamma-band, which could lead to more effective joint outputs and inputs to downstream cortical areas (Singer and Gray, 1995; Singer, 1999). A more recent elaboration of this hypothesis extends gamma-band oscillations to the concept of "communication through coherence", whereby distant cortical areas functionally communicate through coherent activation within the gamma-band (Fries, 2009). The high degree of spiking and gamma band activity demonstrated in this chapter is consistent with the known properties of spiking and LFP activity in the striate cortex under more classical visual stimuli and is now extended to natural scene stimulation. Although not explicitly testing the putative roles of gamma-band oscillations in striate cortex, the results presented in this chapter do extend their robust occurrence during natural scene stimulation. However, the high degree of spike-LFP correlation could in part result from spike signals 'leaking' into the LFP signals, sufficiently to dominate the LFP (Zanos et al., 2011). If this were the case, then nearly all spike/LFP correlations illustrated in this chapter would be closer to 1, instead zero values of 1 were found (Figure 3.3.12 and 3.3.12). To the contrary, a large portion of the spike/LFP correlations were not significant or were at significantly low levels, thereby countering the possibility of spike signal leakage into the LFP signals. In addition, several measures were taken to minimize this potential (*see Section 3.2.10 for details*).

In conclusion, the results presented in this chapter, as well as those cited, suggest that gamma-band oscillations likely reflect a basic cortical process that emerges within

striate cortex through complex, yet known interactions between excitatory and inhibitory neurons, intrinsic cellular properties, contributions from reciprocal thalamocortical interactions and modulatory inputs from brain stem arousal centers. Therefore, the complexity observed in the spiking and LFP activity patterns are determined by the characteristics of the sensory input as well as the internal state of the network.

CHAPTER FOUR

MAIN FINDINGS, CONTRIBUTIONS AND CONCLUSIONS

4.1 Summary of Main Findings and Primary Contributions

In this exploratory work, by investigating response properties of populations of neurons in anesthetized cat striate cortex during natural scene stimulation, I have made several key contributions to our basic understanding of the cortical processing of natural stimuli and more broadly toward the collective pursuit of understanding visual perception. More specifically, in chapter two, I have shown that striate neurons respond briefly, sparsely and reliably to repeated presentations of natural scenes and neighboring neurons, recorded simultaneously, exhibit an unexpected degree of response heterogeneity. These findings lend strong supporting evidence to the hypothesis that sensory cortices efficiently represent information by utilizing principles of sparse coding. The results also counter the widely held concept of the columnar organization of response properties within sensory cortex and these issues are elaborated in detail below, within the context of neocortical microcircuits in the next section. In chapter three I have shown that these brief and sparse spiking responses are significantly correlated with elevated gamma-band (25-90Hz) oscillatory activity, present within the local field potentials, during the presentation of natural scenes. When viewed across the layers of striate cortex, these spike-field correlations were generally highest within the supragranular layers, consistent with known anatomical and physiological properties of the striate cortical microcircuit. Together these findings further our understanding of cortical processing of

complex sensory information and will inform future experimentation and more importantly shed light onto the mechanisms of visual perception.

4.2 Contributions in the Context of Cortical Microcircuits

A prominent feature of mammalian sensory cortices is the orderly arrangement of columns of anatomically connected neurons possessing similar stimulus feature preferences (reviewed in Mountcastle 1997, 2003). In cat striate cortex, columns are thought to consist of narrow vertical chains of cells spanning all layers of the cortex that exhibit similar preferences to visual features such as spatial location, orientation, direction of motion, ocular dominance, and spatial frequency (Hubel and Wiesel, 1962; 1963; 1977). The selectivity of visual response properties is systematically arranged into a smoothly varying map across the cortical surface that is punctuated by local discontinuities (Blasdel and Salma 1986; Hubener et al., 1997; Ohki et al., 2005), although when multiple stimulus features are simultaneously present, these maps can display greater variability than expected (Basole et al. 2003) The resulting functional architecture is thought to maximize the coverage of stimulus features and to minimize the distance between neurons with similar response properties. While this model is well supported by a large body of evidence from both electrophysiological and optical imaging studies, it is based primarily on the responses to the classical set of simple visual stimuli. In chapter two, I present results that counter this generally accepted picture of the functional organization of striate cortex. I have shown that small neighboring groups of cat striate cells respond with an unexpected high degree of sparse and heterogeneous

responses to the presentation of natural scenes. These findings raise important questions regarding our current understanding of the columnar organization of function within striate cortex and more broadly to organization of function within all neocortical areas.

The distinguishing hallmarks of most neocortical areas include the horizontal arrangement of cells into six general laminae and the vertical alignment of neurons into columnar arrangements that take several anatomical forms: macrocolumns, approximately 0.4–0.5mm in diameter (Mountcastle, 1957; Hubel and Wiesel, 1963) and microcolumns or minicolumns approximately 30-80μm in diameter (Mountcastle, 1997; Jones, 2000; Buxhoeveden and Casanova, 2002). Mountcastle (1957) first proposed that the smallest functional unit of information processing within the mammalian cerebral cortex was composed of a column of these vertically aligned cells. This basic unit of function was later termed a 'minicolumn' (Mountcastle, 1997) and its anatomical structure was attributed to the 'ontogenetic columns' described by Rakic (1988). While details of minicolumn architecture are likely to vary across different brain regions (Buxhoeveden and Casanova, 2002; Rockland and Ichinohe, 2004), minicolumns are proposed to consist of 80-100 neurons, spanning all six cortical laminae, stacked in a vertical column orthogonal to the cortical surface (Mountcastle, 1957, 1997; Jones 2000; Favorov et al., 1990, 1994a, b; Buxhoeveden and Casanova, 2002). Pyramidal cell bodies, along with their apical dendritic tufts, are clustered together within an individual minicolumn, thus establishing the anatomical and presumed elementary unit (Mountcastle, 1997). In sensory cortex, macrocolumns are proposed to consist of an estimated 60-80 interconnected minicolumns that are variously named barrel fields, hypercolumns or

segregates (Favorov and Kelly, 1994a, b; Mountcastle, 1997; Hubel and Wiesel, 1977; Buxhoeveden and Casanova, 2002) whereby the standard anatomical basis of a macrocolumn is the physical termination of the thalamic afferents (Mountcastle 1997).

The anatomical arrangement of neocortical cells and the connections between them is clearly columnar in nature and this principle of organization correlates well with the columnar arrangement of neurons possessing similar stimulus preferences. The functional arrangement stimulus preference within the neocortex has been extensively investigated, using a variety of techniques, from a variety of animals, and has been observed within nearly all sensory cortices (Mountcastle, 1957; Hubel and Wiesel, 1963, 1974; 1977; Favorov and Whitsel, 1988; Favorov and Diamond, 1990; Favorov and Kelly, 1994a, b; Blasdel, et al., 1992; Hübener et al., 1997; Amirikian and Georgopoulos, 2003; Krupa et al, 2004; Ohki et al., 2005). Although the columnar hypothesis maybe a parsimonious description of cortical organization and function, issues regarding the anatomical minicolumn and it's proposed functional role have remained quite controversial (Mountcastle, 2003; Rockland and Ichinohe, 2004; Horton and Adams, 2005) and confusion surrounding the various terminology remains (Rakic, 2008). In addition several studies within cat striate cortex have shown that receptive field properties among adjacent striate neurons can display significant differences under more classical stimulus conditions. (Maldonado and Gray, 1996; Maldonado et al., 1997; Hetherington and Swindale, 1999; DeAngelis et al., 1999). Results in chapter two extend the evidence of heterogeneity of response properties among adjacent striate neurons through the use of natural scenes and put into question the general definition of columnar organization.

Given the striking degree of columnar arrangement of the anatomy and physiology of neurons within sensory cortex, it has been proposed that a "canonical" microcircuit is in fact embedded within this arrangement and replicated through an evolutionary expansion of the neocortex (Douglas and Martin, 1989, 2004). Since local synaptic connections dominate the distribution of inputs to any given cortical neuron (Gilbert and Wiesel, 1983; Martin and Whitteridge, 1984; Peters and Yilmaz, 1993; Callaway, 1998, 2002; Thomson and Bannister, 2003; Binzegger et al., 2004) this suggests that neighboring cortical neurons should receive common synaptic inputs (Yoshimura and Callaway, 2005). And within this "canonical" framework, subcircuits within each layer of cortex would acquire direct excitation and disynaptic inhibition, both driven by common inputs, and therefore as the level of excitation increases, so does the level of inhibition, due to the recurrent nature of the local reciprocal connections (Douglas and Martin, 2007b). It is also well established that there exists a greater diversity of inhibitory GABAergic interneurons compared to the more plentiful excitatory pyramidal cells (Whittington and Traub, 2003; Markram et al., 2004) and that a subset of these interneurons engage in gamma (30-80Hz) oscillations (Azouz et al., 1997; Hasenstaub et al., 2005; Cardin et al., 2007; 2009; Cruikshank et al., 2007, reviewed in Bartos et al., 2007). It has been shown that excitatory pyramidal cells also engage in robust gamma activity as well (Gray and McCormick, 1997). Taken together, if increased afferent drive manifests itself as enhanced gamma activity, via the reciprocal connections between excitatory and inhibitory cells, gamma activity could be used as a direct metric of the local networks quasi-stable state. A variant of this concept, termed the "gamma

cycle" stipulates that spiking activity is determined by the absolute phase of ongoing oscillations within the gamma band (Fries et al., 2007). Therefore, during periods of enhanced gamma, i.e. enhanced excitability, functional interactions are dynamically established between local circuit elements and the incoming sensory information. This transient 'state' change within the local network could act as a brief window of opportunity for cell-to-cell interactions, mediating the transfer of, or enhancement of information flow within the cortical microcircuit and onto to the next stage of processing. I have shown in chapter two that local networks of neurons response sparsely and heterogeneously during particular movie segments and in chapter three these epochs co-occur within periods of enhanced gamma activity. I proposed that gamma oscillations could actively select, in a Darwinian sense, which set of afferent inputs, i.e. stimulus related information, is allowed to be processed locally and how that information flows to the next stage of processing within the visual system. Although a bit speculative, this hypothesis could be directly tested using more sophisticated stimulus presentation technologies and data analysis methods, each of which are briefly discussed below in section 4.3.

Overall the general consensus is that neurons sharing similar response properties tend to cluster together within the cortex, yet the results presented in chapter two counters this consensus, at least in the context of natural scene stimulation. The level of decorrelated activity among adjacent neurons suggests either a reexamination of current models of cortical microcircuits or a more intriguing possibility, is that the correlation structure may be dependent on the statistical properties of the stimulus.

4.3 Future Experimentation and Analysis

The exploratory nature of this research employed novel recording and stimulation techniques. The insertion of silicon polytrodes into the cortex proved straightforward yet acquiring and maintaining consistent unit activity throughout and across experimental sessions proved more difficult than anticipated. Although great care was taken to advance the polytrodes 'normal' to the surface of the cortex, the histology confirmed that nearly all recordings were 'off-axis' in at least one plane. In order to determine if penetrations are normal to the surface, electrical stimulation of the afferent thalamic inputs (Jin et al., 2011) could be conducted, although this approach may prove just as difficult to implement and reproduce across experiments. However, the 'off-axis' penetration is likely a non-issue when interpreting the results from the LFP analysis, given that the spread of currents is significantly larger than the size of a putative cortical column.

In chapters two and three I presented results highlighting the fact that unit activity and LFP activity occasionally became entrained to the presentation rates of the natural scenes. Video entrainment of spiking neurons in cat lateral geniculate nucleus and striate cortex have been reported with CRT refresh rates of 60Hz (Wollman and Palmer, 1995); within human and non-human primate visual cortex up to 60Hz (Williams et al., 2004) and within spiking and LFP activity in the visual cortex of tree shrews up to 120Hz (Viet et al., 2011). In addition to these studies, our own studies have documented refresh rate locking of spiking activity at 85, 120 and 150Hz during natural scene stimulation (Herikstad et al., 2011). Therefore additional experiments using natural scenes should include movies, originally captured at higher frames rates, 60Hz or greater, which is now

possible with off the shelf video capture equipment, and video sync refresh rates of 200Hz or greater, to avoid artificial entrainment of the spiking and LFP activity. In addition, these movies should avoid artificial scene transitions, although the movies would need to include increased motion of objects within the scenes in order to induce adequate cortical responses. This may include shooting moving animals and objects with a stationary camera. As shown in figure 3.3.19, ongoing spiking and LFP activity was significantly influenced by scene transitions within the movies, which may lead to inflated spike-field correlations and could lead to erroneous conclusions regarding the processing of natural scenes.

Although technically challenging, additional experimentation using more robust silicon laminar polytrodes in awake and behaving animals viewing both static and dynamic natural scenes should be considered as an alternative. Response properties of neurons in striate cortex of cats are significantly influenced by the amount and type of anesthetic administered (Ogawa et al., 1992; Villeneuve and Casanova 2003). Transitions between awake and anesthetized states have also been explored in rodent visual cortex (Greenberg et al., 2008), illustrating marked differences in overall cellular responsiveness and sparsity. Beyond the specific effects of general anesthetics, the current ‘state’ of the local network can directly influence receptive field properties and the overall responsiveness of visual cortical neurons (Worgotter et al., 1998; Haider et al., 2007; Hasenstaub et al., 2007).

In order move beyond basic descriptive statistics of these large and complex datasets, and transition to better spiking models that can predict responses to novel and

arbitrary stimuli, one must employ more rigorous analytical techniques that exploit the dynamics inherent to the data presented in this thesis. In recent years, an extension of the classic spike-triggered average (STA) methodology (Jones & Palmer, 1987; reviewed in Ringach 2004), termed spike-triggered covariance (STC) analysis was developed to explain a greater degree of the variance of the spiking activity observed for both simple and complex cells in striate cortex using simple (Touryan et al., 2002; Rust et al., 2004; 2005) and natural (Touryan et al., 2005; Felsen et al., 2005; Sharpee et al., 2006) stimuli. Although successful in uncovering additional 'filters' employed in Linear-Nonlinear Poisson (LNP) predictive spiking models (Schwartz et al., 2006), the methodology does not easily generalize to joint responses and has no mechanism of incorporating large fluctuations in overall network activity, as observed in simultaneous recorded EEG and/or LFP signals, and known to significantly influence cellular responses (Arieli et al., 1995, 1996; Tsodyks et al., 1999; Kenet et al., 2003; reviewed in Haider and McCormick, 2009). Generalized Linear Models (GLMs) incorporate joint spiking responses and network interactions (EEG, LFP) in order to model and predict responses to novel stimuli (Paninski, 2003) and have been recently shown to better predict responses during natural scene stimulation compared to more 'classical' stimuli (Haslinger et al., 2012). GLM spiking models could be employed to analyze the datasets collected in this thesis and future dataset, which include large-scale population activity and indirect information about the 'state' of the network, in the form of enhanced gamma frequency band activity. These models may be able to better predict the dynamics of the individual and joint responses to natural scenes discussed in both chapters two and three.

Natural scenes are inherently endowed with statistical regularities and richness not contained in the vast majority of visual stimuli used in past and current experimentation. From an evolutionary perspective natural scenes are more ecologically relevant to the study of the visual system, and therefore may engage and stimulate the striate cortex in markedly different ways compared to classical reduced stimuli. This presumption is based on the fact that the visual system evolved under the constraints of the natural world in order to efficiently represent information most relevant to the organisms' survival. Therefore, one could imagine that additional 'filters' and mechanisms of sensory processing could be uncovered using the above methodologies in combination with natural scenes. I believe this approach will eventually lead to a better understanding of visual perception in the natural world.

REFERENCES CITED

Adelson, E.H., and Bergen, J.R. (1985) Spatiotemporal energy models for the perception of motion. Journal of the Optical Society of America A2: 284–299.

Alonso, J.M. and Martinez, L.M. (1998) Functional connectivity between simple cells and complex cells in cat striate cortex. Nature Neuroscience. 1:395-403.

Amirikian, B., Georgopoulos, A.P. (2003) Modular organization of directionally tuned cells in the motor cortex: is there a short-range order? Proc Natl Acad Sci U S A. 100(21):12474-9.

Arieli, A., Sterkin, A., Grinvald, A., and Aertsen, A. (1996). Dynamics of ongoing activity: explanation of the large variability in evoked cortical responses. Science 273, 1868–1871.

Attneave, F. (1954) Some informational aspects of visual perception. Psychology Reviews 51, 183–193.

Attwell, D., and Laughlin, S.B. (2001) An energy budget for signaling in the grey matter of the brain. Journal of Cerebral Blood Flow and Metabolism. 21, 1133–1145

Azouz, R. and Gray, C.M. (2000) Dynamic Spike Threshold Reveals a Mechanism for Synaptic Coincidence Detection in Cortical Neurons In Vivo. Proc. Natl. Acad. Sci., 97(14): 8110-8115.

Azouz, R. and Gray, C.M. (2003) Adaptive Coincidence Detection and Dynamic Gain Control in Visual Cortical Neurons In Vivo. Neuron, 37:513-523.

Baddeley, R., Abbott, L.F., Booth, M.C., Sengpiel, F., Freeman, T., Wakeman, E.A. and Rolls, E.T. (1997) Responses of neurons in primary and inferior temporal visual cortices to natural scenes. Proceedings of the Royal Society of London. B Biol. Sci., 264, 1775-1783.

Bair, W., Zohary, E. and Newsome, W.T. (2001) Correlated firing in macaque visual area MT: time scales and relationship to behavior. Journal of Neuroscience. 21,1676-1697.

Binzegger, T., Douglas, R.J. and Martin, K.A. (2004) A quantitative map of the circuit of cat primary visual cortex. Journal of Neuroscience. 24:8441-8453.

Dan, Y., Attick, J.J. and Reid, R.C. (1996) Efficient Coding of Natural Scenes in the Lateral Geniculate Nucleus: Experimental Test of a Computational Theory. Journal of Neuroscience. 16:3351-3362.

Barlow, H.B. (1961) The coding of sensory messages. In Thorpe, W.H. and Zangwill, O.L. (Eds), Current Problems in Animal Behaviour. Cambridge University Press, Cambridge, pp. 331–360.

Barlow, H.B. (1961) Possible principles underlying the transformation of sensory messages. In: Sensory Communications, edited by Rosenbluth WA. Cambridge, MA: Cambridge UP 217-234.

Barlow, H. B. (1972) Single units and sensation: a neuron doctrine for perceptual psychology. Perception, 1(4), 371-394.

Barlow, H.B. (2001) Redundancy reduction revisited. Network, 12, 241–253.

Bartos M., Vida, I. and Jonas, P. (2007) Synaptic mechanisms of synchronized gamma oscillations in inhibitory interneuron networks. Nature Reviews Neuroscience. 8, 45–56.

Basole, A., White, L.E. and Fitzpatrick, D. (2003) Mapping multiple features in the population response of visual cortex. Nature, 423:986-990.

Bedard, C. and Destexhe, A. (2009) Macroscopic Models of Local Field Potentials and the Apparent 1/f Noise in Brain Activity. Biophysical Journal. 96, 2589-2603.

Bell, A.J. and Sejnowski, T.J. (1997) The "independent components" of natural scenes are edge filters. Vision Research. 37(23), 3327-3338.

Belitski, A., Gretton, A., Magri, C., Murayama, Y., Montemurro, M.A., Logothetis, N.K., Panzeri, S. (2008) Low-frequency local field potentials and spikes in primary visual cortex convey independent visual information. Journal of Neuroscience 28, 5696-5709.

Belitski, A., Panzeri, S., Magri, C., Logothetis, N. K., and Kayser, C. (2010) Sensory information in local field potentials and spikes from visual and auditory cortices: time scales and frequency bands. Journal of Computational Neuroscience. 29(3), 533-545.

Berens, P., Keliris, G.A., Ecker, A.S., Logothetis, N.K. and Tolias, A.S. (2008) Comparing the feature selectivity of the gamma-band of the local field potential and the underlying spiking activity in primate visual cortex. Frontiers in Systems Neuroscience. 2, 199–207.

Beierlein, M., Gibson, J.R. and Connors, B.W. (2003) Two dynamically distinct inhibitory networks in layer 4 of the neocortex. Journal of Neurophysiology. 90, 2987-3000.

Benjamini, Y., and Hochberg, Y. (1995) Controlling the false discovery rate: a practical and powerful approach to multiple testing. Journal of the Royal Statistical Society. Series B (Methodological), 289-300.

Berry, M.J., Warland, D.K. and Meister, M. (1997) The structure and precision of retinal spike trains. Proceedings of the National Academe of Sciences, USA. 94, 5411-5416.

Bichot NP, Rossi AF, Desimone R. (2005) Parallel and serial neural mechanisms for visual search in macaque area V4. Science 308(5721):529–34

Binzegger, T., Douglas, R.J. and Martin, K.A. (2004) A quantitative map of the circuit of cat primary visual cortex. Journal of Neuroscience. 24, 8441-8453.

Blanche, T.J., Spacek, M.A., Hetke, J.F. and Swindale, N.V. (2005) Polytrodes: high-density silicon electrode arrays for large-scale multiunit recording. Journal of Neurophysiology. 93, 2987-3000.

Blanche, T.J., Freiwald, W.A. and Swindale, N.V. (2006) Neural sparseness in cat and monkey visual cortex studied with silicon polytrode arrays. Program No. 734.20. 2006 Abstract Viewer/Itinerary Planner, Washington, DC: Society for Neuroscience.

Blasdel, G.G. and Salama, G. (1986) Voltage-sensitive dyes reveal a modular organization in monkey striate cortex. Nature, 321:579-585.

Börgers, C., and Kopell, N. (2003) Synchronization in networks of excitatory and inhibitory neurons with sparse, random connectivity. Neural Computation, 15(3), 509-538.

Bryant, H.L. and Segundo, J.P. (1976) Spike initiation by transmembrane current: a white-noise analysis. Journal of Physiology. 260, 279-314.

Buffalo, E.A., Fries, P., Landman, R., Buschman, T.J., and Desimone, R. (2011) Laminar differences in gamma and alpha coherence in the ventral stream. Proceedings of the National Academes of Science, USA. 108, 11262–11267.

Buxhoeveden, D.P., Casanova, M.F. (2002) The minicolumn hypothesis in neuroscience. Brain. 125(Pt 5):935-51.

Buzsáki, G., and Chrobak, J. J. (1995). Temporal structure in spatially organized neuronal ensembles: a role for interneuronal networks. Current Opinion in Neurobiology. *5*(4), 504-510.

Buzsáki, G., and Kandel, A. (1998). Somadendritic backpropagation of action potentials in cortical pyramidal cells of the awake rat. Journal of Neurophysiology, *79*(3), 1587-1591.

Buzsáki G, Draguhn A (2004) Neuronal oscillations in cortical networks. Science. 304,1926–1929.

Buzsáki, G. (2006) Rhythms of the Brain. Oxford University Press.

Buzsáki, G., Anastassiou, C.A. and Koch, C. (2012) The origin of extracellular fields and currents – EEG, ECog, LFP and spikes. Nature Reviews Neuroscience.13, 407-420.

Callaway, E.M. (1998) Local circuits in primary visual cortex of the macaque monkey. Ann. Rev. Neurosci., 21:47-74.

Callaway, E.M. (2002) Cell type specificity of local cortical connections. J. Neurocytol., 31:231-237.

Carandini, M., Demb, J.B., Mante, V., Tolhurst, D.J., Dan, Y., Olshausen, B.A., Gallant, J.L. and Rust, N.C. (2005) Do We Know What the Early Visual System Does? Journal of Neuroscience 25 (46). 10577–10597.

Cardin, J.A., Palmer, L.A., and Contreras, D. (2007). Stimulus feature selectivity in excitatory and inhibitory neurons in primary visual cortex. Journal of Neuroscience. 27,10333–10344.

Cardin, J.A., Carle´n, M., Meletis, K., Knoblich, U., Zhang, F., Deisseroth, K., Tsai, L.H., and Moore, C.I. (2009) Driving fast-spiking cells induces gamma rhythm and controls sensory responses. Nature. 459, 663– 667.

Cavanaugh, J.R., Bair, W. and Movshon, J.A. (2002) Selectivity and spatial distribution of signals from the receptive field surround in macaque V1 neurons. Journal of Neurophysiology. 88, 2547-2556.

Chalk, M., Herrero, J.L., Gieselmann, M.A., Delicato, L.S., Gotthardt, S. and Thiele, A. (2010) Attention reduces stimulus-driven gamma frequency oscillations and spike field coherence in V1. Neuron. 66, 114–125.

Connors, B.W. and Gutnick, M.J. (1990) Intrinsic firing patterns of diverse neocortical neurons. Trends in Neuroscience. 13, 99-104.

Cruikshank, S.J., Lewis, T.J., and Connors, B.W. (2007). Synaptic basis for intense thalamocortical activation of feedforward inhibitory cells in neocortex. Nature Neuroscience 10,462–468.

Dan, Y., Attick, J.J. and Reid, R.C. (1996) Efficient Coding of Natural Scenes in the Lateral Geniculate Nucleus: Experimental Test of a Computational Theory. Journal of Neuroscience. 16, 3351-3362.

David, S.V., Vinje, W.E. and Gallant, J.L. (2004) Natural stimulus statistics alter the receptive field structure of V1 neurons. Journal of Neuroscience. 24, 6991-7006.

David, S.V and Gallant, J.L. (2005) Predicting neuronal responses during natural vision. Network: Computation in Neural Systems. 16, 239-260.

DeAngelis, G.C., Ghose, G.M., Ohzawa, I. and Freeman, R.D. (1999) Functional micro-organization of primary visual cortex: receptive field analysis of nearby neurons. Journal of Neuroscience. 19, 4046-4064.

De Valois, K.K., De Valois, R.L. and Yund, E.W. (1979) Responses of striate cortex cells to grating and checkerboard patterns. Journal of Physiology. 291: 483–505.

DiCarlo, J.J., Lane, J.W., Hsiao, S.S. and Johnson, K.O. (1996) Marking Microelectrode Penetrations with Fluorescent Dyes. Journal of Neuroscience Methods. 64:75-81.

Dimitrov, A. and Cowan, J.D. (1998) Spatial decorrelation in orientation-selective cortical cells. Neural Computation.10,1779-1795.

Dong, D.W. and Atick, J.J. (1995) Statistics of natural time-varying images. Network: Computational Neural Systems 6, 345-358.

Douglas, R.J. and Martin, K.A. (2004) Neuronal circuits of the neocortex. Annual Reviews in Neuroscience. 27:419-451.

Douglas, R.J., and Martin, K.A. (2007a). Mapping the matrix: the ways of neocortex. Neuron 56, 226–238.

Douglas, R.J., and Martin, K.A. (2007b). Recurrent neuronal circuits in the neocortex. Current Biology. 17, 496–500.

Ecker, A.S., Berens, P., Keliris, G.A., Bethge, M., Logothetis, N.K., and Tolias, A.S. (2010) Decorrelated neuronal firing in cortical microcircuits. Science. 327, 584–587.

Einevoll, G. T., Pettersen, K. H., Devor, A., Ulbert, I., Halgren, E., and Dale, A. M. (2007) Laminar population analysis: estimating firing rates and evoked synaptic activity from multielectrode recordings in rat barrel cortex. Journal of neurophysiology. *97*(3), 2174-2190.

Engel, A. K., König, P., Gray, C. M., and Singer, W. (1990) Stimulus‐Dependent Neuronal Oscillations in Cat Visual Cortex: Inter‐Columnar Interaction as Determined by Cross‐Correlation Analysis. European Journal of Neuroscience, 2(7), 588-606.

Engel AK, Konig P, Kreiter AK, Singer W. (1991a) Interhemispheric synchronization of oscillatory neuronal responses in cat visual cortex. Science 252(5010):1177–79

Engel AK, Konig P, Singer W. (1991b) Direct physiological evidence for scene segmentation by temporal coding. Proc. Natl. Acad. Sci. USA 88(20):9136–40

Engel AK, Kreiter AK, Konig P, Singer W. (1991c) Synchronization of oscillatory neuronal responses between striate and extrastriate visual cortical areas of the cat. Proc. Natl. Acad. Sci. USA 88(14):6048–52.

Favorov, O.V., Whitsel, B.L., (1988) Spatial organization of the peripheral input to area 1 cell columns. II. The forelimb representation achieved by a mosaic of segregates. Brain Res. 472(1):43-56.

Favorov, O.V., Diamond, M.E., (1990) Demonstration of discrete place-defined columns segregates in the cat SI. J Comp Neurol. 298(1):97-112.

Favorov, O.V., Kelly, D.G., (1994a) Minicolumnar organization within somatosensory cortical segregates: II. Emergent functional properties. Cerebral Cortex. 4(4):428-42.

Favorov, O.V., Kelly, D.G., (1994b) Minicolumnar organization within somatosensory cortical segregates: I. Development of afferent connections. Cereb Cortex. Jul-Aug;4(4):408-27.

Freeman, R.D. (2003) Cortical columns: a multi-parameter examination. Cereb. Cortex, 13:70-72.

Felsen, G., Touryan, Han, F., and Dan, Y. (2005) Cortical sensitivity to visual features in natural scenes. PLOS Biology. 3, e342.

Felsen, G. and Dan, Y. (2005) A natural approach to studying vision. Nature Neuroscience. 8,1643–46.

Field, D.J. (1987) Relations Between the Statistics of Natural Images and the Response Properties of Cortical Cells. Journal of the Optical Society of America A., 4, 2379-2394.

Friedman-Hill S, Maldonado PE, Gray CM. (2000) Dynamics of striate cortical activity in the alert macaque: I. Incidence and stimulus-dependence of gamma-band neuronal oscillations. Cerebral Cortex 10(11):1105–16

Frien A, Eckhorn R, Bauer R, Woelbern T, Kehr H. (1994) Stimulus-specific fast oscillations at zero phase between visual areas V1 and V2 of awake monkey. Neuroreport 5(17):2273–77

Frien A, Eckhorn R (2000a) Functional coupling shows stronger stimulus dependency for fast oscillations than for low-frequency components in striate cortex of awake monkey. Eur J Neurosci 12:1466 –1478.

Frien A, Eckhorn R, Bauer R, Woelbern T, Gabriel A (2000b) Fast oscillations display sharper orientation tuning than slower components of the same recordings in striate cortex of the awake monkey. Eur J Neurosci 12:1453–1465.

Fries P, Roelfsema PR, Engel AK, Konig P, Singer W. (1997) Synchronization of oscillatory responses in visual cortex correlates with perception in interocular rivalry. Proc. Natl. Acad. Sci. USA 94(23):12699–704

Fries, P., Reynolds, J.H., Rorie, A.E. and Desimone, R. (2001) Modulation of oscillatory neuronal synchronization by selective visual attention. Science. 291, 1560–1563.

Fries P, Schroder JH, Roelfsema PR, Singer W, Engel AK. (2002) Oscillatory neuronal synchronization in primary visual cortex as a correlate of stimulus selection. J. Neurosci. 22(9):3739–54

Fries P. (2005) A mechanism for cognitive dynamics: neuronal communication through neuronal coherence. Trends Cogn. Sci. 9(10):474–80

Fries, P., Nikolić, D., and Singer, W. (2007) The gamma cycle. Trends in neurosciences, 30(7), 309-316.

Fries P, Scheeringa R, Oostenveld R. (2008a) Finding gamma. Neuron 58(3):303–5

Fries P, Womelsdorf T, Oostenveld R, Desimone R. (2008b) The effects of visual stimulation and selective visual attention on rhythmic neuronal synchronization in macaque area V4. J. Neurosci. 28(18):4823–35

Fries, P. (2009) Neuronal gamma-band synchronization as a fundamental process in cortical computation. Annual Reviews in Neuroscience. 32: 209–224.

Gail A, Brinksmeyer HJ, Eckhorn R (2004) Perception-related modulations of local field potential power and coherence in primary visual cortex of awake monkey during binocular rivalry. Cerebral Cortex 14:300 –313.

Gieselmann, M. A., and Thiele, A. (2008) Comparison of spatial integration and surround suppression characteristics in spiking activity and the local field potential in macaque V1. European Journal of Neuroscience, 28(3), 447-459.

Geisler, W.S., Albrecht, D.G., Crane, A.M., and Stern, L. (2001) Motion direction signals in the primary visual cortex of cat and monkey. Visual Neuroscience. 18, 501-516.

Gilbert, C.D. and Wiesel, T.N. (1983) Functional organization of the visual cortex. Progress in Brain Research. 58:209-218.

Gilbert, C.D. (1983) Microcircuitry of the visual cortex. Annual Reviews in Neuroscience. 6:217-247.

Goard, M. and Dan, Y. (2009) Basal forebrain activation enhances cortical coding of natural scenes. Nature Neuroscience. 12, 1444-1449.

Goodell, A.B. and Gray, C.M. (2003) Semi-automated solution to the spike overlap problem using tetrode data obtained from cat visual cortex. In: Program No. 429.9. 2003 Abstract Viewer/Itinerary Planner, edited by Washington DC: Society for Neuroscience.

Gray, C.M., Konig, P., Engel, A.K. and Singer, W. (1989) Oscillatory responses in cat visual cortex exhibit inter-columnar synchronization which reflects global stimulus properties. Nature. 338:334-37.

Gray, C.M. and Singer, W. (1989) Stimulus-specific neuronal oscillations in orientation columns of cat visual cortex. Proc. Natl. Acad. Sci. USA 86:1698-1702.

Gray, C. M., Engel, A. K., König, P., and Singer, W. (1990) Stimulus‐Dependent Neuronal Oscillations in Cat Visual Cortex: Receptive Field Properties and Feature Dependence. European Journal of Neuroscience, 2(7), 607-619.

Gray, C. M. (1994). Synchronous oscillations in neuronal systems: mechanisms and functions. Journal of computational neuroscience, 1(1-2), 11-38.

Gray, C.M., Maldonado, P., Wilson, M. and McNaughton, B. (1995) Tetrodes Markedly Improve the Reliability and Yield of Multiple Single Unit Isolation from Multiunit Recordings in Cat Striate Cortex. Journal of Neuroscience Methods. 63, 43-54.

Gray, C.M. and McCormick, D.A. (1996) Chattering Cells: Superficial Pyramidal Neurons Contributing to the Generation of Synchronous Oscillations in Visual Cortex. Science. 274, 109-113.

Gray CM, Di Prisco GV. (1997) Stimulus-dependent neuronal oscillations and local synchronization in striate cortex of the alert cat. Journal of Neuroscience. 17(9):3239–53.

Greenberg, D.S., Houweiling, A.R., and Kerr, J.N.D., (2008) Population imaging of ongoing neuronal activity in the visual cortex of awake rats. Nature Neuroscience. 11, 749–751

Guo, K., Robertson, R.G., Mahmoodi, S. and Young, M.P. (2005) Centre-surround interactions in response to natural scene stimulation in the primary visual cortex. European Journal of Neuroscience. 21, 536-548.

Haider, B., Duque, A., Hasenstaub, A.R., Yu, Y., and McCormick, D.A. (2007). Enhancement of visual responsiveness by spontaneous local network activity in vivo. Journal of Neurophysiology. 97, 4186–4202.

Haider, B. and McCormick D.A. (2009) Rapid neocortical dynamics: cellular and network mechanisms. Neuron. 62, 171-189.

Haider, B., Krause, M.R., Duque, A., Yu, Y., Touryan, J., Mazer, J.A. and McCormick, D.A. (2010) Synaptic and network mechanisms of sparse and reliable visual cortical activity during nonclassical receptive field stimulation. Neuron. 65, 107-121.

Harris, K.D., Henze, D.A., Csicsvari, J., Hirase, H. and Buzsaki, G. (2000) Accuracy of tetrode spike separation as determined by simultaneous intracellular and extracellular measurements. Journal of Neurophysiology. 84, 401-414.

Hasenstaub, A., Shu, Y., Haider, B., Kraushaar, U., Duque, A., and McCormick, D.A. (2005). Inhibitory postsynaptic potentials carry synchronized frequency information in active cortical networks. Neuron 47, 423–435.

Hasenstaub, A., Sachdev, R.N., and McCormick, D.A. (2007). State changes rapidly modulate cortical neuronal responsiveness. Journal of Neuroscience 27, 9607–9622.

Haslinger, R., Pipa, G., Lima, B., Singer, W., Brown, E.N., Neuenschwander, S. (2012) Context Matters: The Illusive Simplicity of Macaque V1 Receptive Fields. PLoS ONE. 7(7), e39699.

Henrie, J.A. and Shapley, R. (2005) LFP power spectra in V1 cortex: the graded effect of stimulus contrast. Journal of Neurophysiology. 94, 479–490.

Henze, D.A., Z. Borghegyi, J. Csicsvari, A. Mamiya, K.D. Harris, and G. Buzsaki. (2000) Intracellular features predicted by extracellular recordings in the hippocampus in vivo. Journal of Physiology. 84: 390-400.

Herculano-Houzel S, Munk MH, Neuenschwander S, Singer W. 1999. Precisely synchronized oscillatory firing patterns require electroencephalographic activation. *J. Neurosci.* 19(10):3992–4010.

Herikstad, R., Baker, J.L., Lachaux, J.P., Gray, C.M. and Yen, S.C. (2011) Natural Movies Evoke Spike Trains with Low Spike Time Variability in Cat Primary Visual Cortex. The Journal of Neuroscience. 31(44),15844-15860.

Hetherington, P.A. and Swindale, N.V. (1999) Receptive field and orientation scatter studied by tetrode recordings in cat area 17. Visual Neuroscience. 16:637-652.

Horton, J.C. and Adams, D.L. (2005) The cortical column: a structure without a function. Philosophical Transactions of the Royal Society of London B Biological Sciences, 360, 837-862.

Hubel, D.H. (1959) Single unit activity in striate cortex of unrestrained cats. Journal of Physiology. 147, 226-238.

Hubel, D.H. and Wiesel, T.N. (1959) Receptive fields of single neurons in the cat's striate cortex. Journal of Physiology 148, 574–591.

Hubel, D.H. and Wiesel, T.N. (1962) Receptive fields, binocular interaction and functional architecture in the cat's visual cortex. Journal of Physiology. 160, 106-154.

Hubel, D.H. and Wiesel, T.N. (1968) Receptive fields and functional architecture of monkey striate cortex. Journal of Physiology. 195, 215-243.

Hubel, D.H. and Wiesel, T.N. (1977) Ferrier lecture. Functional architecture of macaque monkey visual cortex. Proceedings of the Royal Society of London. 198, 1-59.

Hubener, M., Shoham, D., Grinvald, A. and Bonhoeffer, T. (1997) Spatial relationships among three columnar systems in cat area 17. Journal of Neuroscience. 17, 9270-9284.

Hutcheon, B., and Yarom, Y. (2000) Resonance, oscillation and the intrinsic frequency preferences of neurons. Trends in neurosciences, 23(5), 216-222.

Izhikevich, E. M. (2001) Resonate-and-fire neurons. Neural networks, 14(6), 883-894.

Jarvis, M. R., and Mitra, P. P. (2001) Sampling properties of the spectrum and coherency of sequences of action potentials. Neural Computation, 13(4), 717-749.

Jia, X., Smith, M. A., and Kohn, A. (2011). Stimulus selectivity and spatial coherence of gamma components of the local field potential. The Journal of Neuroscience, 31(25), 9390-9403.

Jin, J., Wang, Y., Swadlow, H.A. and Alonso, J.M. (2011) Population receptive fields of ON and OFF thalamic inputs to an orientation column in visual cortex. Nature Neuroscience.14(2),232-238.

Jones, E.G. (2000) Microcolumns in the cerebral cortex. Proc Natl Acad Sci U S A. May 9;97(10):5019-21.

Jones, H.E., Grieve, K.L., Wang, W. and Sillito, A.M. (2001) Surround suppression in primate V1. Journal of Neurophysiology. 86, 2011-2028.

Jones, J.P. and Palmer, L.A. (1987) The Two Dimensional Spatial Structure of Simple Cell Receptive Fields in the Cat Striate Cortex. J. Neurophysiol., 58:1187-1211.

Juergens, E., Eckhorn, R., Frien, A. and Woelbern, T. (1996) Restricted coupling range in fast oscillations in striate cortex of awake monkey. In: Brain and Evolution. Berlin: Theime, p. 418.

Kajikawa, Y., and Schroeder, C. E. (2011) How local is the local field potential? Neuron. 72(5), 847-858.

Kamondi, A., Acsady, L., Wang, X.J. and Buzsaki, G. (1998) Theta oscillations in somata and dendrites of hippocampal pyramidal cells in vivo: activity-dependent phase-precession of action potentials. Hippocampus. 8: 244–261.

Karube, F., Kubota, Y. and Kawaguchi, Y. (2004) Axon branching and synaptic bouton phenotypes in GABAergic nonpyramidal cell subtypes. Journal of Neuroscience. 24, 2853-2865.

Katzner, S., Nauhaus, I., Benucci, A., Bonin, V., Ringach, D. L., and Carandini, M. (2009) Local origin of field potentials in visual cortex. Neuron, 61(1), 35-41.

Kayser, C., Salazar, R.F. and Konig, P. (2003) Responses to natural scenes in cat V1. Journal of Neurophysiology. 90, 1910-1920.

Kayser C, Kording KP, Konig P. (2004) Processing of complex stimuli and natural scenes in the visual cortex. Current Opinion in Neurobiology. 14, 468–473.

Kayser C, Konig P (2004) Stimulus locking and feature selectivity prevail in complementary frequency ranges of V1 local field potentials. European Journal of Neuroscience, 19:485– 489.

Kayser, C., Montemurro, M. A., Logothetis, N. K., and Panzeri, S. (2009) Spike-phase coding boosts and stabilizes information carried by spatial and temporal spike patterns. Neuron, 61(4), 597-608.

Kenet, T., Bibitchkov, D., Tsodyks, M., Grinvald, A., and Arieli, A. (2003). Spontaneously emerging cortical representations of visual attributes. Nature. 425, 954–956.

Ko, H., Hofer, S.B., Pichler, B., Buchanan, K.A., Sjöström, P.J. and Mrsic-Flogel, T.D. (2011) Functional specificity of local synaptic connections in neocortical networks. Nature 473, 87-91.

Kreiman, G., Hung, C. P., Kraskov, A., Quiroga, R. Q., Poggio, T., and DiCarlo, J. J. (2006) Object selectivity of local field potentials and spikes in the macaque inferior temporal cortex. Neuron, 49(3), 433-445.

Kreiter AK, Singer W. (1996) Stimulus-dependent synchronization of neuronal responses in the visual cortex of the awake macaque monkey. J. Neurosci. 16(7):2381–96

Krupa, D.J., Wiest, M.C., Shuler, M.G., Laubach, M., Nicolelis, M.A. (2004) Layer-specific somatosensory cortical activation during active tactile discrimination. Science. Jun 25;304(5679):1989-92.

Kruse W, Eckhorn R (1996) Inhibition of sustained gamma oscillations (35– 80 Hz) by fast transient responses in cat visual cortex. Proc Natl Acad Sci USA 93:6112– 6117.

Kuffler, S.W. (1953) Discharge patterns and functional organization of mammalian retina. Journal of Neurophysiology, 16, 37–68.

Lamme, V.A.F. (1995) The neurophysiology of figure-ground segregation in primary visual cortex. Journal of Neuroscience 15, 1605–1615.

Laughlin, S.B., de Ruyter van Steveninck, R.R., and Anderson, J.C. (1998) The metabolic cost of neural information. Nature Neuroscience 1, 36-41.

Lemon, R. (1984) Methods of Neuronal Recording in Conscious Animals. Chichester: Wiley.

Lennie, P. (2003) The cost of cortical computation. Current Biology. 13, 493–497.

Leopold DA, Murayama Y, Logothetis NK. (2003) Very Slow Activity Fluctuations in Monkey Visual Cortex: Implication for Functional Brain Imaging. Cerebral Cortex 13, 422-433.

Lindén, H., Tetzlaff, T., Potjans, T. C., Pettersen, K. H., Grün, S., Diesmann, M., and Einevoll, G. T. (2011) Modeling the spatial reach of the LFP. Neuron, 72(5), 859-872.

Liu, J., and Newsome, W. T. (2006) Local field potential in cortical area MT: stimulus tuning and behavioral correlations. The Journal of neuroscience, 26(30), 7779-7790.

Llinas, R. R., Grace, A. A., and Yarom, Y. (1991) In vitro neurons in mammalian cortical layer 4 exhibit intrinsic oscillatory activity in the 10-to 50-Hz frequency range. Proceedings of the National Academy of Sciences, 88(3), 897-901.

Llinás, R. R., and Steriade, M. (2006) Bursting of thalamic neurons and states of vigilance. Journal of neurophysiology, 95(6), 3297-3308.

Logothetis, N.K., Kayser, C. and Oeltermann, A. (2007) In Vivo Measurements of Cortical Impedance Spectrum in Monkeys: Implications for Signal Propagation. Neuron. 55, 809-823.

Maier, A., Adams, G.K., Aura, C. and Leopold, D.A. (2010) Distinct superficial and deep laminar domains of activity in the visual cortex during rest and stimulation. Frontiers in Systems Neuroscience 4, 1–11.

Mainen, Z.F. and Sejnowski, T.J. (1995) Reliability of spike timing in neocortical neurons. Science 268, 1503-1506.

Maldonado, P.E. and Gray, C.M. (1996) Heterogeneity in Local Distributions of Orientation Selective Neurons in the Cat Primary Visual Cortex. Visual Neurosciences. 13, 509-516.

Maldonado, P.E., Goedecke, I., Gray, C.M. and Bonhoeffer, T. (1997) Orientation Selectivity in Pinwheel Centers of Cat Striate Cortex. Science. 276, 1551-1555.

Maldonado PE, Friedman-Hill S, Gray CM. (2000) Dynamics of striate cortical activity in the alert macaque: II. Fast time scale synchronization. Cereb. Cortex 10(11):1117–31

Mann, E. O., and Paulsen, O. (2007) Role of GABAergic inhibition in hippocampal network oscillations. Trends in neurosciences, 30(7), 343-349.

Markram, H., Toledo-Rodriguez, M., Wang, Y., Gupta, A., Silberberg, G. and Wu, C. (2004) Interneurons of the neocortical inhibitory system. Nature Reviews Neuroscience 5, 793-807.

Martin, K.A. and Whitteridge, D. (1984) Form, function and intracortical projections of spiny neurones in the striate visual cortex of the cat. Journal of Neurophysiology. 353, 463-504.

Martin, K.A.C. and Schroder, S. (2013) Functional Heterogeneity in Neighboring Neurons of Cat Primary Visual Cortex in Response to Both Artificial and Natural Stimuli Journal of Neuroscience. 33, 7325-7344.

Martinez, L.M., Wang, Q., Reid, R.C., Pillai, C., Alonso, J.M., Sommer, F.T. and Hirsch, J.A. (2005) Receptive field structure varies with layer in the primary visual cortex. Nature Neuroscience 8, 372-379.

Mazurek, M.E. and Shadlen M.N. (2002) Limits to the temporal fidelity of cortical spike rate signals. Nature Neuroscience. 5, 463-471.

Mechler, F., Reich, D.S. and Victor, J.D. (2002) Detection and discrimination of relative spatial phase by V1 neurons. Journal of Neuroscience. 22, 6129-6157.

Milstein, J., Mormann, F., Fried, I., and Koch, C. (2009) Neuronal shot noise and Brownian 1/f2 behavior in the local field potential. PLoS ONE 4, e4338.

Minlebaev, M., Colonnese, M., Tsintsadze, T., Sirota, A., and Khazipov, R. (2011) Early gamma oscillations synchronize developing thalamus and cortex. Science, 334(6053), 226-229.

Mitzdorf, U. (1985) Current source-density method and application in cat cerebral cortex: investigation of evoked potentials and EEG phenomena. Physiology Reviews. 65, 37–100.

Mitzdorf, U. (1987) Properties of the evoked potential generators: current source-density analysis of visually evoked potentials in the cat visual cortex. International Journal of Neuroscience 33:33–59.

Montemurro, M.A., Rasch, M.J., Murayama, Y., Logothetis, N.K. and Panzeri, S. (2008) Phase-of-firing coding of natural visual stimuli in primary visual cortex. Current Biology. 18, 375-380.

Moruzzi, G., and Magoun, H. W. (1949) Brain stem reticular formation and activation of the EEG. Electroencephalography and clinical neurophysiology, 1(1), 455-473.

Mountcastle, V.B. (1957) Modality and topographic properties of single neurons in cat's somatic sensory cortex. Journal of Neurophysiology 20:408–434.

Mountcastle, V.B. (1997) The columnar organization of the neocortex. Brain, 120:701-722.

Mountcastle, V.B. (2003) Untitled-introduction. Cerebral Cortex.13(1), 2–4.

Movshon, J. A., Thompson, I. D., and Tolhurst, D. J. (1978) Spatial and temporal contrast sensitivity of neurones in areas 17 and 18 of the cat's visual cortex. The Journal of Physiology, 283(1), 101-120.

Munk MH, Roelfsema PR, Konig P, Engel AK, Singer W. 1996. Role of reticular activation in the modulation of intracortical synchronization. *Science* 272(5259):271–74

Naselaris, T., Merchant, H., Amirikian, B. and Georgeopoulos, A. (2005) Spatial Reconstruction of Trajectories of an Array of Recording Microelectrodes. Journal of Neurophysiology. 93:2318-2330.

Nowak, L.G., Azouz, R.A., Sanchez-Vives, M.V., Gray, C.M. and McCormick, D.A. (2003) Electrophysiological Classes of Cat Primary Visual Cortical Neurons In Vivo as Revealed by Quantitative Analyses. Journal of Neurophysiology. 89, 1541-1566.

Nunez, P.L. and Srinivasan, R. (2006) Electric Fields of the Brain: The Neurophysics of EEG, Second Edition. New York: Oxford University Press.

Okun, M., Naim, A., and Lampl, I. (2010) The subthreshold relation between cortical local field potential and neuronal firing unveiled by intracellular recordings in awake rats. The Journal of Neuroscience, 30(12), 4440-4448.

Ohki, K., Chung, S., Ch'ng, Y.H., Kara, P., and Reid, R.C. (2005). Functional imaging with cellular resolution reveals precise micro-architecture in visual cortex. Nature 433, 597–603.

Ogawa T, Shingu K, Shibata M, Osawa M, Mori K. (1992) The divergent actions of volatile anaesthetics on background neuronal activity and reactive capability in the central nervous system in cats. Can J Anaesth. Oct;39(8):862-72.

Olshausen, B.A. and Field, D.J. (1996a) Emergence of simple-cell receptive field properties by learning a sparse code for natural images. Nature, 381:607-609.

Olshausen, B.A., and Field, D.J. (1996b) Natural image statistics and efficient coding. Network. 7, 333–339.

Olshausen, B.A., and Field, D.J. (2004). Sparse coding of sensory inputs. Current Opinions in Neurobiology. 14, 481–487.

Olshausen, B.A., Baker, J.B., Yen, S.C. and Gray, C.M. (2004). Receptive field models fail to predict responses of V1 neurons to natural scenes. Abstract Viewer/Itinerary Planner, Washington, DC: Society for Neuroscience.

Olshausen, B.A., Field, D.J. (2005) How close are we to understanding V1? Neural Computation. 17, 1665-1699.

Paninski, L. (2003) Convergence properties of some spike-triggered analysis techniques Network Computations in Neural Systems. 14, 437–64.

Payne, B., and Peters, A. (Eds.). (2002). The cat primary visual cortex. Elsevier.

Pedroarena, C., and Llinás, R. (1997) Dendritic calcium conductances generate high-frequency oscillation in thalamocortical neurons. Proceedings of the National Academy of Sciences, 94(2), 724-728.

Percival, D. B. (1993) Spectral analysis for physical applications. Cambridge University Press.

Pesaran, B., Pezaris, J.S., Sahani, M., Mitra, P.P. and Andersen, R.A. (2002) Temporal structure in neuronal activity during working memory in macaque parietal cortex. Nature Neuroscience 5, 805– 811.

Pesaran, B., Nelson, M. J., and Andersen, R. A. (2008) Free choice activates a decision circuit between frontal and parietal cortex. Nature, 453(7193), 406-409.

Pesaran, B. (2009) Uncovering the mysterious origins of local field potentials. Neuron. *61*(1), 1-2.

Peters, A. and Yilmaz, E. (1993) Neuronal organization in area 17 of cat visual cortex. Cerebral Cortex, 3:49-68.

Rakic, P., (1988) Specification of cerebral cortical areas. Science. 241(4862):170-6.

Rasch, M., Logothetis, N. K., and Kreiman, G. (2009). From neurons to circuits: linear estimation of local field potentials. The Journal of Neuroscience, 29(44), 13785-13796.

Ray, S., and Maunsell, J. H. (2011) Different origins of gamma rhythm and high-gamma activity in macaque visual cortex. PLoS biology, 9(4), e1000610.

Reid, R.C., Victor, J.D. and Shapley, R.M. (1997) The use of m-sequences in the analysis of visual neurons: linear receptive field properties. Visual Neurosciences. 14(6), 1015-27.

Reich, D.S., Mechler, F. and Victor, J.D. (2001) Independent and redundant information in nearby cortical neurons. Science. 294, 2566-2568.

Roberts, M.J., Lowet, E., Brunet, N.M., Ter Wal, M. Tiesinga, P., Fries, P., and De Weerd, P. (2013) Robust Gamma Coherence between Macaque V1 and V2 by Dynamic Frequency Matching. Neuron. 78(3), 523-536

Rockland KS, Ichinohe N (2004) Some thoughts on cortical minicolumns. Experimental Brain Research 158: 265–277.

Rodriguez R, Kallenbach U, Singer W, Munk MH (2004) Short- and long-term effects of cholinergic modulation on gamma oscillations and response synchronization in the visual cortex. Journal of Neuroscience, 24:10369–10378.

Rodriguez, R., U. Kallenbach, W. Singer and M. H.J. Munk (2010) Stabilization of visual responses through cholinergic activation. Neuroscience165(3), 944-954.

Rickert J, Oliveira SC, Vaadia E, Aertsen A, Rotter S, Mehring C (2005) Encoding of movement direction in different frequency ranges of motor cortical local field potentials. Journal of Neuroscience. 25:8815– 8824.

Ringach, D.L., Hawken, M.J. and Shapley, R. (2002) Receptive field structure of neurons in monkey primary visual cortex revealed by stimulation with natural image sequences. Journal of Vision. 2, 12–24.

Ringach, D.L. (2004) Mapping receptive fields in primary visual cortex. Journal of Physiology, 558, 717-728.

Ruderman, D.L. and Bialek, W. (1994) Statistics of natural images: Scaling in the woods. Physical Review Letters. 73, 814-817.

Rust, N. C., Schwartz, O., Movshon, J. A., and Simoncelli, E. P. (2004). Spike-triggered characterization of excitatory and suppressive stimulus dimensions in monkey V1. Neurocomputing. 58–60C, 793–799.

Rust, N. C., Schwartz, O., Movshon, J. A., and Simoncelli, E. P. (2005). Spatiotemporal elements of macaque V1 receptive fields. Neuron. 46, 945–956.

Rust, N.C. and Movshon, J.A. (2005) In praise of artifice. Nature Neuroscience 8, 1647-1650.

Scherberger H, Jarvis MR, Andersen RA (2005) Cortical local field potential encodes movement intentions in the posterior parietal cortex. Neuron 46:347–354.

Schiller, P.H., Finlay, B.L. and Volman, S.F. (1976) Short-term response variability of monkey striate neurons. Brain Research. 105, 347-349.

Schwartz O, Pillow JW, Rust NC, Simoncelli EP. (2006) Spike-triggered neural characterization J Vis. Jul 17;6(4):484-507.

Shadlen, M.N., and Newsome, W.T. (1998). The variable discharge of cortical neurons: implications for connectivity, computation, and information coding. Journal of Neuroscience. 18, 3870–3896.

Sharpee, T. O., Sugihara, H., Kurgansky, A. V., Rebrik, S. P., Stryker, M. P., and Miller, K. D. (2006). Adaptive filtering enhances information transmission in visual cortex. Nature. 439, 936–942.

Sillito, A.M., Grieve, K.L., Jones, H.E., Cudeiro, J., and Davis, J. (1995) Visual cortical mechanisms detecting focal orientation discontinuities. Nature. 378, 492-496.

Simoncelli, E.P. and Olshausen, B.A. (2001) Natural image statistics and neural representation. Annual Reviews in Neuroscience. 24, 1193-1216.

Singer, W. (1999) Neuronal synchrony: a versatile code for the definition of relations? Neuron, 24(1), 49-65.

Simoncelli, E.P. (2003) Vision and the statistics of the visual environment. Current Opinions in Neurobiology. 13, 144-149.

Singer, W. (1981) Topographic organization of orientation columns in the cat visual cortex. A deoxyglucose study. Experimental Brain Research 44, 431-436.

Singer, W., and Gray, C. M. (1995) Visual feature integration and the temporal correlation hypothesis. Annual review of neuroscience, 18(1), 555-586.

Smith, M.A., and Kohn, A. (2008) Spatial and temporal scales of neuronal correlation in primary visual cortex. Journal of Neuroscience 28, 12591–12603.

Skottun BC, Zhang J, and Grosof DH. (1994) On the directional selectivity of cells in the visual cortex to drifting dot patterns. Visual Neurosciences. 11,885-897.

Smith, M.A., Jia, X., Zandvakili, A. and Kohn, A. (2013) Laminar dependence of neuronal correlations in visual cortex Journal of Neurophysiology. 109, 940-947.

Smyth, D., Willmore, B., Baker, G.E., Thompson, I.D. and Tolhurst, D.J. (2003) The receptive-field organization of simple cells in primary visual cortex of ferrets under natural scene stimulation. Journal of Neuroscience 23, 4746–4759.

Sohal VS, Zhang F, Yizhar O, Deisseroth K (2009) Parvalbumin neurons and gamma rhythms enhance cortical circuit performance. Nature 459: 698–702.

Steriade, M., McCormick, D. A., and Sejnowski, T. J. (1993) Thalamocortical oscillations in the sleeping and aroused brain. Science, *262*(5134), 679-685.

Steriade, M., Timofeev, I., and Grenier, F. (2001). Natural waking and sleep states: a view from inside neocortical neurons. Journal of neurophysiology, *85*(5), 1969-1985.

Steriade, M., Timofeev, I., Dürmüller, N., and Grenier, F. (1998) Dynamic properties of corticothalamic neurons and local cortical interneurons generating fast rhythmic (30–40 Hz) spike bursts. Journal of Neurophysiology, 79(1), 483-490.

Stuart, G. J., and Sakmann, B. (1994) Active propagation of somatic action potentials into neocortical pyramidal cell dendrites. Nature, 367(6458), 69-72.

Sullivan, D., Csicsvari, J., Mizuseki, K., Montgomery, S., Diba, K., and Buzsáki, G. (2011) Relationships between hippocampal sharp waves, ripples, and fast gamma oscillation: influence of dentate and entorhinal cortical activity. The Journal of Neuroscience, 31(23), 8605-8616.

Swindale, N.V. (1991) Coverage and the design of striate cortex. Biological Cybernetics. 65, 415-424.

Swindale, N.V. (2000) How many maps are there in visual cortex? Cerebral Cortex. 10, 633-643.

Talebi, V., and Baker, C. L. (2012) Natural versus Synthetic Stimuli for Estimating Receptive Field Models: A Comparison of Predictive Robustness. The Journal of Neuroscience, *32*(5), 1560-1576.

Taylor K, Mandon S, Freiwald WA, Kreiter AK (2005) Coherent oscillatory activity in monkey area V4 predicts successful allocation of attention. Cerebral Cortex 15:1424 – 1437.

Thomson D. (1982) Spectrum estimation and harmonic analysis. Proc IEEE 70:1055–1096.

Thomson, D. J. and Chave, A. D. (1991). Advances in Spectrum Analysis and Array Processing, chapter Jackknifed Error Estimates for Spectra, Coherences, and Transfer Functions, pages 58–113. Prentice Hall.

Thomson, A.M., West, D.C., Wang, Y. and Bannister, A.P. (2002) Synaptic connections and small circuits involving excitatory and inhibitory neurons in layers 2-5 of adult rat and cat neocortex: triple intracellular recordings and biocytin labeling in vitro. Cerebral Cortex, 12:936-953.

Thomson, A.M. and Bannister, A.P. (2003) Interlaminar connections in the neocortex. Cerebral Cortex 13, 5-14.

Tolhurst, D.J., Movshon, J.A. and Dean, A.F. (1983) The statistical reliability of signals in single neurons in cat and monkey visual cortex. Vision Research. 23, 775-785.

Tolhurst, D.J., Smyth, D. and Thompson, I.D. (2009) The sparseness of neuronal responses in ferret primary visual cortex. Journal of Neuroscience. 29, 2355-2370.

Touryan, J., Lau, B., and Dan, Y. (2002). Isolation of relevant visual features from random stimuli for cortical complex cells. The Journal of Neuroscience. 22, 10811–10818.

Touryan, J., Felsen, G., and Dan, Y. (2005). Spatial structure of complex cell receptive fields measured with natural images. Neuron. 45, 781–791.

Tsodyks, M., Kenet, T., Grinvald, A. and Arieli, A. (1999) Linking spontaneous activity of single cortical neurons and the underlying functional architecture. Science, 286:1943-1946.

Tusa, R. J., Palmer, L. A., and Rosenquist, A. C. (1978) The retinotopic organization of area 17 (striate cortex) in the cat. Journal of Comparative Neurology, 177(2), 213-235.

Uhlhaas, P. J., and Singer, W. (2006) Neural synchrony in brain disorders: relevance for cognitive dysfunctions and pathophysiology. Neuron, 52(1), 155-168.

Uhlhaas, P. J., and Singer, W. (2010) Abnormal neural oscillations and synchrony in schizophrenia. Nature Reviews Neuroscience, 11(2), 100-113.

Van Der Werf, J., Jensen, O., Fries, P., and Medendorp, W. P. (2008) Gamma-band activity in human posterior parietal cortex encodes the motor goal during delayed prosaccades and antisaccades. The Journal of Neuroscience, 28(34), 8397-8405.

Villeneuve, M.Y. and Casanova, C. (2003) On the use of isoflurane versus halothane in the study of visual response properties of single cells in the primary visual cortex. Journal of Neuroscience Methods. 129(1), 19-31.

Vinje, W.E. and Gallant, J.L. (2000) Sparse coding and decorrelation in primary visual cortex during natural vision. Science. 287(5456), 1273-1276.

Vinje, W.E. and Gallant, J.L. (2002) Natural stimulation of the nonclassical receptive field increases information transmission efficiency in V1. Journal of Neuroscience 22(7), 2904-2915.

Vinck, M., Lima, B., Womelsdorf, T., Oostenveld, R., Singer, W., Neuenschwander, S., and Fries, P. (2010) Gamma-phase shifting in awake monkey visual cortex. The Journal of Neuroscience, 30(4), 1250-1257.

Vogels, R., Spileers, W. and Orban, G.A. (1989) The response variability of striate cortical neurons in the behaving monkey. Experimental Brain Research. 77:432-436.

Walker, G.A., Ohzawa, I., and Freeman, R.D. (1999) Asymmetric suppression outside the classical receptive field of the visual cortex. Journal of Neuroscience 19, 10536-10553.

Webb, B.S., Tinsley, C.J., Barraclough, N.E., Parker, A. and Derrington, A.M. (2003) Gain control from beyond the classical receptive field in primate primary visual cortex. Visual Neurosciences. 20, 221-230.

Weliky, M., Fiser, J., Hunt, R.H. and Wagner, D.N. (2003) Coding of natural scenes in primary visual cortex. Neuron. 37, 703-718.

Whittington, M. A., Traub, R. D., Kopell, N., Ermentrout, B., and Buhl, E. H. (2000) Inhibition-based rhythms: experimental and mathematical observations on network dynamics. International Journal of Psychophysiology, 38(3), 315-336.

Whittington, M. A., and Traub, R. D. (2003) Interneuron Diversity series: Inhibitory interneurons and network oscillations in vitro. Trends in neurosciences, 26(12), 676-682.

Whittington, M. A., Cunningham, M. O., LeBeau, F. E., Racca, C., and Traub, R. D. (2011) Multiple origins of the cortical gamma rhythm. Developmental neurobiology, 71(1), 92-106.

Williams, P. E., Mechler, F., Gordon, J., Shapley, R., & Hawken, M. J. (2004) Entrainment to video displays in primary visual cortex of macaque and humans. The Journal of neuroscience, 24(38), 8278-8288.

Willmore, B., Watters, P.A., and Tolhurst, D.J. (2000) A comparison of natural-image-based models of simple-cell coding. Perception. 29, 1017-1040.

Willmore, B. and Tolhurst, D.J. (2001) Characterizing the sparseness of neural codes. Network. 12, 255-270.

Wollman D.E. Palmer L.A. (1995) Phase locking of neuronal responses to the vertical refresh of computer display monitors in cat lateral geniculate nucleus and striate cortex, Journal of Neuroscience Methods, Volume 60, Issues 1–2, August. 107-113.

Womelsdorf, T., Fries, P., Mitra, P.P. and Desimone, R. (2006) Gamma-band synchronization in visual cortex predicts speed of change detection. Nature. 439, 733–736.

Womelsdorf, T., Schoffelen, J.M., Oostenveld, R., Singer, W., Desimone, R., Engel, A.K. and Fries, P. (2007) Modulation of neuronal interactions through neuronal synchronization. Science 316, 1609 –1612.

Wörgötter, F., Suder, K., Zhao, Y., Kerscher, N., Eysel, U. T., and Funke, K. (1998) State-dependent receptive-field restructuring in the visual cortex. Nature, 396(6707), 165-168.

Wörgötter, F., Eysel, U.T. (2000) Context, state and the receptive fields of striatal cortex cells. Trends in Neuroscience. 23, 497-503.

Xing, D., Yeh, C. I., and Shapley, R. M. (2009) Spatial spread of the local field potential and its laminar variation in visual cortex. The Journal of Neuroscience, 29(37), 11540-11549.

Yen. S.C., Baker, J.L. and Gray, C.M. (2007) Heterogeneity in the Responses of Adjacent Neurons to Natural Stimuli in Cat Striate Cortex. Journal of Neurophysiology. 97, 1326-1341.

Yang, J. W., An, S., Sun, J. J., Reyes-Puerta, V., Kindler, J., Berger, T., ... and Luhmann, H. J. (2013) Thalamic network oscillations synchronize ontogenetic columns in the newborn rat barrel cortex. Cerebral Cortex, 23(6), 1299-1316.

Yao, H. and Li, C.Y. (2002) Clustered organization of neurons with similar extra-receptive field properties in the primary visual cortex. Neuron. 35, 547-553.

Yao, H., Shi, L., Han, F., Gao, H., and Dan, Y. (2007). Rapid learning in cortical coding of visual scenes. Nature Neuroscience. 10, 772–778.

Yoshimura, Y., Dantzker, J.L. and Callaway, E.M. (2005) Excitatory cortical neurons form fine-scale functional networks. Nature. 433, 868-873.

Zanos TP, Mineault PJ, Pack CC (2011) Removal of spurious correlations between spikes and local field potentials. Journal of Neurophysiology, 105:474–486.

Zanos, S., Zanos, T. P., Marmarelis, V. Z., Ojemann, G. A., and Fetz, E. E. (2012) Relationships between spike-free local field potentials and spike timing in human temporal cortex. Journal of Neurophysiology, 107(7), 1808-1821.